1972
Quarterly
Technical
Progress
Review
Volume 15-3

Reactor Technology

A publication of the
Office of Information Services
U.S. Atomic Energy Commission
Prepared in Cooperation
with
The American Nuclear Society

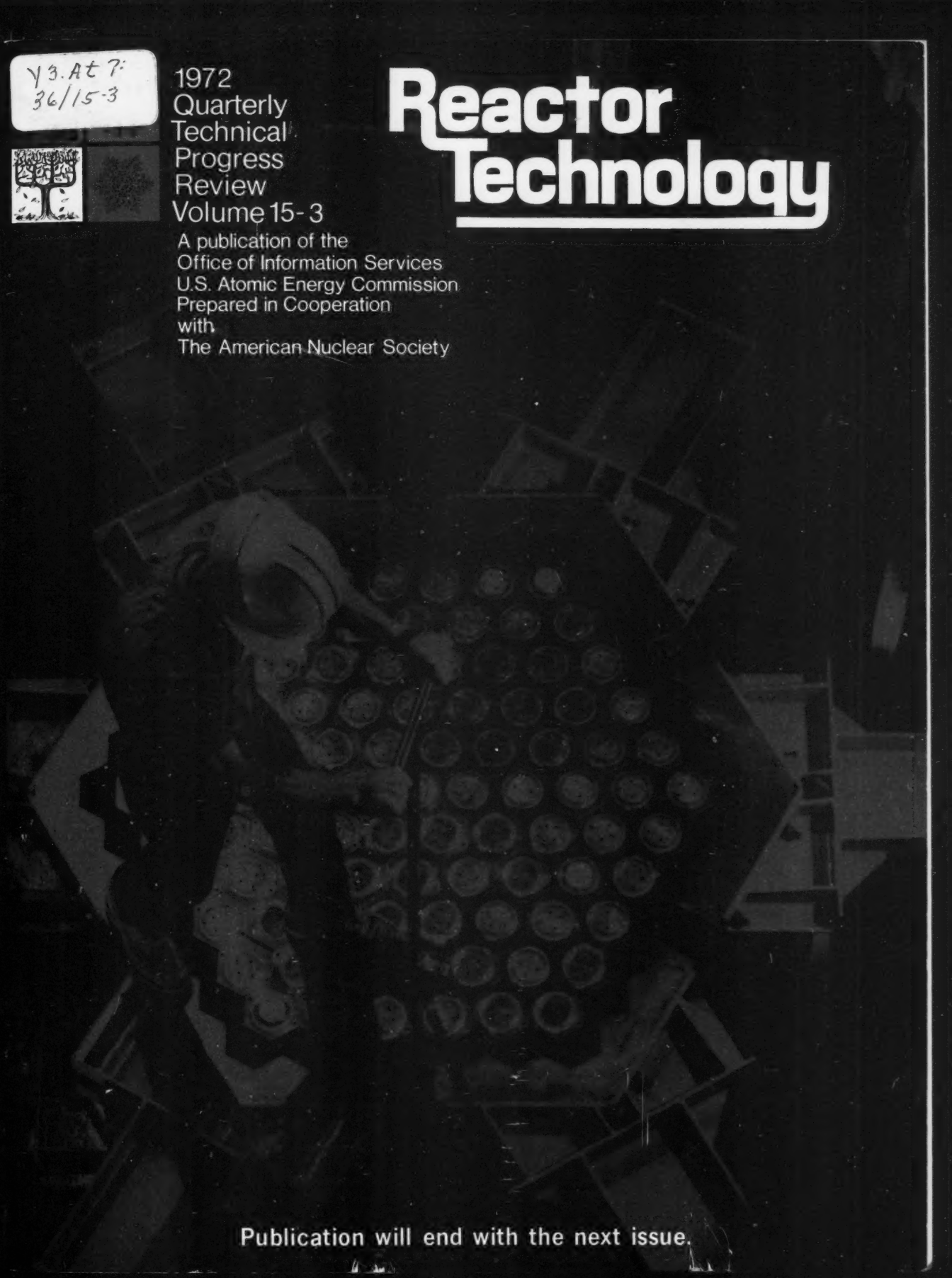

Publication will end with the next issue.

TECHNICAL PROGRESS REVIEW

The United States Atomic Energy Commission publishes *Nuclear Safety* as a bimonthly technical progress review to meet the needs of industry and government for concise summaries of current developments. This journal digests and evaluates the latest findings in its area of nuclear technology and science.

Nuclear Safety is prepared in cooperation with the Nuclear Safety Information Center at Oak Ridge National Laboratory. Editor, Wm. B. Cottrell; managing editor, J. Paul Blakely; advisory editor, W. H. Jordan.

Subscription Information. *Nuclear Safety* may be purchased from the Superintendent of Documents, U. S. Government Printing Office, Washington, D. C. 20402, at $3.50 per year (six issues) or $0.60 per issue.

Postage and Remittance. Postpaid within the United States, Canada, Mexico, and all Central and South American countries except Argentina, Brazil, Guyana, French Guiana, Surinam, and British Honduras. For these Central and South American countries and all other countries: for each annual subscription, add $1.00; for single issues, add one-fourth of the single-issue price. Payment should be by check, money order, or document coupons, and MUST accompany order. Remittances from foreign countries should be made by international money order or draft on an American bank payable to the Superintendent of Documents or by UNESCO book coupons.

Availability of Reports Cited in This Review

United States Atomic Energy Commission (USAEC) reports are available at the libraries listed on the inside front cover of each issue of *Nuclear Science Abstracts*. USAEC reports are also sold by the following governmental and international organizations: (1) National Technical Information Service (NTIS), U. S. Department of Commerce, Springfield, Va. 22151; (2) International Atomic Energy Agency (IAEA), Vienna, Austria; and (3) National Lending Library, Boston Spa, England.

Other U. S. Government agency reports identified in this journal are generally available from NTIS.

Reports from other countries are generally available at the same U. S. libraries as maintain collections of USAEC reports, and from IAEA and the originating country. **United Kingdom Atomic Energy Authority (UKAEA)** reports are sold by Her Majesty's Stationery Office, London. **Atomic Energy of Canada Limited (AECL)** reports are sold by the Scientific Document Distribution Office, Atomic Energy of Canada Limited, Chalk River, Ontario, Canada. UKAEA and AECL reports issued after March 1, 1967, are sold by NTIS to purchasers in the United States and its territories. IAEA publications are sold in the United States by UNIPUB, P. O. Box 433, New York, N. Y. 10016.

Private-organization reports should be requested from the originator.

Reactor Technology

Vol. 15, No. 3 Fall 1972

RETNA$_B$ 15(3) 185-242 (1972)

REVIEW ARTICLE

AMERICAN NUCLEAR SOCIETY—CRITICAL REVIEWS

MISCELLANY

COVER: An engineer at WADCO Corporation, Richland, Wash., rotates one of the mock fuel bundles in the Fast Flux Test Facility's Simulated Core Mockup prior to taking measurements with a laser. A Battelle–Northwest photograph.

(Publication of this journal will end with the next issue, Vol. 15, No. 4.)

Superintendent of Documents, U. S. Government Printing Office, Washington, D. C. 20402, $3.00 per year.

Publication of this journal will cease with Vol. 15, No. 4,
because of a lack of funds.

The General Manager of the U. S. Atomic Energy Commission has determined that the publication of this periodical is necessary in the transaction of the public business required by law of this agency. Use of funds for printing this periodical has been approved by the Director of the Office of Management and Budget through Dec. 31, 1972.

Low-Cycle Fatigue of Reactor Structural Materials

By C. E. Jaske, J. S. Perrin, and H. Mindlin*

Abstract: *Low-cycle fatigue and creep–fatigue are important considerations in evaluation and development of design information for reactor structural materials. Strain-controlled low-cycle fatigue tests of axially loaded specimens of Alloy 800, 304 stainless steel, and 316 stainless steel have been conducted at several laboratories. Fatigue curves for these three alloys have been developed at temperatures from 70 to 1500°F. Hold times at peak strain and slower strain rates have been shown to greatly reduce cyclic-fatigue resistance at temperatures between 1000 and 1400°F. The linear-life-fraction damage rule has been used to evaluate creep–fatigue damage interaction in tension hold-time tests, but it does not provide a proper explanation of the damage mechanisms. These materials exhibited significant cyclic strain hardening at all temperatures studied. The hardening mechanism was influenced by strain rate, number of strain cycles, and prior heat treatment of the alloy. Aging of material at test temperature prior to test had a significant influence on both creep–fatigue resistance and cyclic hardening at temperatures near 1100 to 1200°F but had little effect at temperatures near 1000 to 1050°F.*

During normal operation of a nuclear power plant, the pressure vessel and such related components as piping are subjected to transient loading during startup, shutdown, or variations in the steady-state operation conditions. During these transient conditions, components at elevated temperatures are subjected to nonuniform thermal stresses large enough to exceed the elastic limit and therefore to cause local plastic flow and introduction of residual stresses. The result of this can be damage from both fatigue and creep such that the component may fail in a relatively low number of cycles.

Low-cycle fatigue is normally associated with the presence of cyclic macroscopic plastic strains. For many structural materials that are cyclically loaded under such conditions, fatigue failures occur in relatively short lifetimes of less than 10^5 cycles. The problem of low-cycle fatigue failure has received increasing consideration in recent years. The *ASME Boiler and Pressure Vessel Code, Section III*,[1] of the American Society of Mechanical Engineers (ASME) requires a fatigue analysis of pressure-vessel and related components used in nuclear reactors and provides fatigue design curves for use at temperatures up to 700°F for carbon, low-alloy, and high-tensile steels and at temperatures up to 800°F for austenitic steels, Ni–Cr–Fe alloy, Ni–Fe–Cr alloy, and Ni–Cu alloy. Design rules for use of 304 and 316 stainless steels at temperatures above 800°F are covered[2] in ASME Code Case 1331-5. Rules for use of solution-annealed Alloy 800 are to be added to the next revision of this Code Case.

Before design rules for the above-mentioned materials can be developed, experimental information on their low-cycle fatigue behavior must be obtained. This review will cover the special experimental procedures normally used in low-cycle fatigue testing. In addition, the types of low-cycle fatigue results which have been and are currently being obtained by investigators on three specific materials (Alloy 800, 304 stainless steel, and 316 stainless steel) will be presented and discussed. These materials are all of current interest for nuclear reactor applications.

*The authors are Senior Researcher, Associate Fellow, and Division Chief, respectively, at Battelle Memorial Institute, Columbus Laboratories, Columbus, Ohio 43201.

EXPERIMENTAL PROCEDURES

Low-cycle fatigue testing techniques have evolved relatively recently; a review that contains descriptions of approaches used at a number of laboratories has been published.[3] During low-cycle testing, specimens are normally run under strain control rather than load control. Usually specimens are tested using uniaxial loading, although some work is done by loading the specimen in bending.

The most versatile type of machine for low-cycle fatigue testing is the closed-loop, electrohydraulic, servo-controlled testing system.[4] With such a system, any type of strain–time waveform desired can be programmed. For continuous-cycling tests, strain is usually programmed to follow a fully reversed triangular waveform (Fig. 1) with a constant strain rate, $\dot{\epsilon}$, and a constant total strain range, $\Delta\epsilon_t$. Initial loading is usually compressive (as shown in Fig. 1) because it is more representative of actual service conditions. Time-

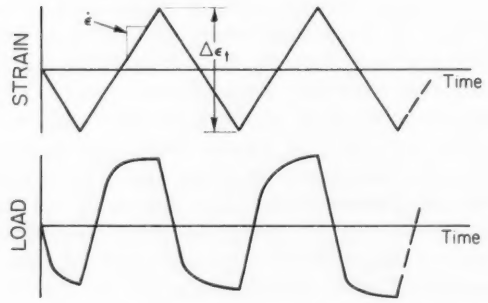

Fig. 1 Schematic of program waveform for fully reversed continuous-cycling fatigue test.

dependent or creep deformation is usually introduced through a hold time, t_h, at peak strain as illustrated in Fig. 2. At elevated temperature and significantly high strain levels, stress relaxation usually takes place during the hold period. Load is applied from a hydraulic actuator to the test specimen, and load is measured using a load cell.

Two common types of specimen configuration (Fig. 3) are used in uniaxial loading tests; both have a circular cross section. The cylindrical type [Fig. 3(*a*)] has a constant cross section and a longitudinal gauge section, whereas the hourglass type [Fig. 3(*b*)] has a minimum diameter at the center of the test section and a diametral gauge length. Other types include hollow, tubular specimens and specimens with a notched gauge section to localize failure.

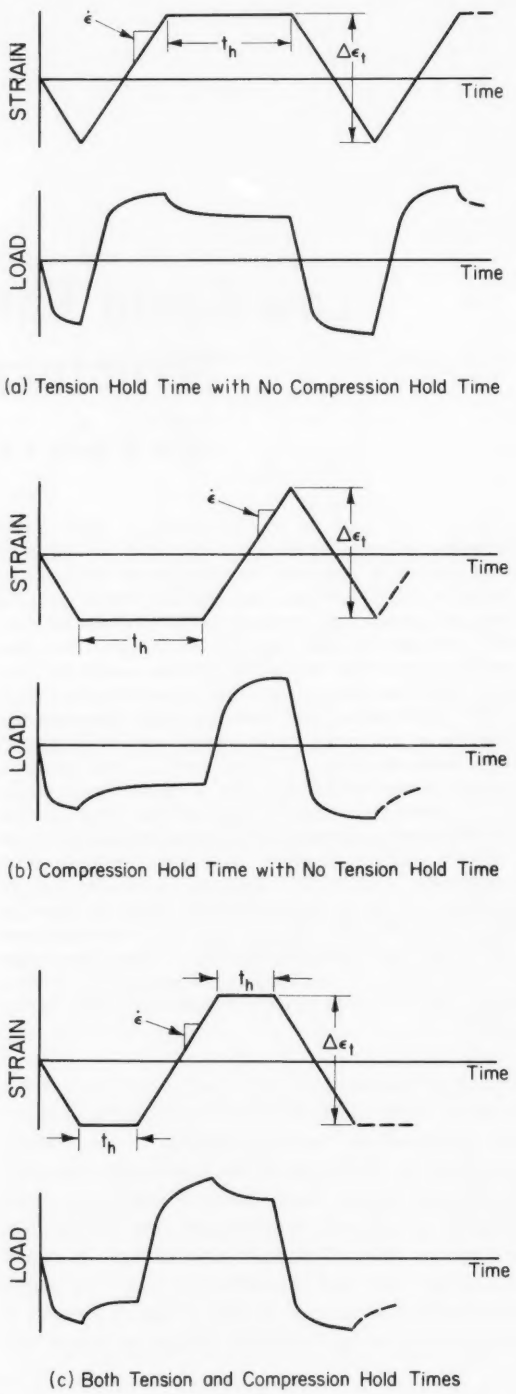

Fig. 2 Schematic of program waveforms for fatigue tests with hold times.

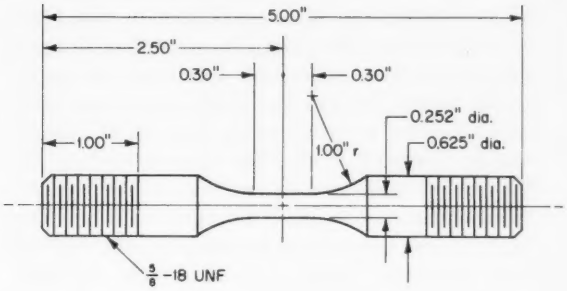

(a) Cylindrical

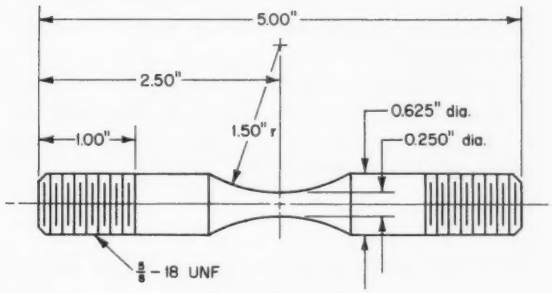

(b) Hourglass Shaped

Fig. 3 Typical configurations of low-cycle fatigue specimens.

Strain can be controlled and measured with either a longitudinal (Fig. 4) or diametral (Fig. 5) extensometer. The longitudinal extensometer is used with a specimen of uniform gauge section and has the advantage of measuring the axial strain directly. However, the extensometer must be mounted carefully so that the specimen surface is not disturbed at the point of attachment. Also, the specimen must be machined with very small diameter variations along the gauge length, and temperature must be uniform along the gauge length. The diametral extensometer has the advantages that temperature has to be controlled over a short length, the extensometer is following the behavior of the specimen right at the location of ultimate failure, and the possibility of buckling failure is minimized. However, to control axial strain with an hourglass-shaped specimen requires that the diametral strain and load be automatically combined and converted to equivalent axial strain during testing.[5]

Heating the specimen to the desired test temperature can be accomplished by such methods as direct resistance heating of the specimen, induction heating, or putting a furnace around the entire specimen. Temperature is normally measured by attaching

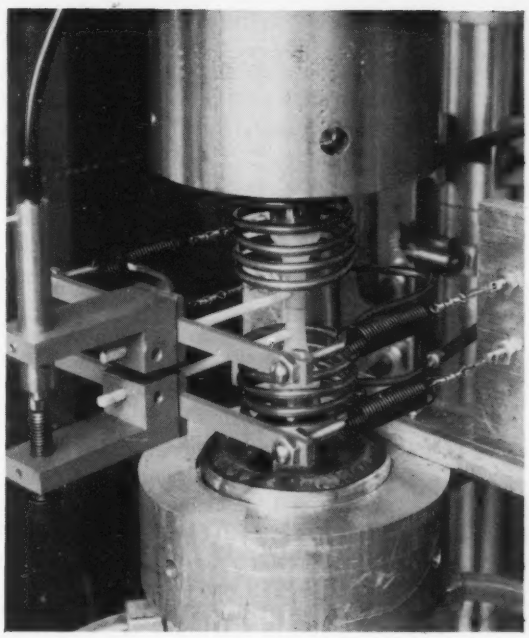

Fig. 4 Apparatus for low-cycle fatigue testing of cylindrical specimens at elevated temperature.

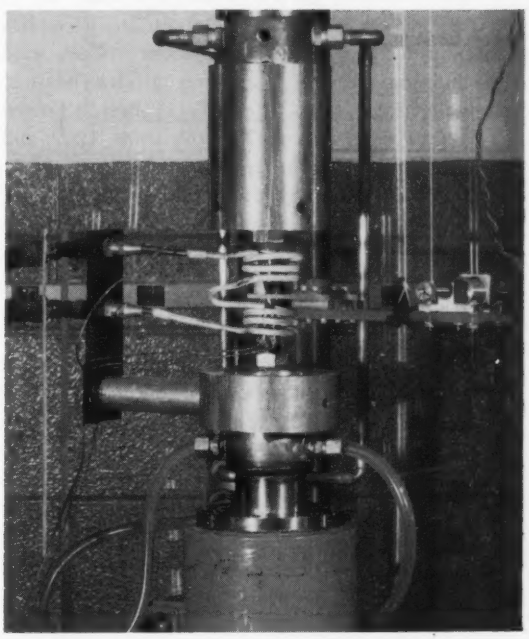

Fig. 5 Apparatus for low-cycle fatigue testing of hourglass-shaped specimens at elevated temperature.

thermocouples directly to the specimen surface. In some cases infrared pyrometry is also used.

MATERIALS

In recent years a number of experimental programs have been conducted under the sponsorship of the U. S. Atomic Energy Commission (USAEC) to evaluate the low-cycle fatigue resistance of structural reactor materials. An extensive investigation of the plastic fatigue properties of 304, 348, and 316 stainless steels was conducted at Nuclear Systems Programs, General Electric Company (GE–NSP), from 1964 to 1969 (Ref. 6). Constant-amplitude, axial-load, strain-controlled tests of all three alloys were conducted[7] at 800, 1200, and 1500°F with strain rates of 4×10^{-3}, 4×10^{-4}, and 4×10^{-5} sec^{-1}. The influence of hold time at peak strain was studied for 304 and 316 stainless steels at 1200°F (Ref. 8). The notched low-cycle fatigue behavior of carbon steel, 2¼ Cr–1 Mo steel, and 304 stainless steel was investigated at room temperature and 550°F in a 4-year program conducted at the Materials and Processes Laboratory of the General Electric Company.[9] In another program conducted at GE–NSP, the constant-amplitude, axial-load, strain-controlled low-cycle fatigue behavior of Alloy 800 was examined at temperatures[10] from 800 to 1400°F. In subsequent work at Battelle's Columbus Laboratories (BCL), low-cycle fatigue studies were conducted on specimens from four different heats of solution-annealed Alloy 800 (Ref. 11). Best-fit fatigue curves were developed at 70, 800, 1000, 1200, and 1400°F (Ref. 11), cyclic-stress–strain data were obtained at the same temperatures,[12] and the influence of hold times at peak strain was examined at 1000, 1200, and 1400°F (Ref. 13).

In current work at BCL,[14–17] low-cycle fatigue design information on 304 and 316 stainless steels is being developed for use at temperatures up to 1200°F. This work includes determination of monotonic- and cyclic-stress–strain response, continuous-cycling fatigue resistance, the effect of aging and hold time on fatigue life, cumulative damage under variable-amplitude loading, and creep–fatigue damage interaction. Developing an understanding of the microstructural phenomena involved in low-cycle fatigue failure of 304 and 316 stainless steels in the 800 to 1200°F temperature regime is the goal of experimental work being performed at Argonne National Laboratory (ANL).[18–27] The type of failure mode has been qualitatively related to creep–fatigue damage interaction, and the importance of material condition (i.e., annealed, stress relieved, or aged) prior to testing has been emphasized. Also, fatigue crack-propagation experiments and computerized simulation of cyclic-loading-behavior studies are being initiated for both materials. Primary effort of a program at Aerojet Nuclear Company (ANC) has been directed to the influence of irradiation on creep–fatigue of 304 and 316 stainless steels and Alloy 800 (Refs. 28–31). Irradiated and unirradiated specimens of both stainless steels have been tested at 1100°F under constant-amplitude, strain-controlled axial loading with and without hold times at peak tensile strain. The effect of irradiation on fatigue and creep–fatigue of these two stainless steels and of Alloy 800 at 1292°F was also examined.

Details of the work summarized above are reported in the following sections for each of the three materials of primary interest: (1) Alloy 800, (2) 304 stainless steel, and (3) 316 stainless steel.

Alloy 800

Curves of total strain range vs. fatigue life are available at a strain rate of 4×10^{-3} sec^{-1} for mill-annealed Alloy 800 at 800, 1000, and 1100°F and for solution-annealed Alloy 800 at 1000, 1200, 1300, and 1400°F (Ref. 10). The fatigue resistance of this material decreased with increasing temperature, and the fatigue resistance of the mill-annealed material was superior to that of the solution-annealed material at temperatures below 1100°F. A few specimens tested at a strain rate of 4×10^{-4} sec^{-1} had slightly lower fatigue strength than comparable ones tested at the faster rate.

Since the solution-annealed material was of primary interest for use at high temperatures, subsequent studies were conducted on the same heat of material used by Conway[10] (specimens from this heat were designated as Group A material) and from three additional heats of Alloy 800 (specimens were designated as belonging to Groups B, C, and D). Groups A and D were from standard heats of Alloy 800, whereas Group B was duplex solution-annealed and Group C had a high carbon content (0.09% C compared to 0.05–0.06% C for the other heats). Best-fit fatigue curves for all the results on solution-annealed material at 4×10^{-3} sec^{-1} are shown in Fig. 6. Values of plastic strain range, $\Delta\epsilon_p$, and elastic strain range, $\Delta\epsilon_e$, were related to fatigue life, N_f, by the following polynomial equation:

$$\log \Delta\epsilon_p \text{ (or } \log \Delta\epsilon_e) = A_1 + A_2 \log N_f + A_3 (\log N_f)^2 \quad (1)$$

where, A_1, A_2, and A_3 are best-fit regression coefficients. (See Table 1.) The value of $\Delta\epsilon_t$ (the total strain range) is simply the sum of $\Delta\epsilon_p$ and $\Delta\epsilon_e$ for any particular value of N_f. For all cases but $\Delta\epsilon_p$ at 800°F, the data fell close to a straight line on the log-log plots and the constant A_3 was deleted. Results for all four heats of material were about the same, and the fatigue results at each temperature were well approximated by a single $\Delta\epsilon_t$ vs. N_f curve.

Brinkman et al.[31] have shown that irradiation of Alloy 800 to fluences of 0.3 to 5.0×10^{22} neutrons/cm^2 ($E > 0.1$ MeV) at 1292 to 1382°F produced a significant reduction in fatigue life at 1292°F. For $\Delta\epsilon_t$ from 0.003 to 0.024, fatigue life was reduced by factors as large as 35. (See Fig. 7.) This severe degradation in fatigue resistance was caused by irradiation-induced embrittlement of the Alloy 800 and was correlated with corresponding changes in tensile

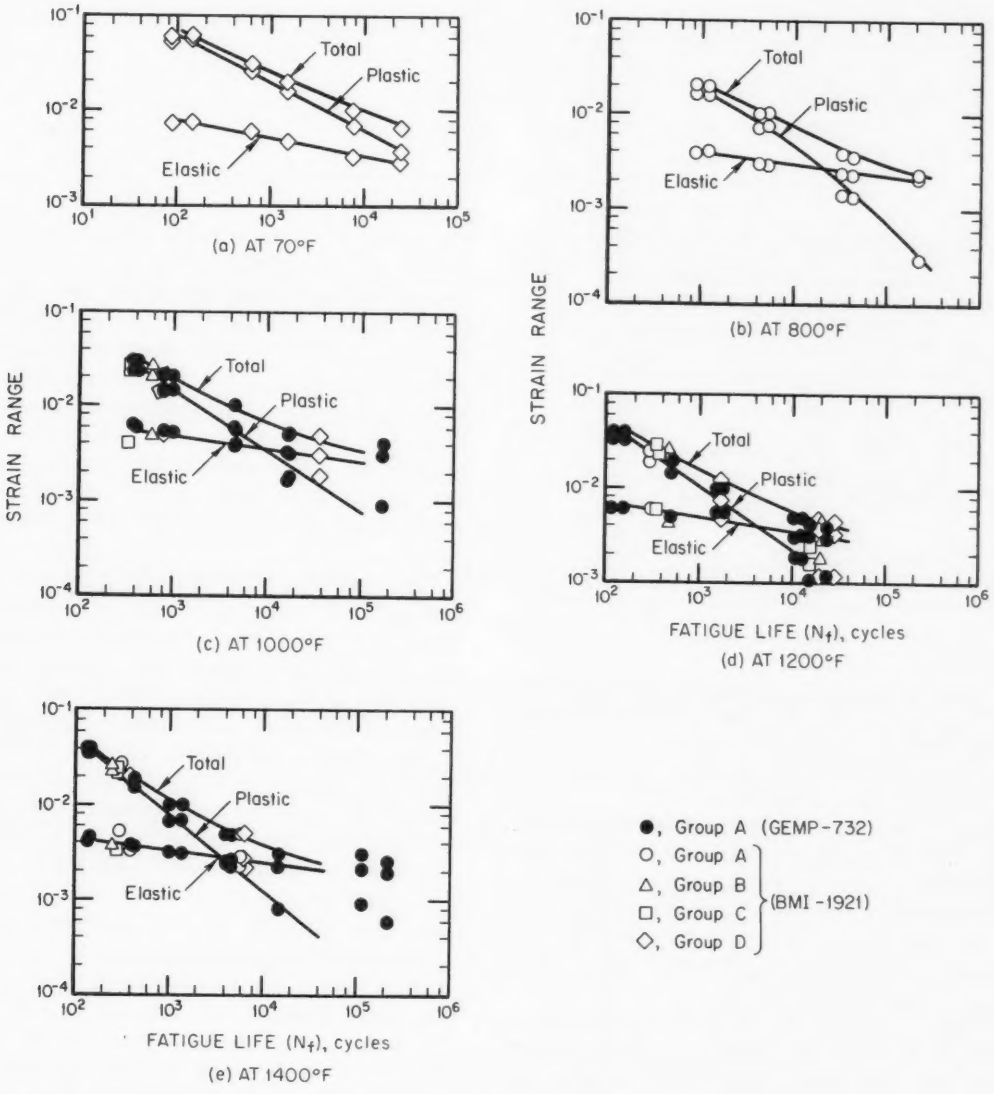

Fig. 6 Fatigue curves for solution-annealed Alloy 800 at a strain rate of 4×10^{-3} sec^{-1}. (From Conway[10] and Jaske et al.[11])

Table 1 Summary of Best-Fit Regression Coefficients for Solution-Annealed Alloy 800 Fatigue Curves

Temp., °F	Type of strain range	Best-fit value for indicated constant			References from which data were taken
		A_1	A_2	A_3	
70	$\Delta\epsilon_p$	−0.225	−0.499		11
	$\Delta\epsilon_e$	−1.76	−0.177		
800	$\Delta\epsilon_p$	−1.54	0.294	−0.124	11
	$\Delta\epsilon_e$	−2.06	−0.120		
1000	$\Delta\epsilon_p$	−0.0143	−0.621		10, 11
	$\Delta\epsilon_e$	−1.93	−0.128		
1200	$\Delta\epsilon_p$	−0.0421	−0.657		10, 11
	$\Delta\epsilon_e$	−1.89	−0.0148		
1400	$\Delta\epsilon_p$	0.264	−0.793		10, 11
	$\Delta\epsilon_e$	−2.11	−0.127		

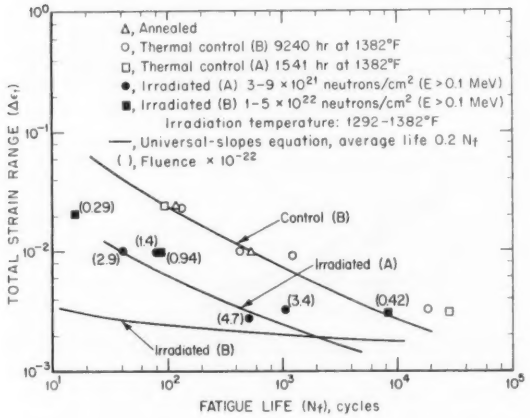

Fig. 7 Effect of irradiation on the fatigue life of Alloy 800 at 1292°F and at a strain rate of 8 × 10^{-4} sec^{-1}. (From Brinkman et al.[31])

properties using the modified method of universal slopes.[32,33] As shown in Fig. 7, the modified universal-slopes equation provided a good prediction of the fatigue life of the unirradiated control specimens and the specimens irradiated to low fluences. For specimens irradiated to high fluences, it gave a conservative prediction.

Tension hold times [Fig. 2(*a*)] detrimentally affect the fatigue life of solution-annealed Alloy 800, whereas compression [Fig. 2(*b*)] or combined tension and compression holds [Fig. 2(*c*)] have only a small effect or no significant effect on fatigue life.[13] Results of tests at constant lengths of tensile hold time can be summarized as shown in Fig. 8. At each temperature the $\Delta\epsilon_t$ vs. N_f relation can be approximated by a straight line for a given length of hold time, and these straight lines all intercept the one-cycle-to-failure line at the point which is a linear extrapolation of the no-hold-time fatigue curve. These results imply that tensile hold times have a more detrimental influence on fatigue as their length increases and that the detrimental effect is more pronounced at low strain ranges than at high strain ranges. Values of the slopes and intercepts of the curves in Fig. 8 are summarized in Table 2.

The hold-time results discussed above were all for material from Group A. Results of a few tension hold-time tests conducted on specimens from Groups B and C showed more heat-to-heat variation than for continuous cycling. Duplex solution-annealed material (Group B) had slightly inferior creep–fatigue resistance to the standard material at 1000 and 1200°F and about the same at 1400°F. High-carbon-content material (Group C) had markedly better creep–fatigue resistance than the standard material at 1000 and 1200°F but was slightly worse at 1400°F.

In recent work at BCL,[17] 10-min tension hold-time tests were conducted on both as-received and aged (150 hr at 1200°F and 1000 hr at 1200°F) specimens from the Group D material. Tests were conducted at total strain ranges of 0.02 and 0.01 at 1200°F, and results were compared with previous data on Group A material.[13] As shown in Fig. 8(*b*) (compare open, partially filled, and completely filled diamond symbols), greater hold-time fatigue resistance was observed for the aged material than for the as-received

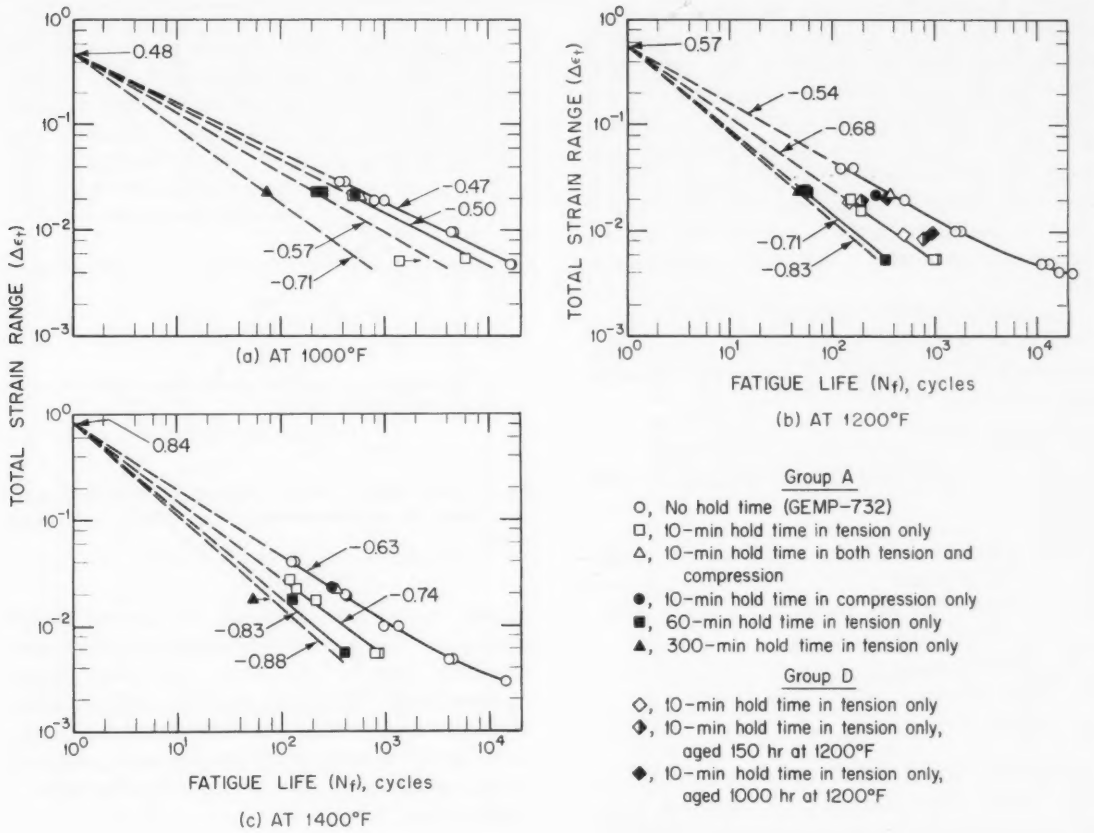

Fig. 8 Effect of hold time on fatigue life of solution-annealed Alloy 800 at a strain rate of 4×10^{-3} sec^{-1}. (From Conway[10] and Jaske et al.[13])

Table 2 Slope and Intercept Values That Define Tension Hold-Time Fatigue Curves for Solution-Annealed Alloy 800

Temp., °F	Intercept at $N_f = 1$	Length of tension hold time, min	Slope of $\Delta\epsilon_t$ vs. N_f curve	References from which data were taken
1000	0.48	0	−0.47	10
		10	−0.50	13
		60	−0.57	13
		300	−0.71	13
1200	0.57	0	−0.54	10
		10	−0.68	13
		60	−0.79	13
		300	−0.83	13
1400	0.84	0	−0.63	10
		10	−0.74	13
		60	−0.83	13
		300	−0.88	13

material. As-received specimens had about the same hold-time fatigue lives as expected for the previously studied heat. However, specimens that were aged 150 hr had about 1½ times as much fatigue life, and those which were aged 1000 hr had over 2¼ times as much life. It was also noted that increased hold-time fatigue life was accompanied by decreased cyclically stable stress range. Thus the aged material was subjected to less time-dependent damage than the as-received material because it had lower stabilized stress values.

Examination of the cyclically stable relaxation curves from the tension hold-time tests showed that they could be represented by using the following relation of Gittus:[34]

$$\ln(\sigma_0/\sigma) = \frac{A}{1+m^t}1 + m \qquad (2)$$

where σ_0 = initial stress, ksi, at the beginning of the hold period
σ = instantaneous stress, ksi, at some point during the hold period
t = time, min
A = a constant
m = a constant

Using Eq. 2 to define stable stress-relaxation curves, creep–fatigue damage interaction was computed using a linear damage rule of the form suggested by ASME Code Case 1331-5 (Ref. 2). Total damage, D, was defined as

$$D = \Sigma n/N_f + \Sigma \Delta t/t_r \qquad (3)$$

where n = number of cycles applied at a particular load condition
N_f = number of cycles to failure for continuous cycling at the same load condition
Δ_t = increment of time that creep stress is at a given level
t_r = stress-rupture life, hr, at the above-mentioned level of creep stress

Results of creep–fatigue damage calculations that were made for Alloy 800 are presented in Fig. 9. Considerable scatter in the results is related to large variations in the values of the creep damage term ($\Sigma \Delta t/t_r$) because t_r is very sensitive to the level of stress at these temperatures. Thus small errors in measurement of stress and normal scatter in rupture life will inherently cause large variations in creep

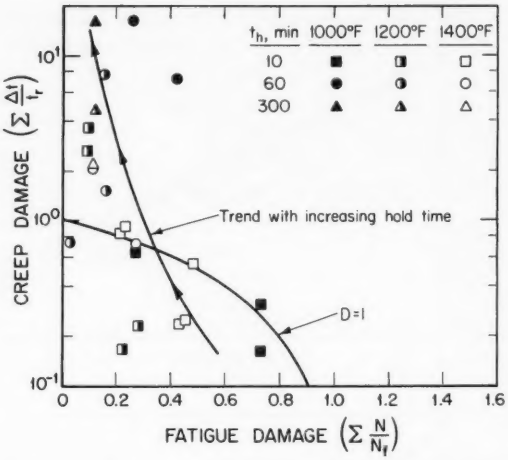

Fig. 9 Creep–fatigue damage interaction for tension hold-time tests of solution-annealed Alloy 800. (From Jaske et al.[11])

damage summations. However, the general overall trend of the damage results was significant. Data were reasonably close to the $D = 1$ curve when fatigue damage ($\Sigma n/N_f$) was greater than 0.5. At lower values of fatigue damage than 0.5, the results were significantly greater than $D = 1$. The damage values tended to increase as the length of tension hold time increased as shown in Fig. 10.

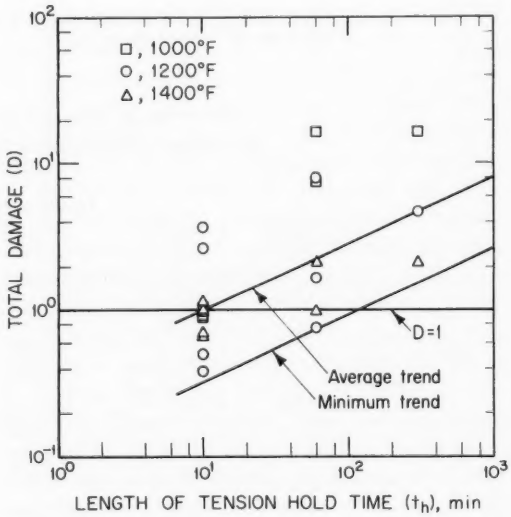

Fig. 10 Effect of length of tension hold time on total damage for solution-annealed Alloy 800. (From Jaske et al.[11])

Incremental step tests have been used to obtain comparative monotonic and cyclic-stress–strain curves[12] for solution-annealed Alloy 800. (See Fig. 11.) Results from the step tests provide a fairly good correlation with those from constant-amplitude tests. (Compare solid curves with plotted symbols in Fig. 11.) At strain amplitudes lower than the maximum used in the step test, there is some deviation in results between the two methods of defining stable stress–strain behavior. This deviation indicates that prior history has an influence on such behavior; thus, in the variable-amplitude step test, the alloy has a "memory" for high-level strain cycles that influence subsequent strain cycles at low strain levels. Since the cyclic-

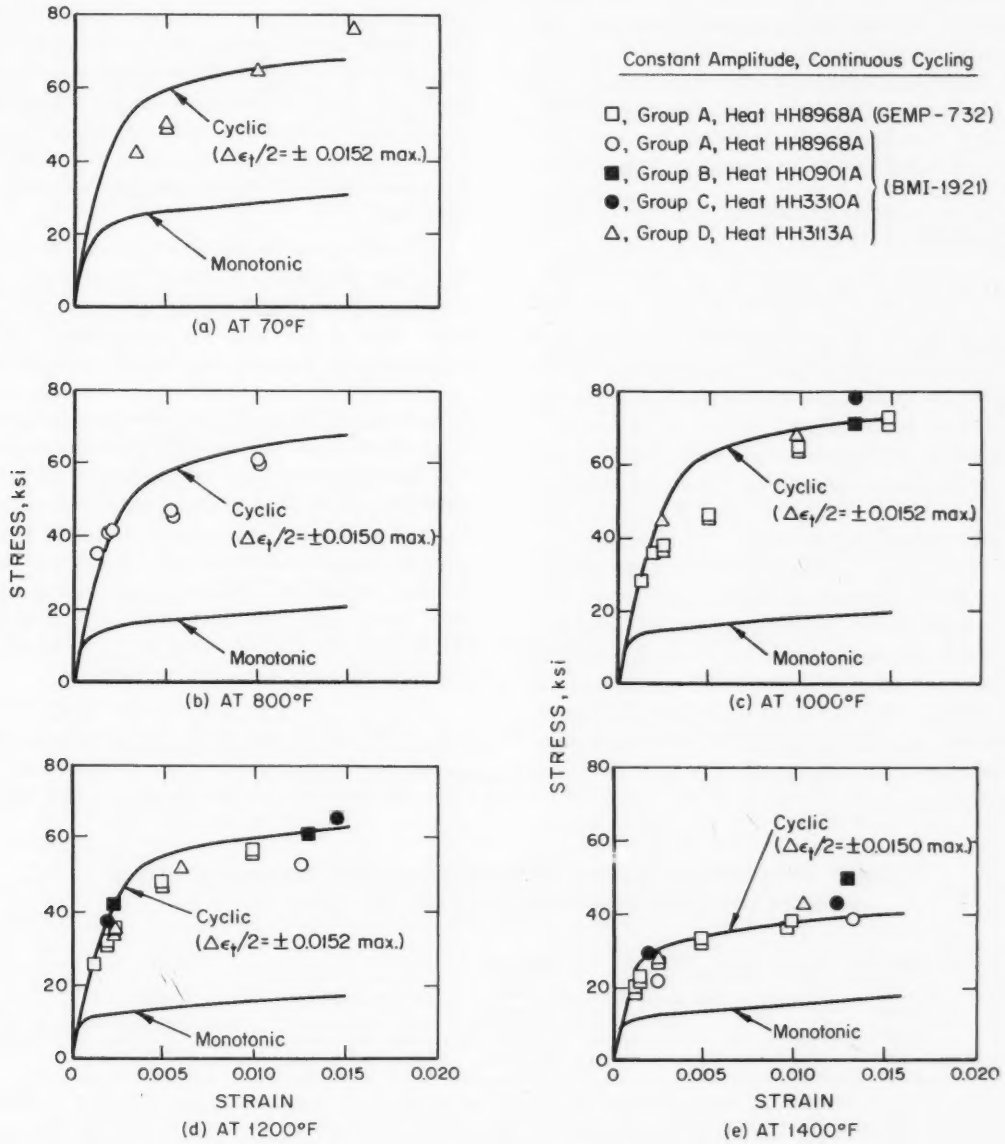

Fig. 11 Comparison of monotonic- and cyclic-stress–strain curves for solution-annealed Alloy 800 at a strain rate of 4×10^{-3} sec^{-1}. (From Jaske et al.[11,12])

stress–strain curves fell significantly above the monotonic ones, a large amount of cyclic hardening occurred. Comparing the cyclic with the monotonic yield strength (Table 3) shows that the alloy cyclically hardened by factors from 2.3 to 4.4 with a maximum amount of hardening at 1200°F.

The cyclic-stress–strain curves in Fig. 11 were approximated by the following function:

$$\Delta\sigma/2 = K'(\Delta\epsilon_p/2)^{n'} \quad (4)$$

where $\Delta\sigma/2$ = cyclically stable stress amplitude, ksi
$\Delta\epsilon_p/2$ = cyclically stable plastic-strain amplitude
K' = cyclic-strength coefficient, ksi
n' = cyclic-strain-hardening exponent

Knowing the modulus of elasticity, E, values of $\Delta\epsilon_p/2$ were defined by the relation

$$\Delta\epsilon_p/2 = \Delta\epsilon_t/2 - \Delta\sigma/2E \quad (5)$$

Analogous equations were used for the monotonic-stress–strain curves, and both monotonic- and cyclic-strength coefficients and strain-hardening exponents are summarized in Table 3.

Data from constant-amplitude tests[31] of Alloy 800 showed that irradiation had no significant effect on cyclic-stress–strain behavior at 1292°F. (See Fig. 12.) The small increase in yield strength (20 to 23 ksi) from the monotonic to the cyclic case indicated only a small amount of cyclic hardening for this heat of material. The main differences between this material and that used in the other studies[12] are that the carbon content was 0.03% instead of 0.05 to 0.06% and that the final anneal was at 1904°F instead of at 2100°F. Further studies are necessary to determine why this heat of material has relatively stable cyclic-stress–strain response.

304 Stainless Steel

The problem of predicting low-cycle fatigue life at a geometrical notch has been studied by Krempl.[9] Circumferentially notched, cylindrical specimens and edge-notched flat plate specimens of 304 stainless steel were tested at room temperature and 550°F under fully reversed and zero-to-tension uniaxial loading conditions. Completely reversed bending tests of notched specimens were also performed at room temperature. In these tests, values of theoretical stress concentration factor, K_t, ranged from 1.9 to 3.3. In all these tests, creep deformation was considered to be insignificant. Both the number of cycles to crack initiation (considered to be a crack 0.005 to 0.015 in. long) and to total failure of the specimen were determined.

In the range of fatigue lives between 10^2 and 10^5 cycles, no shakedown to elastic action at the notch root was observed, and for the cylindrical specimens about 70% of the total life was involved in crack propagation.[35] Knowing the applied nominal elastic stress amplitude and mean stress, the value of K_t, fatigue resistance of unnotched material, and the cyclic-stress–strain behavior of the material, a method was developed to predict fatigue life of the notched specimens that had been tested under load-controlled conditions. The method provided conservative predictions that may be of design use but did not provide accurate predictions. Additional experimental work at both room and elevated temperatures is required before a more accurate understanding of notched low-cycle fatigue behavior can be developed.

Studies at GE–NSP,[6-8] at BCL,[14-17] at ANL,[18-27] and at ANC[28-31] have all been conducted on material from one heat (No. 55697) of annealed (1 hr at 1950°F) 304 stainless steel; ANL has also

Table 3 Comparison of Monotonic- and Cyclic-Stress–Strain Properties of Solution-Annealed Alloy 800 at a Strain Rate of 4×10^{-3} sec^{-1} (From Jaske et al.[12])

Max. total strain range, %	Temp., °F	0.2% offset tensile yield strength, ksi		Ratio of cyclic to monotonic yield strength	Strength coefficient, ksi		Strain-hardening exponent	
		Monotonic	Cyclic		Monotonic	Cyclic	Monotonic	Cyclic
3.0	70	24.9	56.6	2.27	59.2	106	0.148	0.099
3.0	800	15.9	55.5	3.49	41.2	118	0.156	0.120
3.0	1000	15.0	61.3	4.08	30.1	115	0.113	0.098
3.0	1200	12.2	53.5	4.38	27.9	92.1	0.123	0.087
3.0	1400	12.5	32.5	2.60	28.8	62.1	0.100	0.101

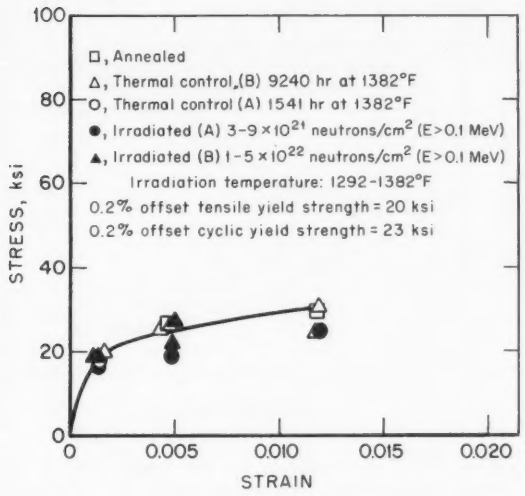

Fig. 12 Effect of irradiation on cyclic-stress–strain behavior of Alloy 800 at 1292°F and at a strain rate of 8×10^{-4} sec^{-1}. (From Brinkman et al.[31])

conducted a few tests at 1100°F on specimens from a similar heat (No. 9T2796) of this alloy.[26] In the work at GE–NSP, specimens were machined to final configuration and then reannealed (½ hr at 1998°F).[6] Specimens at BCL were tested in the as-received annealed condition.[14-17] Material tested at ANL was in the same annealed condition used by GE–NSP as well as in a stress-relieved condition (¼ hr at 1400°F) and in an aged condition (159 and 1000 hr at test temperature prior to testing).[25-27] At ANC, material has been tested in an annealed (½ hr at 1967°F) condition, in several aged conditions, and in irradiated conditions.[28-31]

Combining results from all four laboratories, fatigue curves can be defined for 304 stainless steel at 70, 800, 1000, 1200, and 1500°F and at a strain rate of 4×10^{-3} sec^{-1}. There is a general trend of decreased fatigue resistance with increased temperature. However, for the annealed material, there is only a slight difference in fatigue strength between 1000 and 1200°F (Ref. 14). Work at ANL[25] showed that aged material (1000 hr at 1050°F) and stress-relieved material tested at 1050°F had significantly better fatigue strength than annealed material tested at 1050°F. However, at 1200°F all three conditions had essentially the same fatigue resistance. This effect of heat treatment was related to precipitation of $M_{23}C_6$ carbides. Higher elevated-temperature fatigue resistance was related to more advanced carbide precipitation. Thus, for longer testing times and higher temperatures, the influence of initial heat treatment is expected to have a small effect on fatigue life because precipitation will have time to stabilize relatively early in the test.

Equation 1 was again used to define best-fit fatigue curves as summarized in Table 4. Data on solution-

Table 4 Summary of Best-Fit Regression Coefficients for 304 Stainless-Steel Fatigue Curves

Temp., °F	Material condition	Type of strain range	Best-fit value for indicated constant A_1	Best-fit value for indicated constant A_2	References from which data were taken
70	Annealed	$\Delta\epsilon_p$	−0.608	−0.403	16
		$\Delta\epsilon_e$	−1.13	−0.303	
800	Stress relieved	$\Delta\epsilon_p$	−0.422	−0.451	7
		$\Delta\epsilon_e$	−1.18	−0.191	
1000	Annealed	$\Delta\epsilon_p$	−0.0429	−0.610	14
		$\Delta\epsilon_e$	−1.02	−0.208	
1100	Annealed	$\Delta\epsilon_p$	−0.620	−0.467	25
		$\Delta\epsilon_e$	−1.18	−0.176	
1100	Aged 1000 hr at 1100°F	$\Delta\epsilon_p$	−0.541	−0.441	25
		$\Delta\epsilon_e$	−1.86	−0.177	
1200	Annealed and stress relieved	$\Delta\epsilon_p$	+0.113	−0.681	7, 14
		$\Delta\epsilon_e$	−1.88	−0.188	

annealed material at 1100°F are for both heats that were tested by ANL, and data for aged material are for the second heat (No. 9T2796).[25] Berling and Slot[7] have shown that decreasing the strain rate from 4×10^{-3} sec^{-1} to 4×10^{-4} and 4×10^{-5} sec^{-1} caused a corresponding reduction in cyclic-fatigue life at both 1202 and 1501°F. (See Fig. 13.)

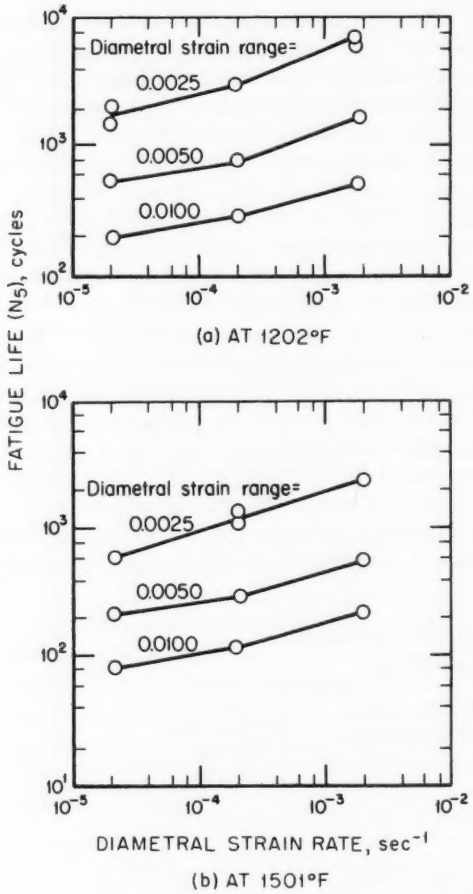

Fig. 13 Effect of strain rate on fatigue life of 304 stainless steel at 1202 and 1501°F. (From Berling and Slot.[7])

Irradiation of 304 stainless steel to fluences between 1.5 and 3.0×10^{22} neutrons/cm^2 ($E > 0.1$ MeV) at 1292 to 1382°F caused about a factor of 2 reduction in fatigue life[31] at 1292°F. (See Fig. 14.) The modified universal-slopes equation[32,33] predicted a similar reduction in fatigue life based upon changes in

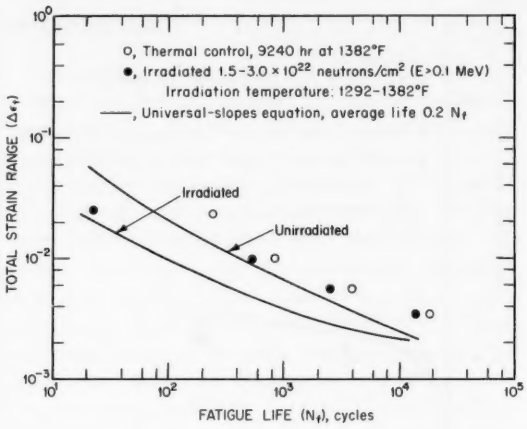

Fig. 14 Effect of irradiation on the fatigue life of 304 stainless steel at 1292°F and at a strain rate of 8×10^{-4} sec^{-1}. (From Brinkman et al.[31])

irradiated tensile properties and gave a conservative prediction of actual fatigue life.

At both 1000 and 1200°F, tension hold times caused a significant reduction in fatigue life compared to results for continuous cycling. At 1200°F, compression and combined tension–compression hold times did not significantly affect cyclic-fatigue life. Results at 1200°F were for annealed specimens tested at GE–NSP,[8] and those at 1000°F were for annealed specimens tested at BCL.[36] As was true in the case of Alloy 800, the tension hold-time data can be represented by a series of curves for each constant length of hold time. (Refer to Fig. 15 and Table 5). For hold times up to 5 hr at 1000°F, cyclic-fatigue resistance was reduced as length of hold time increased [Fig. 15(*a*)]; for hold times up to ½ hr, the same was true at 1200°F [Fig. 15(*b*)]. However, at 1200°F there was a saturation in the hold-time effect for hold times from ½ to 10 hr, where there was little difference in fatigue life as length of hold time increased. This saturation is probably related to the enhanced carbide precipitation at the grain boundaries discussed earlier.

For this alloy, Eq. 2 was also found to describe cyclically stable relaxation behavior both at 1000°F (Ref. 36) and at 1200°F (Ref. 37). Equation 3 was used to calculate creep–fatigue damage at 1000°F (Ref. 36) and at 1200°F (Ref. 38), and the results are summarized in Fig. 16. The damage values fall near or well below the $D = 1$ curve, and the trend of values is different for different strain ranges. (No such trend was noted for Alloy 800.) Fatigue damage tended to

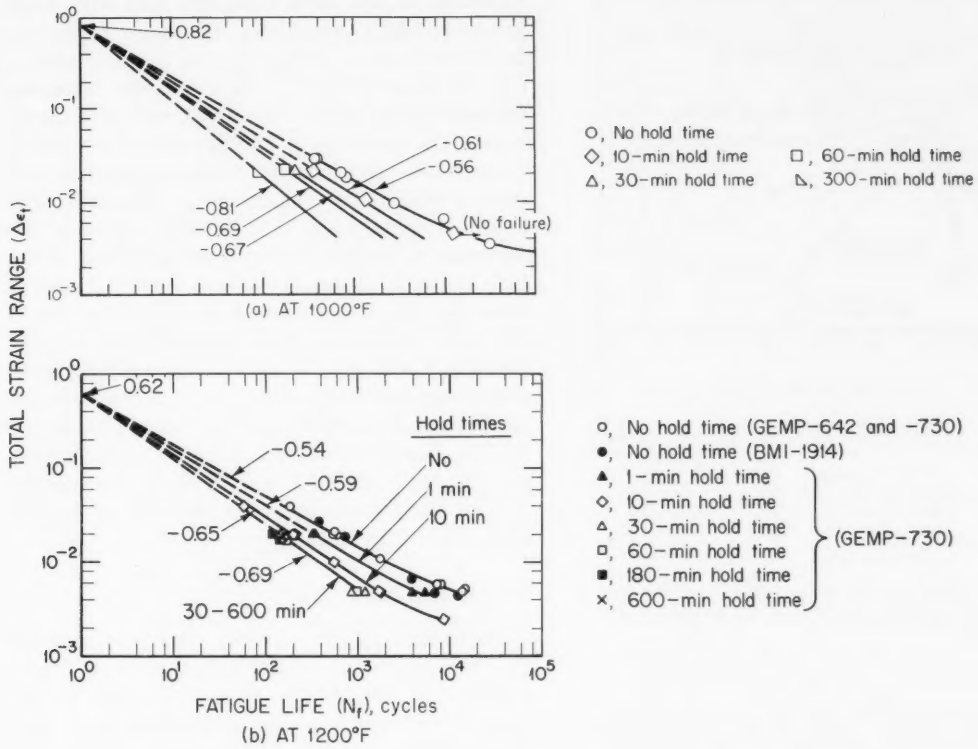

Fig. 15 Effect of hold time on fatigue life of 304 stainless steel at a strain rate of 4×10^{-3} sec^{-1}. (From Conway[8] and Jaske et al.[36])

Table 5 Slope and Intercept Values That Define Tension Hold-Time Fatigue Curves for Annealed 304 Stainless Steel

Temp., °F	Intercept at $N_f = 1$	Length of tension hold time, min	Slope of $\Delta\epsilon_t$ vs. N_f curve	References from which data were taken
1000	0.83	0	−0.56	14
		10	−0.61	36
		30	−0.67	36
		60	−0.69	36
		300	−0.81	36
1200	0.62	0	−0.54	7, 14, 37
		1	−0.59	8, 37
		10	−0.65	8, 37
		30 to 60	−0.69	8,37

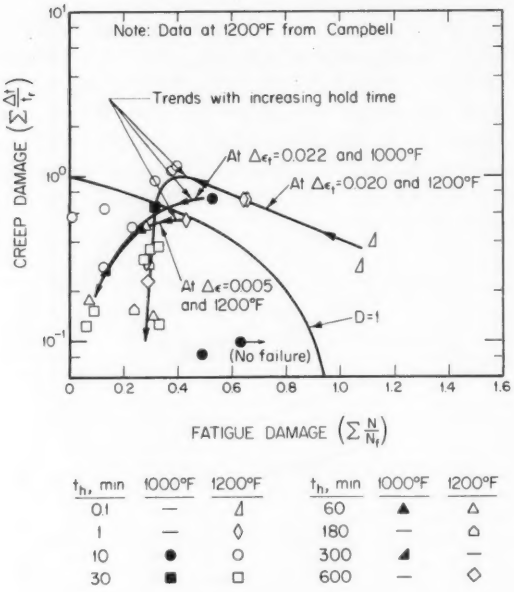

t_h, min	1000°F	1200°F	t_h, min	1000°F	1200°F
0.1	—	Δ	60	▲	△
1	—	◊	180	—	⌂
10	●	○	300	◢	—
30	■	□	600	—	◇

Fig. 16 Creep–fatigue damage interaction for tension hold-time tests of annealed 304 stainless steel. (From Jaske et al.[36] and Campbell.[38])

decrease toward a limit as the length of hold time increased, whereas the creep damage tended to first increase slightly and then decrease rapidly. Total-damage values decreased as a function of hold time as illustrated in Fig. 17. Type 304 stainless steel was irradiated to fluences of 1.65 to 5.02 x 10^{21} neutrons/cm^2 ($E > 0.1$ MeV) at 842°F and tested with tensile hold times at $\Delta\epsilon_t = 0.01$ and at 1100°F (Ref. 30). Compared with control specimens that were aged at 752°F for 8760 hr and at 770°F for 3096 hr, irradiation reduced the tension hold-time fatigue life by a factor of approximately 4. Total damage, as calculated by Eq. 3, was between 1 and 3 for the control specimens with tensile hold times from 0.01 to 1.0 hr. However, the total damage was between 0.17 and 0.72 for irradiated specimens with hold times from 0.1 to 5.0 hr.

Incremental step tests were used to develop the monotonic- and cyclic-stress–strain curves shown in Fig. 18 (Refs. 12 and 15). At high strain amplitudes, results of the incremental step tests correlate fairly well with the constant-amplitude data points. However, at low strain amplitudes, the step-test curves reflect the fact that the material was previously hardened at a higher level and is thus harder than observed in constant-amplitude data. This same "memory" behavior of the material was shown by less cyclic hardening for specimens from step tests with lower maximum strain amplitudes. (Compare curves for $\Delta\epsilon_t/2 = 0.015$ max. to those for $\Delta\epsilon_t/2 = 0.005$ max. in Figs. 18(*c*) and (*d*).) It was also shown that decreasing the strain rate from 4 x 10^{-3} to 4 x 10^{-5} sec^{-1} caused more cyclic hardening at 1000°F and less at 1200°F. These results imply that the hardening mechanism is time dependent as well as cycle dependent. The time-dependent hardening is probably related to the formation of carbides discussed earlier. Values of the ratio of cyclic to monotonic yield strength (Table 6) show that this alloy hardened by factors from 1.9 to 3.0, with maximum cyclic hardening at 1000°F. Equation 4 was again found to well represent both monotonic- and cyclic-stress–strain curves, and the appropriate constants are listed in Table 6. Irradiation of 304 stainless steel to 3.5 x 10^{21} neutrons/cm^2 ($E > 0.1$ MeV) at 842°F was shown to only slightly increase the amount of cyclic hardening at 1100°F (Ref. 30).

316 Stainless Steel

Material from one heat (No. 65608) of annealed 316 stainless steel has been used in low-cycle fatigue programs at GE–NSP,[6] BCL,[15-17] ANL,[25] and ANC.[28-31] Specimens used at GE–NSP were reannealed (½ hr at 1958°F) and then stress relieved (1 hr

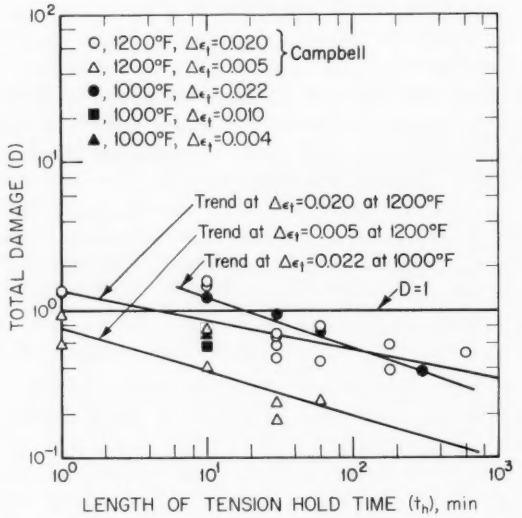

Fig. 17 Effect of length of tension hold time on total damage of annealed 304 stainless steel. (From Jaske et al.[36] and Campbell.[38])

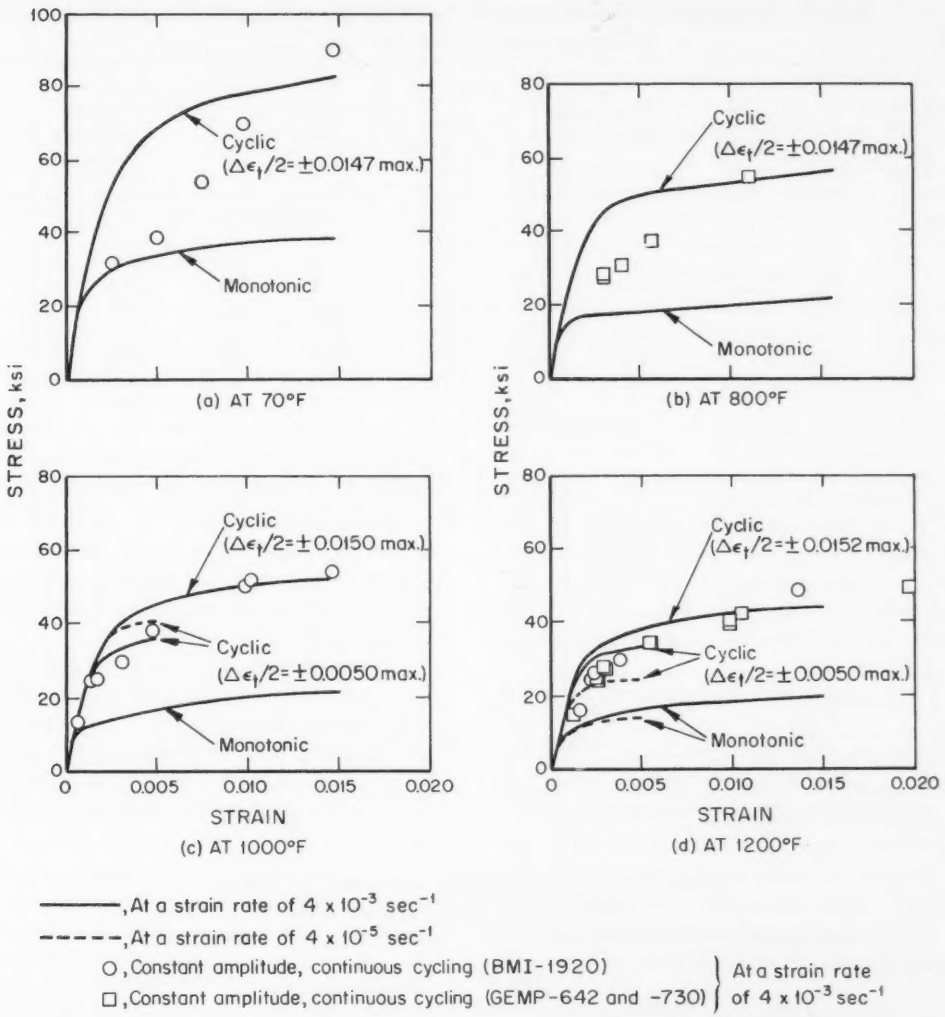

Fig. 18 Comparison of monotonic- and cyclic-stress–strain curves for annealed 304 stainless steel. (From Jaske et al.[12,15])

at 1400°F) after final machining.[6] This same treatment was used for some of the specimens tested at 1050°F by ANL.[23,25] ANL has also used specimens in the annealed condition at both 1050 and 1202°F and specimens that were aged (1000 hr at 1050°F) in tests at 1050°F (Ref. 25). All specimens tested at BCL were either in the annealed condition or were aged for 1000 hr at either 1050 or 1200°F prior to testing.[15-17] Annealed, aged, and irradiated materials have been used in the experimental work at ANC.[28-31]

For constant-amplitude, continuous cycling of 316 stainless steel, fatigue curves are available at 70, 800, 900, 1050, 1200, and 1500°F. With increasing temperature, there is a general trend of decreasing low-cycle fatigue resistance. At both 1050 and 1200°F, there was no significant difference in fatigue strength between stress-relieved specimens tested at ANL[23] and annealed specimens tested at BCL.[16] Material that was aged at test temperature for 1000 hr before testing at 1050 and 1200°F had slightly better fatigue strength than the other two heat-treatment conditions at strain ranges above 0.005 (Refs. 16 and 17). At strain ranges below 0.005, the aging had no significant effect on fatigue life. Results of tests at 1100°F showed a similar

Table 6 Comparison of Monotonic- and Cyclic-Stress–Strain Properties for Annealed 304 Stainless Steel (From Jaske et al.[12])

Max. total strain range, %	Temp., °F	Strain rate, sec^{-1}	0.2% offset tensile yield strength, ksi		Ratio of cyclic to monotonic yield strength	Strength coefficient, ksi		Strain-hardening exponent	
			Monotonic	Cyclic		Monotonic	Cyclic	Monotonic	Cyclic
3.0	70	4×10^{-3}	31.4	66.3	2.11	77.3	177	0.152	0.163
3.0	800	4×10^{-3}	17.5	48.3	2.76	37.7	98.9	0.126	0.116
3.0	1000	4×10^{-3}	14.6	43.5	2.98	43.6	80.6	0.164	0.097
1.0	1000	4×10^{-3}	14.6	34.3	2.35	86.7	82.6	0.293	0.143
1.0	1000	4×10^{-5}	14.6	40.0	2.74	87.0	98.2	0.288	0.141
3.0	1200	4×10^{-3}	14.2	36.6	2.58	41.8	65.2	0.172	0.101
1.0	1200	4×10^{-3}	14.2	32.4	2.28	81.8	68.4	0.182	0.120
1.0	1200	4×10^{-5}	13.2	24.6	1.86	40.4	44.8	0.183	0.155

influence of aging (either 3096 hr at 1112°F or 8760 hr at 1382°F on low-cycle fatigue resistance of 316 stainless steel.[30] The effect of strain rate has been reported by Berling and Slot[7] and is similar to that discussed earlier for 304 stainless steel. Best-fit fatigue curves were defined using Eq. 1, and the results are listed in Table 7.

When 316 stainless steel was irradiated to fluences between 1.3 and 2.4×10^{22} neutrons/cm^2 ($E > 0.1$ MeV) at 1292 to 1382°F, fatigue life at 1292°F was reduced by a factor of approximately 2, which was similar to comparable data for 304 stainless steel.[31] (See Fig. 19.) Just as for the 304 alloy, the modified universal-slopes equation[32,33] predicted a similar amount of reduction in fatigue life because of the difference between tensile properties of the irradiated and unirradiated material, and the prediction of actual fatigue life was conservative.

As was true for both Alloy 800 and 304 stainless steel, experimental work has shown that tension hold times detrimentally affect the cyclic-fatigue life of 316 stainless steel[6,16,17,30] at temperatures from 1050 to 1200°F. In the same temperature range, limited tests at $\Delta\epsilon_t = 0.02$ have shown that compression and combined

Table 7 Summary of Best-Fit Regression Coefficients for 316 Stainless-Steel Fatigue Curves

Temp., °F	Material condition	Type of strain range	Best-Fit value of indicated constant		References from which data were taken
			A_1	A_2	
70	Annealed	$\Delta\epsilon_p$	−0.176	−0.499	17
		$\Delta\epsilon_e$	−1.75	−0.179	
800	Annealed	$\Delta\epsilon_p$	−0.374	−0.484	7, 17
		$\Delta\epsilon_e$	−1.62	−0.219	
900	Annealed	$\Delta\epsilon_p$	−0.396	−0.495	17
		$\Delta\epsilon_e$	−1.74	−0.196	
1050	Annealed	$\Delta\epsilon_p$	−0.552	−0.497	17
		$\Delta\epsilon_e$	−1.76	−0.186	
1050	Aged for 1000 hr at 1050°F	$\Delta\epsilon_p$	0.209	−0.727	17
		$\Delta\epsilon_e$	−1.97	−0.120	
1200	Annealed	$\Delta\epsilon_p$	−0.264	−0.560	7, 17
		$\Delta\epsilon_e$	−1.91	−0.153	
1200	Aged for 1000 hr at 1200°F	$\Delta\epsilon_p$	0.0871	−0.680	17
		$\Delta\epsilon_e$	−1.88	−0.180	

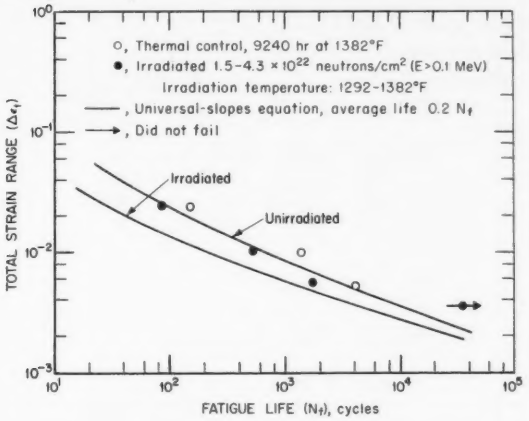

Fig. 19 Effect of irradiation on the fatigue life at 316 stainless steel at 1292°F and at a strain rate of 8×10^{-4} sec^{-1}. (From Brinkman et al.[31])

compression and tension hold times have no significant effect on cyclic-fatigue life.[17] The effect of tension hold time on fatigue life is illustrated in Fig. 20. For annealed material at 1050 and 1100°F [Figs. 20(*a*) and (*b*)], fatigue resistance decreased as the length of tensile hold time increased. (See Table 8.) However, at 1200°F, a saturation in this kind of behavior trend was noted, and similar fatigue lives were obtained for tension hold times from 0.1 to 1.0 hr. This saturation behavior is similar to that described previously for 304 stainless steel at 1200°F.

Aging of specimens for at least 1000 hr at test temperature prior to testing provided additional insight on the hold-time fatigue behavior of this alloy. At 1050°F [Fig. 20(*a*)], aging had little influence on the cyclic-fatigue life of tension hold-time specimens. At 1100°F [Fig. 20(*b*)], aging improved the hold-time fatigue life to a noticeable degree, and, at 1200°F [Fig. 20(*c*)], aging produced a very large increase in hold-time fatigue resistance. The extremely beneficial influence of aging at the highest of these three temperatures is probably related to the type of carbide precipitation discussed previously for the 304 alloy. Further study is required to see if this trend is limited to the 1200°F temperature region or if it is carried on to higher temperatures.

Both ANC[30] and BCL[17] have used Eq. 2 to describe the cyclically stable stress-relaxation response to this alloy and have computed creep–fatigue stress-relaxation response of this alloy and have computed creep–fatigue damage interaction by means of Eq. 3. As shown in Fig. 21, damage values for the annealed material fell somewhat below the $D = 1$ curve. The dispersion of points was not a definite function either of strain range, as was true in the case of 304 stainless steel, or of hold time (see Fig. 22), as in the case of both Alloy 800 and 304 stainless steel, but did reflect normal scatter in such experimental results. At 1050°F, damage values for aged material were about the same as those for annealed material. However, at 1100 and 1200°F, damage values for aged material fell close to or significantly above the $D = 1$ curve. The hold-time fatigue lives of specimens that were irradiated to fluences of 1.7 to 28.6×10^{20} neutrons/cm^2 ($E > 0.1$ MeV) at 842°F were about a factor of 2 to 4 below those of control specimens that were aged for 8760 hr at 752°F. In terms of total damage calculated by means of Eq. 3, similar results were obtained for both the irradiated and control specimens because the damage calculation did account for the effect of irradiation on fatigue life. For hold times from 0.01 to 1.0 hr, damage values between 0.51 and 0.85 were computed for the control specimens, and damage values between 0.28 and 0.85 were computed for the irradiated specimens.

Cyclic-stress–strain curves from incremental-step tests of 316 stainless steel[17] are presented in Fig. 23. The overall data trends for this alloy are similar to those discussed for 304 stainless steel. High-level strain cycles caused the stable stress on subsequent low-level cycles to be higher than for constant-amplitude loading. This phenomenon was more evident at room temperature [Fig. 23(*a*)] than it was at elevated temperatures. The cyclic-stress–strain "memory" of the material resulted in less cyclic hardening for tests that were conducted at lower maximum-strain amplitudes.

The complexity of cyclic-hardening behavior is further pointed out by the influence of aging and strain rate on cyclic hardening at 1050 and 1200°F. At 1050°F [Fig. 23(*c*)], the aged material showed slightly less cyclic hardening than the annealed material, whereas no significant difference in monotonic-stress–strain response was noted. Decreasing the strain rate from 4×10^{-3} to 4×10^{-5} sec^{-1} resulted in both more monotonic and more cyclic hardening at this temperature. At 1200°F [Fig. 23(*d*)], aging significantly reduced the amount of cyclic hardening and had little effect on the monotonic response. When strain rate was decreased from 4×10^{-3} to 4×10^{-5} sec^{-1}, more monotonic hardening was exhibited, but significantly less cyclic hardening was evident.

As shown by the ratios of cyclic to monotonic yield strength in Table 9, this alloy cyclically hardened

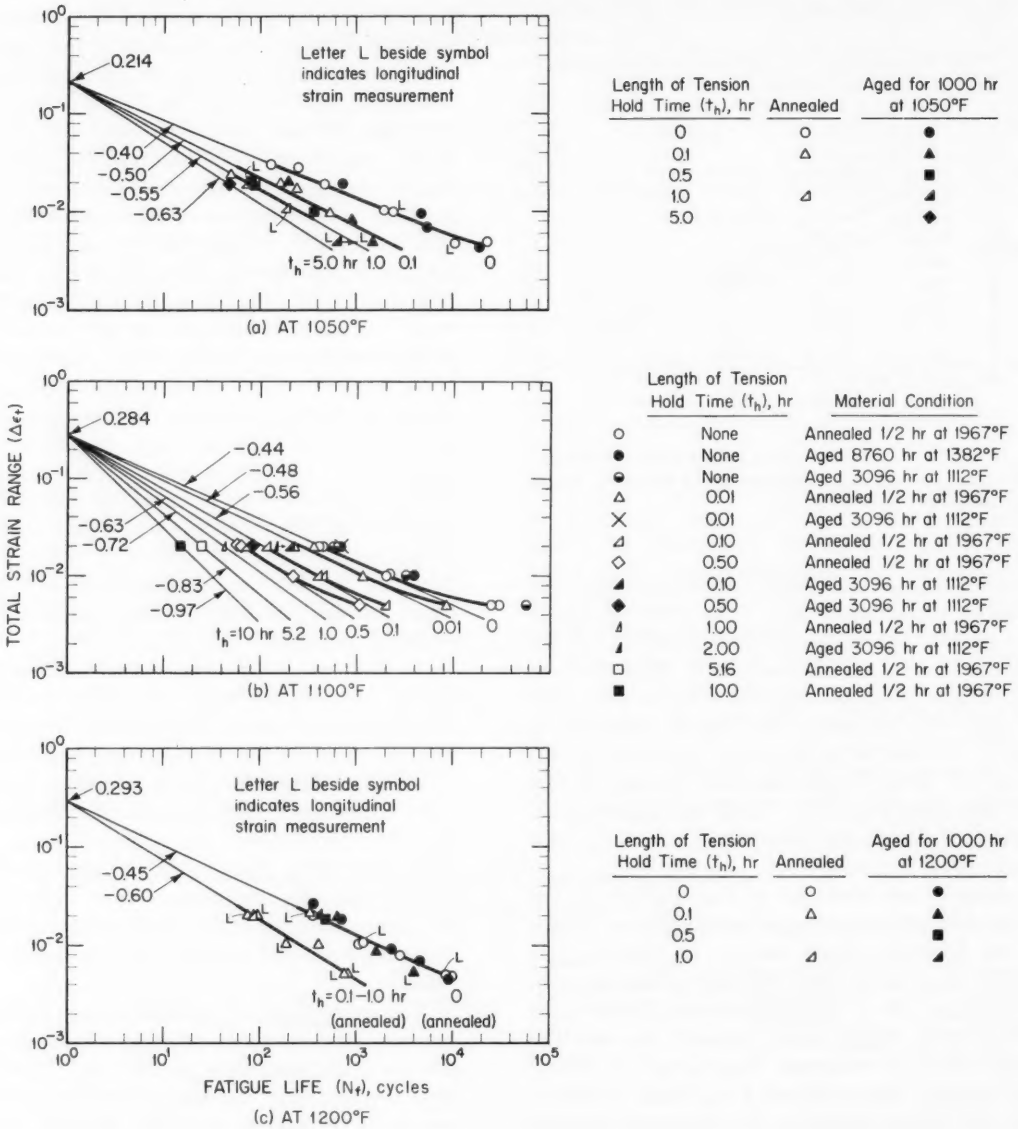

Fig. 20 Effect of hold time on fatigue life of 316 stainless steel at a strain rate of 4×10^{-3} sec^{-1}. (Parts *a* and *c* from Jaske et al.[17] and Part *b* from Brinkman et al.[30])

by factors between 1.3 and 2.6 with a maximum amount of hardening at 1050°F. Both monotonic- and cyclic-stress–strain curves were well represented by Eq. 4 using the appropriate constants in Table 9. Irradiation of 316 stainless steel to 1.2×10^{21} neutrons/cm^2 ($E > 0.1$ MeV) at 842°F caused only a slight increase in cyclic hardening at 1100°F (Ref. 30).

SUMMARY

Data from axially loaded, strain-controlled tests of unnotched specimens are being used to evaluate the low-cycle fatigue behavior of reactor structural materials and to provide creep–fatigue design information on these materials. For continuous cycling (with-

Table 8 Slope and Intercept Values That Define Tension Hold-Time Fatigue Curves for Annealed 316 Stainless Steel

Temp., °F	Intercept at $N_f = 1$	Length of tension hold time, hr	Slope of $\Delta\epsilon_t$ vs. N_f curve	References from which data were taken
1050	0.214	0	−0.40	17
		0.1	−0.50	
		1.0	−0.55	
		5.0	−0.63	
1100	0.284	0	−0.44	30
		0.01	−0.48	
		0.10	−0.56	
		0.50	−0.63	
		1.0	−0.72	
		5.2	−0.83	
		10.0	−0.97	
1200	0.293	0	−0.45	17
		0.1 to 1.0	−0.60	

out hold times), fatigue curves have been developed for Alloy 800 and 304 and 316 stainless steels over temperatures from 70 to 1500°F at a strain rate of 4×10^{-3} sec^{-1}. Decreasing the strain rate down to 4×10^{-5} sec^{-1} caused significant reduction in the low-cycle fatigue resistance of these alloys at temperatures of 1200 and 1500°F (Ref. 7). In the 1100 to 1200°F temperature range, Alloy 800 and 304 stainless steel have similar low-cycle fatigue strength, whereas 316 stainless steel has slightly lower fatigue strength than the 304 alloy.[26] Irradiation reduced the fatigue life of the stainless steels by a factor of about 2 and of the Alloy 800 by factors up to 35 at 1292°F (Ref. 31).

Tension hold times had a detrimental effect on the low-cycle fatigue resistance of all three alloys at temperatures of 1000°F and greater. In contrast, compression or combined compression–tension hold times had little or no effect on low-cycle fatigue

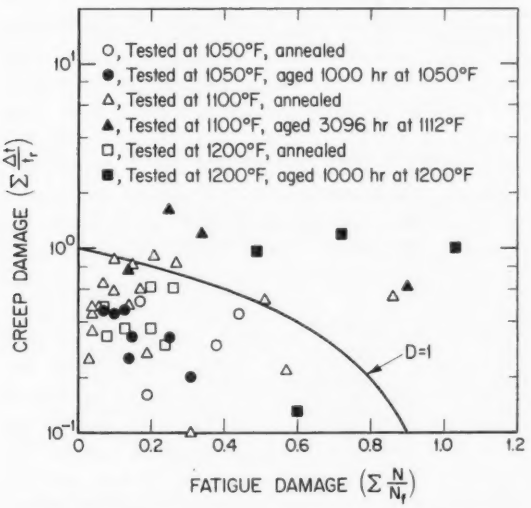

Fig. 21 Creep-fatigue damage interaction for tension hold-time tests of 316 stainless steel. (Results at 1050 and 1200°F from Jaske et al.[17] and at 1100°F from Brinkman et al.[30])

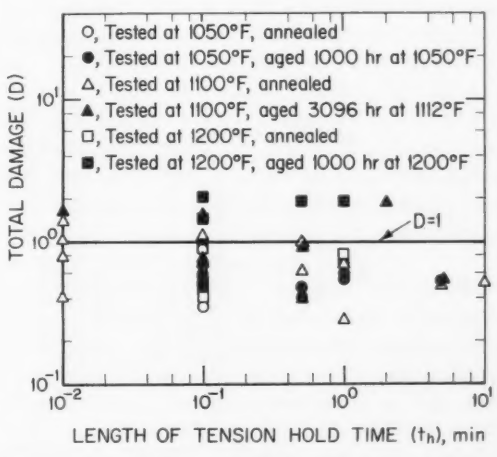

Fig. 22 Effect of length of tension hold time on total damage of 316 stainless steel. (Results at 1050 and 1200°F from Jaske et al.[17] and at 1100°F from Brinkman et al.[30])

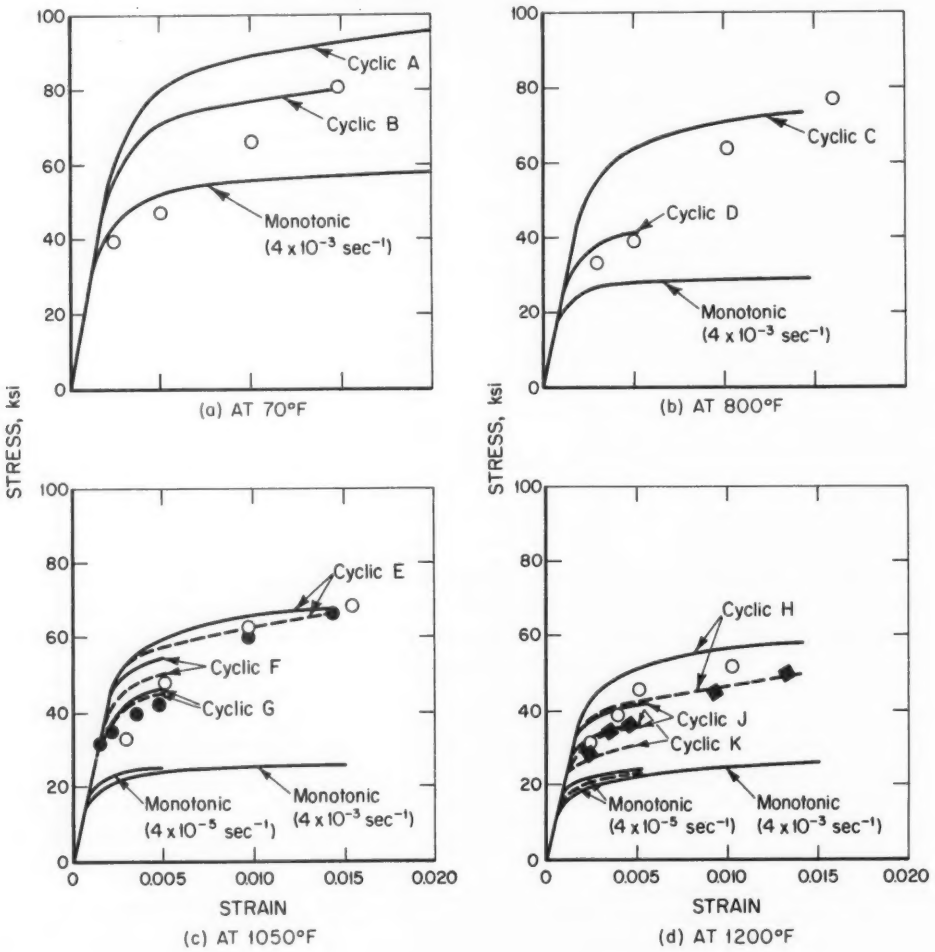

Incremental Step

———, Annealed

– – – – – –, Aged 1000 hr at test temperature

Constant Amplitude, Continuous Cycling

○, Annealed

●, Aged 1000 hr at 1050°F

◆, Aged 1000 hr at 1200°F

	$\dot{\epsilon}$, sec^{-1}	$\Delta\epsilon/2_{max.}$
Cyclic A	4×10^{-3}	±0.0289
Cyclic B	4×10^{-3}	±0.0145
Cyclic C	4×10^{-3}	±0.0146
Cyclic D	4×10^{-3}	±0.005
Cyclic E	4×10^{-3}	±0.0145

	$\dot{\epsilon}$, sec^{-1}	$\Delta\epsilon/2_{max.}$
Cyclic F	4×10^{-5}	±0.005
Cyclic G	4×10^{-3}	±0.005
Cyclic H	4×10^{-3}	±0.0145
Cyclic J	4×10^{-3}	±0.005
Cyclic K	4×10^{-5}	±0.005

Fig. 23 Comparison of monotonic- and cyclic-stress–strain curves for 316 stainless steel. (From Jaske et al.[17])

Table 9 Comparison of Monotonic- and Cyclic-Stress–Strain Properties of 316 Stainless Steel (from Jaske et al.[17])

Temp., °F	Strain rate, sec^{-1}	Max. total strain range, %	0.2% offset yield strength, ksi		Ratio of cyclic to monotonic yield strength	Strength coefficient, ksi		Strain-hardening exponent	
			Monotonic	Cyclic		Monotonic	Cyclic	Monotonic	Cyclic
70	4×10^{-3}	5.78	39.4	80.6	2.05	86.1	146	0.095	0.099
70	4×10^{-3}	2.90	39.4	69.9	1.77	84.2	133	0.086	0.109
800	4×10^{-3}	2.93	26.8	63.1	2.35	47.4	118	0.102	0.104
800	4×10^{-3}	1.00	26.8	39.8	1.48	62.3	104	0.140	0.154
1050	4×10^{-3}	2.92	22.3	58.9	2.64	40.9	102	0.100	0.089
1050	4×10^{-3}	1.00	22.3	45.2	2.03	55.8	91.1	0.142	0.113
1050	4×10^{-5}	0.99	24.1	53.7	2.23	46.0	100	0.106	0.101
1050*	4×10^{-3}	2.87	22.3	56.8	2.55	46.2	92.3	0.122	0.078
1050*	4×10^{-3}	0.98	22.3	43.7	1.96	46.3	113	0.119	0.151
1050*	4×10^{-5}	1.00	24.1	49.2	2.04	43.2	96.4	0.096	0.109
1200	4×10^{-3}	2.90	20.3	50.3	2.48	48.3	99.7	0.142	0.115
1200	4×10^{-3}	0.97	20.3	40.5	1.99	47.8	71.1	0.143	0.090
1200	4×10^{-5}	0.98	22.9	35.3	1.54	42.8	67.3	0.102	0.106
1200†	4×10^{-3}	2.90	20.3	41.5	2.04	54.6	73.3	0.159	0.094
1200†	4×10^{-3}	0.98	20.3	34.2	1.68	49.1	70.9	0.112	0.116
1200†	4×10^{-5}	1.00	21.6	28.8	1.33	52.9	48.0	0.147	0.081

*Aged 1000 hr at 1050°F.
†Aged 1000 hr at 1200°F.

resistance. In terms of hold-time fatigue resistance of the annealed material, 304 stainless steel was superior to 316 stainless steel, which was in turn superior to the Alloy 800. Since aging had a large beneficial influence on hold-time fatigue behavior of both 316 stainless steel and Alloy 800 at 1200°F (Ref. 17), a direct comparison of the three alloys cannot be adequately made until more data on the influence of aging are available. The effect of aging is related to carbide precipitation,[25] and the beneficial influence of aging corresponds directly with the amount of cyclic hardening observed (i.e., less hardening was observed when aging was beneficial).[17] Because experimental results indicate that aging is probably beneficial when it has an effect on elevated-temperature creep–fatigue resistance, information developed on annealed material will provide conservative estimates for design use. However, it should be pointed out that, although aging may inhibit high-temperature damage mechanisms, it may enhance fatigue damage at lower temperatures. It has been shown that heat treatment of 316 stainless steel to produce 2 to 3 vol.% $(CrFe)_{23}C_6$ carbides will reduce the room-temperature low-cycle fatigue resistance as compared with solution-annealed material.[39] Thus the influence of combined thermal–mechanical (rather than just isothermal) cycling on fatigue resistance of these alloys should be investigated in future work.

Use of the linear-life-fraction damage rule to evaluate creep–fatigue damage interaction gave different results for each of the three alloys. Calculated damages values varied as a function of both strain range and hold time for 304 stainless steel, varied as a function of hold time but not of strain range for Alloy 800, and did not vary as a function of either strain range or hold time for 316 stainless steel. Such different trends indicate that relating creep damage done during cyclic relaxation to monotonic-creep-rupture behavior does not explain the time-dependent damage done in hold-time fatigue tests.

The incremental step test provided a useful method of investigating the cyclic-stress–strain behavior of these alloys. The cyclic-stress–strain response of all three materials at low strain levels was definitely influenced by prior cyclic hardening at high strain levels. Such behavior was more pronounced for the stainless steels than it was for the Alloy 800. This influence of variable-amplitude loading is an important consideration in design applications where materials are subjected to spectra of loads rather than constant-

amplitude loading. All three alloys cyclically hardened by a significant amount from the annealed condition. Alloy 800 hardened by factors from 2.3 to 4.4 with a maximum amount of 1200°F, 304 stainless steel hardened by factors from 1.9 to 3.0 with a maximum amount at 1000°F, and 316 stainless steel hardened by factors from 1.3 to 2.6 with a maximum amount at 1050°F. The cyclic-stress–strain response of both stainless steels was influenced by strain rate. (The effect of strain rate on Alloy 800 was not examined.) At 1000 to 1050°F, decreasing the strain rate caused increased cyclic hardening, and, at 1200°F, it caused decreased cyclic hardening.

ACKNOWLEDGMENTS

The authors' studies on low-cycle fatigue were sponsored by the U. S. Atomic Energy Commission under contract No. W-7405-eng-92.

REFERENCES

1. Rules for Construction of Nuclear Power Plant Components, *ASME Boiler and Pressure Vessel Code, Section III,* The American Society of Mechanical Engineers, New York, July 1971.
2. Interpretations of ASME Boiler and Pressure Vessel Code, Case 1331-5, The American Society of Mechanical Engineers, New York, August 1971.
3. *Manual on Low-Cycle Fatigue Testing,* American Society for Testing and Materials, Special Technical Publication No. 465, Philadelphia, 1969.
4. Building a System for Testing Small Metal Specimens, *Closed Loop,* 1(8): 3–6 (1968), MTS System Corp., Minneapolis.
5. T. Slot, R. H. Stentz, and J. T. Berling, Controlled-Strain Testing Procedures, American Society for Testing and Materials, Special Technical Publication No. 465, pp. 100–128, Philadelphia, 1969.
6. J. B. Conway, Evaluation of Plastic Fatigue Properties of Heat-Resistant Alloys, USAEC Report GEMP-740, Nuclear Systems Programs, General Electric Company, December 1969.
7. J. T. Berling and T. Slot, Effect of Temperature and Strain Rate on Low-Cycle Fatigue Resistance of AISI 304, 316, and 348 Stainless Steels, in *Fatigue at High Temperature,* American Society for Testing and Materials, Special Technical Publication No. 459, pp. 3–30, Philadelphia, 1969 (also USAEC Report GEMP-642, Nuclear Systems Programs, General Electric Company, June 1968).
8. J. T. Berling and J. B. Conway, Effect of Hold Time on the Low-Cycle Fatigue Resistance of 304 Stainless Steel at 1200°F, in *Proceedings of the First International Conference on Pressure Vessel Technology,* The American Society of Mechanical Engineers, pp. 1233–1246, New York, 1969 (also USAEC Report GEMP-702, Nuclear Systems Programs, General Electric Company, June 1969).
9. E. Krempl, The Effect of Stress Concentration on the Low-Cycle Fatigue of Three Low-Strength Structural Steels at Room Temperature, USAEC Report GEAP-10170, General Electric Company, San Jose, Calif., March 1970.
10. J. B. Conway, Short-Term Tensile and Low-Cycle Fatigue Studies of Incoloy 800, USAEC Report GEMP-732, Nuclear Systems Programs, General Electric Company, December 1969.
11. C. E. Jaske, H. Mindlin, and J. S. Perrin, Low-Cycle Fatigue and Creep–Fatigue of Incoloy Alloy 800, Topical Report, USAEC Report BMI-1921, Battelle Memorial Institute, Columbus Laboratories, February 1972.
12. C. E. Jaske, H. Mindlin, and J. S. Perrin, Cyclic-Stress–Strain Behavior of Two Alloys at High Temperature, to be published in Special Technical Publication, American Society for Testing and Materials.
13. C. E. Jaske, H. Mindlin, and J. S. Perrin, Influence of Hold-Time and Temperature on the Low-Cycle Fatigue of Incoloy 800, Paper No. 71-WA/PVP-7, The American Society of Mechanical Engineers, 1971 (to be published in *Journal of Engineering for Industry).*
14. C. E. Jaske, H. Mindlin, and J. S. Perrin, Low-Cycle Fatigue Evaluation of Reactor Materials, in Progress on LMFBR Cladding, Structural, and Component Materials Studies During July 1970 Through June 1971, Annual Report, Final Report, USAEC Report BMI-1914, pp. A-1–A-44, Battelle Memorial Institute, Columbus Laboratories, July 1971.
15. C. E. Jaske, H. Mindlin, and J. S. Perrin, Low-Cycle Fatigue Evaluation of Reactor Materials, in Progress on LMFBR Cladding, Structural, and Component Materials Studies During July Through September 1971, Quarterly Report, USAEC Report BMI-1920, Battelle Memorial Institute, Columbus Laboratories, October 1971.
16. D. L. Keller, Progress on LMFBR Cladding, Structural, and Component Materials Studies During October Through December 1971, USAEC Report BMI-1922, Battelle Memorial Institute, Columbus Laboratories, January 1972.
17. Final Report, July 1971 Through June 1972, to be published by Battelle Memorial Institute, Columbus Laboratories.
18. R. W. Weeks, R. Carlander, and Che-Yu-Li, Low-Cycle Fatigue, in Reactor Development Program Progress Report, USAEC Report ANL-7742, pp. 108–109, Argonne National Laboratory, September 1970.
19. R. W. Weeks, W. F. Burke, and Che-Yu-Li, USAEC Report ANL-7758, p. 76, November 1970.*
20. R. W. Weeks, W. F. Burke, C. Tome, and Che-Yu-Li, USAEC Report ANL-7776, pp. 75–79, January 1971.
21. R. W. Weeks, C. F. Cheng, and Che-Yu-Li, USAEC Report ANL-7825, p. 5.8, May 1971.
22. C. F. Cheng and R. W. Weeks, USAEC Report ANL-7845, p. 5.2, July 1971.
23. C. F. Cheng, USAEC Report ANL-7861, p. 5.2, September 1971.
24. C. F. Cheng, USAEC Report ANL-7887, p. 5.3, November 1971.

*References 19 to 27 are Argonne National Laboratory Reactor Development Program Progress Reports.

25. C. F. Cheng, C. Y. Cheng, and D. R. Diercks, USAEC Report ANL-RDP-1, p. 5.6, January 1972.
26. C. F. Cheng and C. Y. Cheng, USAEC Report ANL-RDP-3, p. 5.2, March 1972.
27. C. F. Cheng and C. Y. Cheng, USAEC Report ANL-RDP-5, May 1972.
28. C. R. Brinkman, G. E. Korth, and J. M. Beeston, Elevated-Temperature Fatigue of Cladding and Structural Materials, Quarterly Progress Report—Irradiation Effects on Reactor Structural Materials for May, June, and July 1971, Aerojet Nuclear Company, August 1971.
29. Quarterly Progress Report for November and December 1971 and January 1972, Aerojet Nuclear Company, February 1972.
30. C. R. Brinkman, G. E. Korth, and R. R. Hobbins, Estimates of Creep–Fatigue Interaction in Irradiated and Unirradiated Stainless Steels, to be published in *Nuclear Technology*.
31. C. R. Brinkman, G. E. Korth, and J. M. Beeston, The Influence of Irradiation on the Creep–Fatigue Behavior of Several Austenitic Stainless Steels and Incoloy 800 at 700°C, to be published in Special Technical Publication, American Society for Testing and Materials.
32. S. S. Manson, Fatigue: A Complex Subject—Some Simple Approximations, *Exp. Mech.*, 5(7): 193–226 (July 1965).
33. G. R. Halford and S. S. Manson, Application of a Method of Estimating High-Temperature Low-Cycle Fatigue Behavior of Materials, *Trans. Amer. Soc. Metals*, **61**: 94–101 (1968).
34. J. H. Gittus, Implications of Some Data on Relaxation Creep in Nimonic 80A, *Phil. Mag.*, **9**: 749–753 (1964).
35. E. Krempl, Notched High-Strain Fatigue Behavior of Three Low-Strength Structural Steels, in *Proceedings of the First International Conference of Pressure Vessel Technology*, The American Society of Mechanical Engineers, pp. 1319–1328, New York, 1969.
36. C. E. Jaske, H. Mindlin, and J. S. Perrin, Combined Low-Cycle Fatigue and Stress Relaxation of Alloy 800 and Type 304 Stainless Steel at Elevated Temperature, paper to be presented at 1972 Symposium on Fatigue at Elevated Temperatures, University of Connecticut, Storrs, Conn., June 1972.
37. J. B. Conway, An Analysis of the Relaxation Behavior of AISI 304 and 316 Stainless Steel at Elevated Temperature, USAEC Report GEMP-730, Nuclear Systems Programs, General Electric Company, December 1969.
38. R. D. Campbell, Creep–Fatigue Interaction Correlation for 304 Stainless Steel Subjected to Strain–Controlled Cycling with Hold Times at Peak Strain, *J. Eng. Ind.* **93**(4): 887–892 (November 1971).
39. J. T. Barnby and F. M. Peace, The Effect of Carbides on the High-Strain Fatigue Resistance of an Austenitic Steel, *Acta Met.*, **19**: 1351–1358 (December 1971).

AMERICAN NUCLEAR SOCIETY—CRITICAL REVIEWS

The Atomic Energy Commission has contracted with the American Nuclear Society to prepare for publication on a regular basis detailed Critical Review articles written by experts selected from the ANS membership and reviewed by an advisory committee of top leaders and scientists in the field. In this issue the article is on pages 210–238.

Comments on the article should be communicated directly to the ANS Critical Review Advisory Committee or Editor, 244 E. Ogden Avenue, Hinsdale, Ill. 60521.

ANS GUIDELINES FOR PREPARING CRITICAL REVIEWS FOR *REACTOR TECHNOLOGY*

One interpretation of the words "Critical Review" emphasizes the word *critical.* That type of article would have as its purpose the discussion of a single subject, which has been uncertain and perhaps controversial, in considerable depth. An example might be a critical review of the values of alpha for plutonium, assessing all the work done and arriving at a best current estimate. This paper is primarily addressed to specialists on the particular subject, and serves as an authoritative source for the information they use.

In the second interpretation of a Critical Review, the emphasis is on the word *review,* in the sense of survey. Such a paper would be broader and probably more descriptive in scope. A paper on "Solubility of Metallic Elements in Liquid Sodium" is an example of this category. Such a paper would be addressed to a much broader group of readers and written in a fashion that would be of interest to the majority of reactor technologists. It would provide enough of an introduction that the specialist from another field could immediately appreciate why the subject is important.

The criteria for these two types of articles may not be very different:

1. The paper should be based on a thorough coverage of relevant work on the subject from many sources. A review based on the work of only one individual or group is better suited for publication in one of the regular society journals. The review should be critically selective, reporting only the most valid results and indicating why some prior results have a questionable status. The review should call attention to significant gaps where more work is required in the subject of the article.

2. The paper must include an evaluation, a critical appraisal, of the field being covered. It should be more than merely a survey of the work being done in the field.

3. The paper should be timely, on a subject of active current interest.

4. The scope of articles acceptable as Critical Reviews includes all the subject areas identified for *Reactor Technology* (Economics, Physics, Mechanics, Construction, Fuel Elements, Fuel Cycles, Fluid and Thermal Technology, Fuel Processing, Components, Operating Performance), as well as Materials (including Source and Special Nuclear), Environmental Effects, and Effluent Management. Not desired are (1) reports of original research proposed for first publication and (2) review articles directed toward the specialist in the field of nuclear safety (which is covered by the AEC's bimonthly review *Nuclear Safety*).

5. The paper should be organized so that it is of immediate practical use to the readers. Such organization requires: attention to consistent use of units, presentation of important data in summary curves or tables, and a fully adequate bibliography to the original literature.

All papers are reviewed, at the proposal and the draft stage, by several referees expert in the subject field. Referees may require revisions, expansions, or deletions to make the paper acceptable for publication. Details on size, honorarium, style, etc., can be obtained from ANS.

Flux Synthesis Methods in Reactor Physics

By Weston M. Stacey, Jr.*

Abstract: *Use of flux synthesis methods to compute the neutron distribution and other important parameters in nuclear reactors is reviewed. Spatial, spectral, and angular synthesis methods are discussed. Examples are described which illustrate common methods of selecting trial functions and which represent the current state of the art. Recent advances in the underlying theory and in the development of specific applications are discussed, experience with the different synthesis methods is assessed, and promising areas for further development activity are suggested.*

Synthesis, which derives from the Greek, means literally the action of putting together. Webster defines it as the "composition or combination of parts or elements so as to form a whole." Thus, in a literal sense, most of the methods that comprise the repertoire of the reactor physicist may be classified as synthesis methods. Such a classification, although serving to unify a minuscule portion of the universe, has little pragmatic advantage. To most reactor physicists the term "flux synthesis" conjures up a vaguely delineated class of methods having to do with the combining of simpler or lower dimensional solutions to obtain a more complex or higher dimensional solution.

Meyer[1] seems to be the first to have published a synthesis technique for constructing multidimensional flux solutions from lower dimensional calculations. His idea was to calculate a different two-dimensional planar flux solution for each of several axial zones. These planar solutions were then used to obtain planar-averaged cross sections and transverse bucklings for the corresponding axial zones, and one or more axial shapes were calculated corresponding to the planar regions over which the cross sections and transverse bucklings were computed. Finally the planar and axial shapes were multiplied together to yield a three-dimensional flux distribution. Wachspress et al.[2] improved on this by using the planar solutions to define coupling coefficients between contiguous planar regions (channels), rather than transverse bucklings. Thus, in their multichannel synthesis technique, the axial-shape calculations (for the axial shapes corresponding to the different planar regions or channels) are coupled rather than independent as in Meyer's method.

Selengut[3] precipitated the subsequent development of synthesis methods by providing a theoretical foundation based on variational theory and by introducing the idea of "blending" or combining two or more lower dimensional solutions. Calame and Federighi[4] were the first to exploit Selengut's ideas. They derived variationally a method to synthesize "hard" and "soft" Maxwellian spectra to obtain spatially dependent thermal-neutron spectra. Their method was originally referred to as the overlapping group method but has more recently come to be designated the spectral synthesis, or space–energy synthesis, method.

Kaplan[5] employed Selengut's idea of blending to extend Meyer's technique. In Kaplan's method the planar solutions calculated for the different axial zones were all used over the entire axial domain, rather than each planar solution being used only in the corresponding axial zone as in Meyer's method. Axial-shape functions corresponding to the different planar solu-

*Applied Physics Division, Argonne National Laboratory, Argonne, Ill. 60439.

tions were determined by solving a coupled set of axial-shape equations. In Kaplan's method a single axial-shape function was associated with each planar solution, and all the planar solutions were used in every axial zone, which has given rise to the designation single-channel continuous spatial synthesis. Kaplan also noted that the synthesis equations could be derived on the basis of the weighted residual method, as well as variationally, and that the equations obtained from the two derivations were essentially equivalent.

Pomraning and Clark[6] appear to be the first to have exploited Selengut's ideas with respect to synthesizing the angular distribution of the neutron flux. They demonstrated that the synthesis equations were, in fact, the P_N equations when the Legendre polynomials were used to expand the angular flux and that the use of a different set of polynomials led, via the synthesis formalism, to an improved form of diffusion theory.

An idea of Selengut's[7] was also the basis for the next advance in the development of synthesis methods. He proposed a variational principle that would admit discontinuous trial solutions. Wachspress and Becker[8] exploited this idea to combine the blending formalism of Kaplan and the earlier multichannel idea of Wachspress et al. to obtain a multichannel synthesis formalism in which the planar solutions were blended with axial shapes calculated for each planar region or channel. These axial shapes satisfied coupled equations. Yasinsky and Kaplan[9] also employed Selengut's variational principle to derive an axially discontinuous extension of Kaplan's single-channel synthesis in which different sets of planar shapes were blended in the different axial zones.

Subsequent to these pioneering papers, the literature of the field has been swollen with reports of development and application of synthesis methods and extensions of the supporting theory. It is the purpose of this article to review this work critically and selectively, with emphasis on that work which provides a measure of the current state of the art. The review also touches on several areas in which essentially synthesis-like procedures were employed in the derivation of approximations.

There is no generally accepted classification of synthesis methods or nomenclature for the different approximations. However, to facilitate the organization of the article, it is convenient to establish some conventions before proceeding. To this end, those methods which most logically may be characterized as the combining of spatial shapes, energy spectra, or angular functions will be referred to as spatial, spectral, and angular synthesis, respectively. Some typical synthesis approximations are so classified below.

Spatial Synthesis:

$$\phi(x,y,z,E,\Omega,t) = \sum_{n=1}^{N} \psi_n(x,y)\rho_n(z,E,\Omega,t) \quad (1)$$

or

$$\sum_{n=1}^{N} \psi_n(x,y,z)\rho_n(E,\Omega,t) \quad (2)$$

or

$$\sum_{n=1}^{N} \psi_n(x,y,E)\rho_n(z,\Omega,t) \quad (3)$$

Spectral Synthesis:

$$\phi(x,y,z,E,\Omega,t) = \sum_{n=1}^{N} \psi_n(E)\rho_n(x,y,z,\Omega,t) \quad (4)$$

Angular Synthesis:

$$\phi(x,y,z,E,\Omega,t) = \sum_{n=1}^{N} \psi_n(\Omega)\rho_n(x,y,z,E,t) \quad (5)$$

where ψ_n = known expansion function
ρ_n = unknown expansion coefficient
x,y,z = spatial coordinates
E = energy
Ω = direction
t = time

It should be emphasized that the synthesis approximations are generally based on discrete approximations (e.g., multigroup treatment of energy, finite-difference treatment of space, and P_N treatment of angle), rather than on the integro-differential Boltzmann equation; however, it is notationally convenient to indicate continuous variables above.

In the derivation of synthesis approximations, it is necessary to select weighting functions as well as trial solutions (or trial functions as they are frequently called). The synthesis equations, in essence, are requirements that the combining coefficients, with which the trial functions are combined, are selected such that the synthesized solution satisfies the neutron balance equation in a weighted integral sense, for as many different weighting functions as there are trial functions. Three different types of weighting functions are common: (1) Galerkin weighting, in which the weighting functions are identical with the trial functions; (2) adjoint weighting, in which the weighting functions are trial adjoint solutions; and (3) subdomain weighting, in which the weighting functions are unity over a subdomain and zero elsewhere.

SPATIAL SYNTHESIS

The effort devoted to the development of spatial synthesis far exceeds that expended on the other categories of synthesis; thus it is not surprising that the greatest success has been realized in this area. Although the blending method of Kaplan has enjoyed the most extensive development, the nonblending method of Meyer has been successfully extended as well. The multichannel blending method, although promising, has never quite caught on, due to certain difficulties that may now be eliminated by a new formulation. The use of piecewise polynomials was introduced several years ago in the spatial synthesis context and has recently engendered considerable enthusiasm now that a more systematic development is taking place under the name of finite-element methods. Coarse-mesh rebalancing methods have recently, and correctly, come to be viewed as a variant of the spatial synthesis method.

Nonblending Methods of Spatial Synthesis

Nonblending methods, because of their relative simplicity, probably have been used more widely, if less extensively, than the more powerful blending methods. In the simplest of these methods, a single, but different, planar solution is used within each axial zone to obtain planar-averaged group constants for the calculation of an axial shape, which is then multiplied by the planar solutions to construct a three-dimensional solution. This method, which has probably been used at some time at every installation concerned with reactor analysis, can provide a useful approximation in those situations in which the planar and axial flux distributions, to a good approximation, are separable within the different axial regions. Such situations become vanishingly few as calculational models become more realistic and reactor designs progress beyond their initial stages.

Iteration between the axial- and planar-shape calculations is one means of improving the accuracy of the nonblending method. Travelli and Helm[10] employed an iterative nonblending synthesis method to calculate the spatial distribution of the sodium-void reactivity effect in the fast reactor critical facilities ZPR-6, Assemblies 2 and 3, which were large, single-zoned, reflected reactors. Both the real and adjoint fluxes were assumed separable in r and z coordinates over the whole reactor. One-dimensional 26-group calculations in r and z geometries were run through a rapidly converging iteration scheme by modifying the (uniform) transverse bucklings to obtain a pair of calculations yielding identical k_{eff} and with transverse bucklings which summed to the material buckling. Direct two-dimensional 26-group calculations were performed for comparison. The results are summarized in Table 1, and the spatially detailed comparison for Assembly 2 is shown in Fig. 1. The time required for this relatively simple synthesis method was only 1% of that for the direct two-dimensional solution, yet it yielded quite accurate results for this geometrically simple model.

Table 1 Synthesis[10] of Sodium-Void Reactivity Worth for ZPR-6

	Assembly 2		Assembly 3	
	Synthesis	Direct	Synthesis	Direct
Total sodium void (10^{-2} δk/k)	−2.00	−2.03	−1.68	−1.71
Central sodium void (10^{-2} $\delta k/k$)	−5.57	−5.68	−3.37	−3.46
k_{eff}	0.999	0.998	0.998	0.997

Hutchins et al.[11] employed an iterative extension of Meyer's synthesis method to calculate the important properties of a 1000-MW(e) PuO_2–UO_2 liquid-metal-cooled fast breeder reactor (LMFBR), using 16-group diffusion theory. Initial radial solutions were obtained through the core, followed by the calculation of

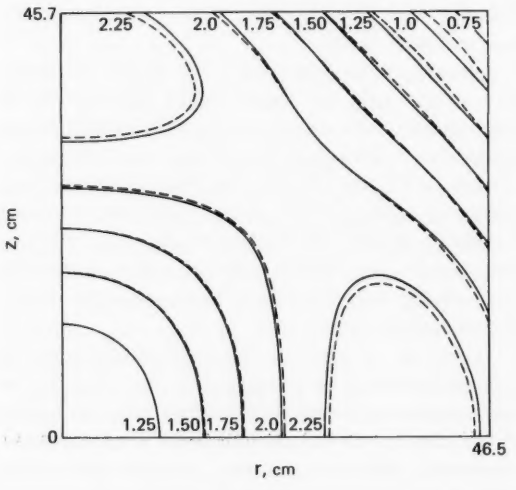

Fig. 1 Spatial distribution of sodium-void effect[10] (-1×10^{-2} $\Delta k/k$) in ZPR-6, Assembly 2. —, synthesis; - - -, direct 2D.

flux-adjoint weighted radial bucklings. Axial calculations were performed in from one to four core zones using the bucklings from the initial radial solution. (Up to this point the method is identical to Meyer's.) Next the axial regions were homogenized by flux-adjoint weighting with the axial solutions. A final radial solution was made, using the axially homogenized cross sections, and combined with the axial shapes to construct the two-dimensional flux. This synthesis solution was a factor of 20 faster than a direct two-dimensional solution of the same problem.

Results of the synthesis and direct solutions are compared in Table 2. The distribution of power by regions was accurate to 1% in the core and 10% in the corner blanket. Detailed power distributions in the core were accurate to with 5%. The maximum sodium loss coefficient was accurate to within 10%, and the Doppler coefficient was computed more accurately.

Table 2 Results for a 1000-MW(e) Fast Reactor Using Synthesis and Conventional Two-Dimensional Solutions[11]

	Synthesis solution	Conventional solution
k_{eff}	0.9999	1.0002
Total breeding ratio	1.338	1.333
Internal conversion ratios		
Core zone 1	0.9170	0.9172
Core zone 2	0.7109	0.7112
Percent power by region		
Core zone 1	50.4	50.7
Core zone 2	39.2	39.0
Radial blanket	2.81	2.73
Axial blanket	7.13	7.06
Corner blanket	0.46	0.51
Maximum sodium loss reactivity, $\Delta k/k$	+0.0235	+0.0221

Blending Methods of Spatial Synthesis

Blending methods were formulated by Kaplan.[3] Subsequent theoretical developments have extended the methodology to time-dependent problems[12] to accommodate the use of different sets of planar solutions in different axial regions[9,13-17] and to accommodate the use of different sets of planar solutions during different intervals of time.[18,19] The accuracy of the blending methods has been tested by a relatively large number of numerical studies performed for both thermal[9,12,20-24] and fast[25-27] reactor models. These tests have been generally successful, except for certain anomalies that will be discussed in a subsequent section, and have demonstrated the power of the synthesis blending methods.

An example presented by Yasinsky and Kaplan[9] serves to represent the rather complex models that have been successfully treated with a blending synthesis method, as well as illustrating the choice of trial functions (planar solutions) and demonstrating the advantages of axially discontinuous single-channel synthesis. They considered the thermal reactor model shown in Fig. 2, represented by two-group diffusion theory. Nine radial trial functions were considered. Trial functions 1 to 5 were one-dimensional solutions representative of radial slices through the correspondingly numbered axial compositions. "Transition" trial functions 6 to 9 were one-dimensional radial solutions obtained using the averaged material constants of axial compositions 1–2, 2–3, 3–4, and 4–5, respectively. Table 3 describes the trial functions used in two discontinuous synthesis solutions (1.a and 1.b), together with the axial zone within which each set of trial functions was used, the motivation being to retain in any axial zone only those trial functions representative of that zone and adjacent zones.

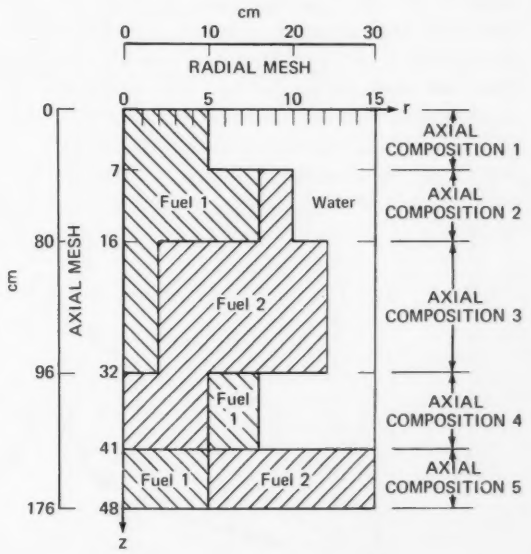

Fig. 2 PWR reactor model for two-dimensional synthesis test calculations.[9]

Table 3 Sets of Trial Functions for Discontinuous Synthesis Solutions[9]

Test problem	Fast trial functions	Thermal trial functions	Axial mesh range
1.a	1,2	1,2	0–9
	2,3	2,3	10–24
	3,4	3,4	25–38
	4,5	4,5	39–48
1.b	1,2	1,2,6	0–9
	2,3	2,3,7	10–24
	3,4	3,4,8	25–38
	4,5	4,5,9	39–48

Two continuous synthesis solutions were also performed, using a single set of trial functions over the entire axial domain. Continuous synthesis solution 1.c used trial functions 1 to 5 in both energy groups, resulting in 10 equations (two groups x five trial functions) to be solved, as compared to four equations (two groups x two trial functions) and five equations (two fast and three thermal trial functions) for discontinuous solutions 1.a and 1.b, respectively. Continuous synthesis solution 1.d used trial functions 2 and 3 in both energy groups, resulting in four equations to be solved. Galerkin weighting was used in all cases.

Thermal-flux distributions computed with the four synthesis calculations are compared with the results of a direct two-dimensional finite-difference solution in Figs. 3 to 6. Of particular interest is the superiority of synthesis solution 1.a relative to synthesis solution 1.d, both of which required the same core storage and computational effort to solve the synthesis equations, thus illustrating the advantage of using the discontinuous synthesis method. However, the computational effort needed to obtain trial functions was much greater for solution 1.a than for solution 1.d. The continuous synthesis solution 1.c is as good as or better than either of the discontinuous synthesis solutions. The former (1.c) required less effort in trial-function calculation and more effort in the solution of the synthesis equations (plus more core storage) than the latter.

Depletion problems have been treated with synthesis by first doing depletion calculations on planar models corresponding to different axial zones. The planar flux solutions obtained at the different depletion steps were then used as trial functions in a three-dimensional synthesis depletion.

Larsen[24] recently examined the idea of recomputing trial functions at selected points during the depletion, thus eliminating the need for the planar depletion calculations. He reported several continuous

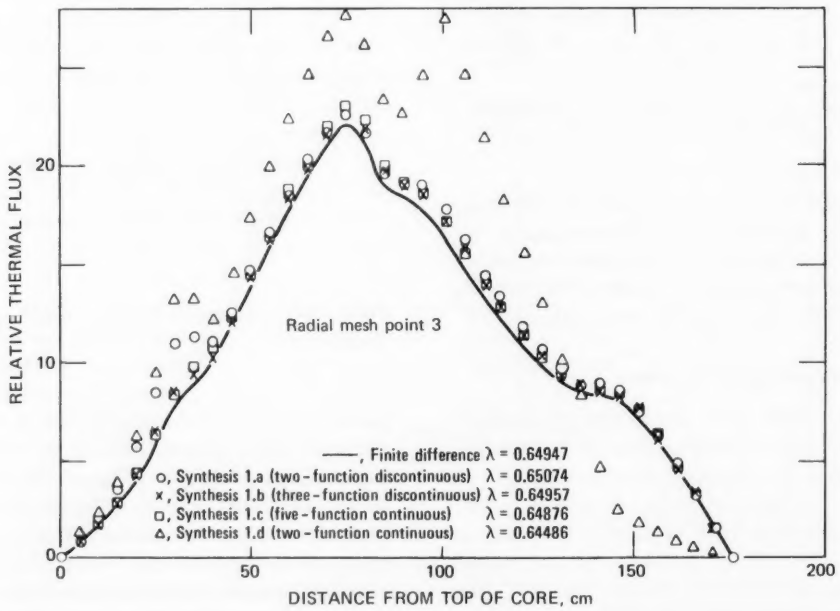

Fig. 3 Thermal-flux distribution: comparison of spatial synthesis with direct calculations.[9]

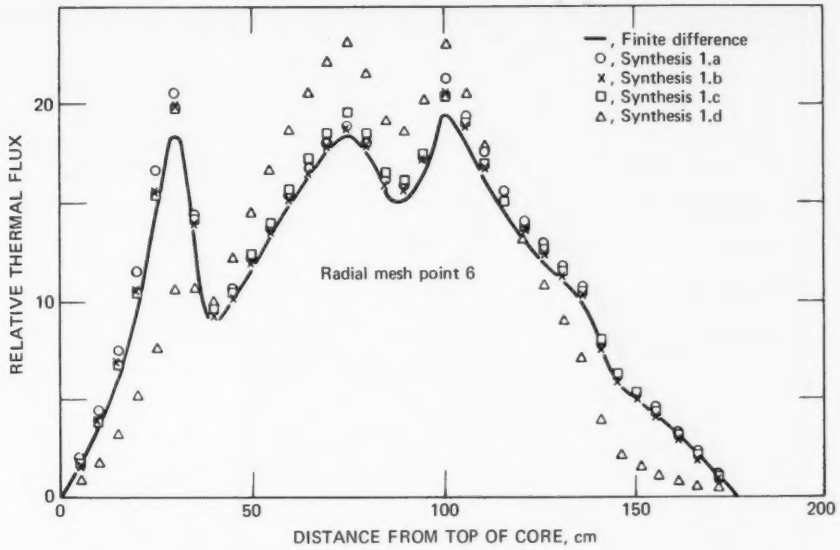

Fig. 4 Thermal-flux distribution: comparison of spatial synthesis with direct calculations.[9]

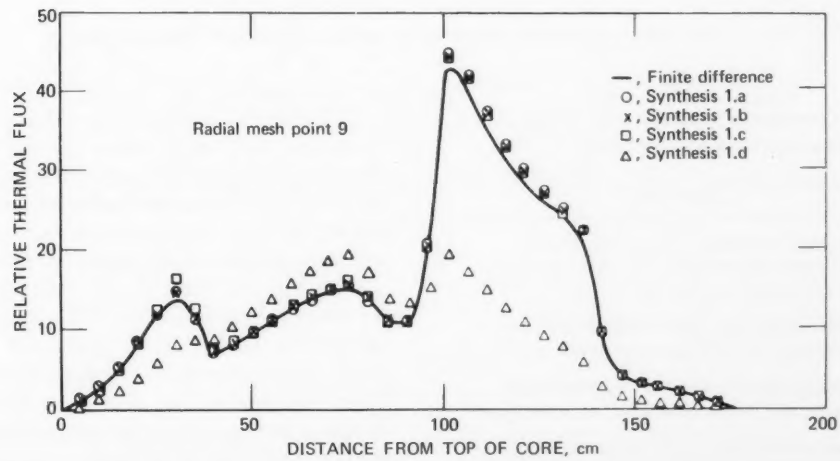

Fig. 5 Thermal-flux distribution: comparison of spatial synthesis with direct calculations.[9]

synthesis calculations for a two-dimensional two-group thermal reactor model representative of the Yankee pressurized-water reactor (PWR), as described in Table 4. His results are compared with the results of a direct two-dimensional solution (DBU) in Fig. 7. Recomputation of the trial functions resulted in a significant increase in accuracy, and there was no apparent advantage in using adjoint, rather than Galerkin, weighting.

Although the majority of the applications of the blending synthesis method have been to thermal reactors, where the fine structure in the spatial flux distribution is quite detailed, some recent work[25,26] has demonstrated the utility of the method for fast-breeder reactor applications as well. Pilate et al.[25] have made continuous synthesis calculations for three-dimensional models of the experimental facilities ZPR-3/48 and SNEAK-2C, using a five-group dif-

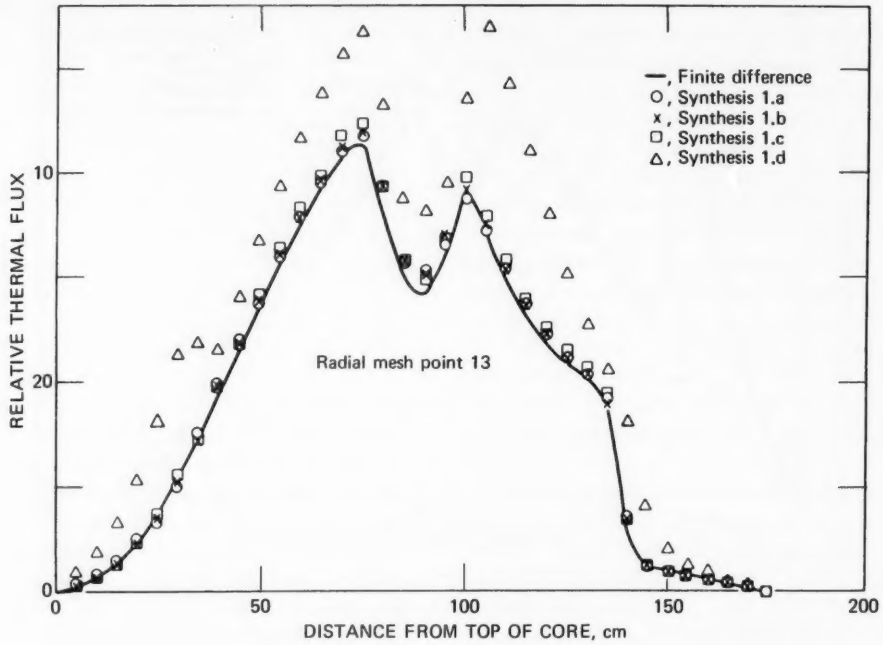

Fig. 6 Thermal-flux distribution: comparison of spatial synthesis with direct calculations.[9]

Table 4 Continuous Synthesis (SYNTRON) Calculations for PWR Depletion[24]

Case	Description
I	Two trial functions in fast group and three in the thermal group; no trial-function recalculation; Galerkin weighting
II	Same as case I but with trial-function recalculation at 750 MWd/ton of uranium
III	Same as case I but with trial-function recalculation at 750 and 2000 MWd/ton of uranium
IV	Same as case III but with adjoint weighting

fusion-theory representation, which have compared favorably with the results of a direct three-dimensional finite-difference calculation. The synthesis calculations, including the trial-function computations, were a factor of 10 or better quicker than the corresponding direct calculations.

The geometrical model used for the SNEAK-2C calculation is shown in Fig. 8, where MASURCA and SNEAK refer to different fuel types and R2 is a radial blanket. Eight different planar shapes were considered as trial functions, as indicated in Table 5. The first four corresponded to planar slices through the core and axial blanket regions with and without the control rod present, and the second four were auxiliary shapes, similar to Green's functions (see the next subsection), which emphasized certain important regions.

The k_{eff} calculated for the reference rod-out and the rod fully inserted cases by the continuous synthesis calculations (KASY) are compared with the results of direct three-dimensional calculations (TRITON) and direct two-dimensional calculations through the core midplane with an estimated axial buckling (DIXY) in Table 6. The synthesis calculations were quite adequate for predicting k_{eff} and were remarkably accurate for predicting the worth of the control rod. Percent of errors in fission rate (absorption rate in the control rod) for the synthesis calculation, relative to the direct three-dimensional calculation, are plotted for z–y plane at $y = 71.7$ cm in Fig. 9.

Luco[26] compared continuous synthesis and direct finite-difference solutions for a two-dimensional model of a 1000-MW(e) LMFBR with middle-of-cycle (MOC) composition, represented by six-group diffusion theory. He used five different radial flux solutions as trial functions: trial function 1 was a radial solution

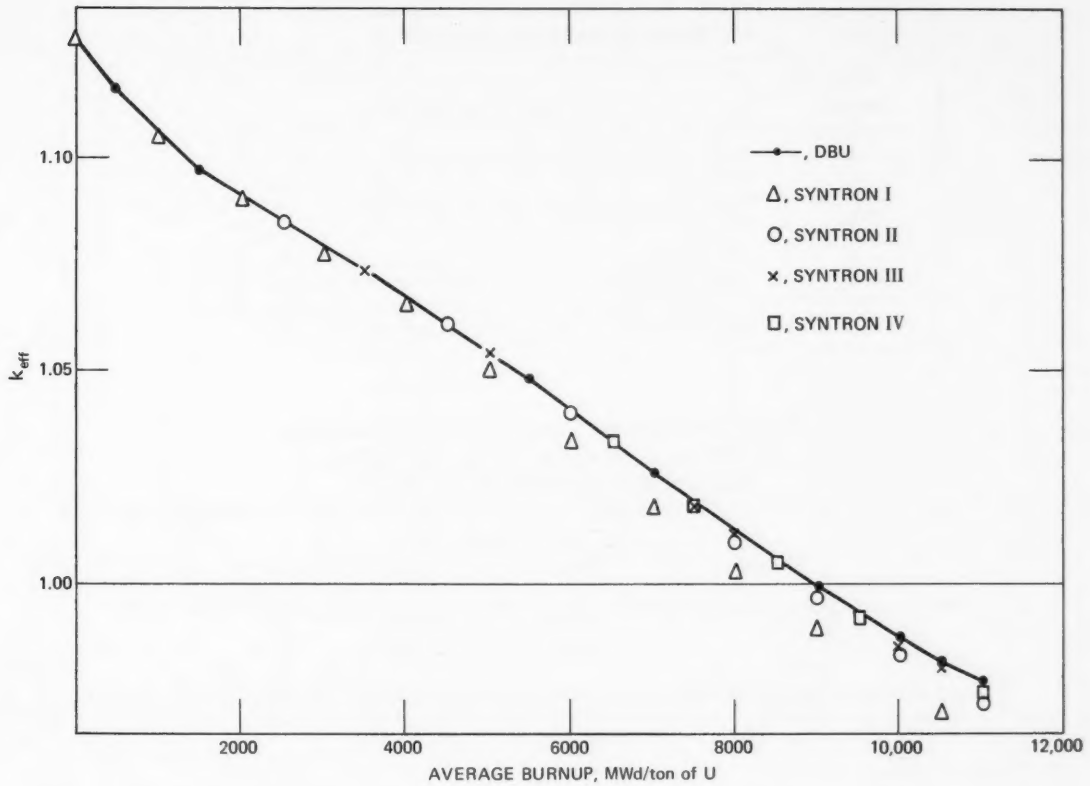

Fig. 7 Comparison of spatial synthesis (SYNTRON) and direct (DBU) depletion calculations for a two-dimensional PWR model.[24]

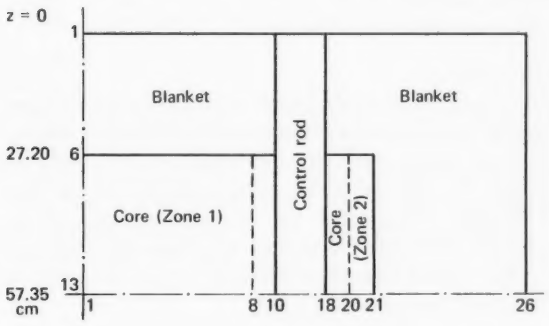

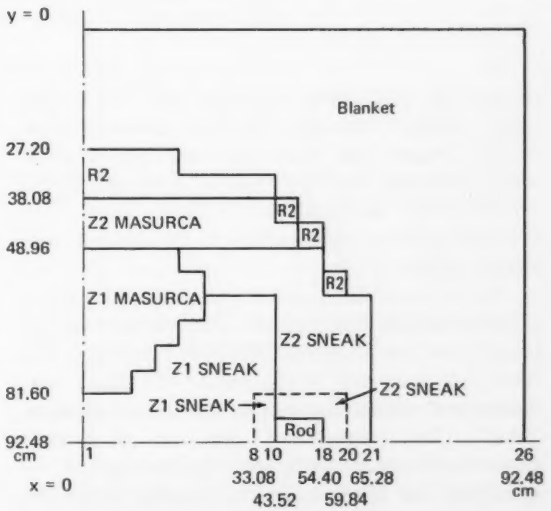

Fig. 8 Calculational model for SNEAK-2C fast reactor critical assembly.[25]

Table 5 Two-Dimensional Trial Functions[25] for Synthesis Calculation of SNEAK-2C

Trial function	Planar (x,y) configuration
1	Plane at z = 57.35 cm with tantalum rod, $B_z^2 = 1.16 \times 10^{-3}/\text{cm}^2$
2	Plane at z = 57.35 cm without tantalum rod, $B_z^2 = 1.16 \times 10^{-3}/\text{cm}^2$
3	Plane at z = 20.00 cm with tantalum rod, $B_z^2 = 0$
4	Plane at z = 20.00 cm without tantalum rod, $B_z^2 = 0$
5	Z_1 SNEAK fuel in rod position, tantalum absorber elsewhere, $B_z^2 = 0$
6	Z_1 SNEAK fuel in core zone 1, tantalum absorber elsewhere, $B_z^2 = 0$
7	Z_1 SNEAK fuel in core zone 2, tantalum absorber elsewhere, $B_z^2 = 0$
8	Blanket material in radial blanket, tantalum elsewhere, $B_z^2 = 0$

Table 6 Criticality and Control-Rod-Worth Calculations for SNEAK-2C: Comparison of Spatial Synthesis (KASY) and Direct (TRITON) Solutions[25]

Methods	k_{eff} Reference		k_{eff} Rod in		Δk (10^{-4})
TRITON		0.9770		0.9600	170
(DIXY)*		(0.9813)		(0.9639)	(174)
KASY†					
One trial function	(2)	0.9764	(1)	0.9594	170
Two trial	(2,4)	0.9768	(1,3)	0.9598	170
functions	(2,6)	0.9768	(1,6)	0.9598	170
	(2.7)	0.9767			
	(2,8)	0.9766			
			(1,5)	0.9595	
Three trial	(2,4,6)	0.9769	(1,3,6)	0.9599	170
functions	(2,4,8)	0.9768	(1,3,8)	0.9598	170
			(1,2,3)	0.9598	

*Two-dimensional results obtained with an estimated B^2.
†The numbers of the trial function used are indicated in parentheses.

through the core region; trial functions 2 to 4 were radial solutions through the three different axial blanket regions; and trial function 5 was a radial solution through the axial reflector, with an external volume source distributed as the fission source from the radial solution corresponding to the adjacent axial blanket region.

Synthesis calculations were performed using the 5, 3 (core, middle axial blanket, and reflector), and 1 (core) trial functions, with Galerkin weighting. The results are compared to the results of a direct two-dimensional finite-difference calculation (DIF2D) in Table 7. (The designations C, AB, and RB indicate core, axial blanket, and radial blanket regions, respectively, and BR indicates the breeding ratio.) The synthesis calculations were quite accurate.

Luco performed another calculation using the same trial functions on the same model, but with a composition corresponding to beginning-of-cycle (BOC), to test the possibility of using a single set of trial functions (calculated for one composition) for an entire fuel-cycle calculation. Results of the synthesis and a direct two-dimensional finite-difference calculation are compared in Table 8.

Green's Functions Trial Solutions

Green's functions trial solutions were introduced by Dougherty and Shen[28] and subsequently applied by others.[29-31] These authors suggested the use of flux solutions to problems in which the fission source was set to zero except in a limited region. By consecutively

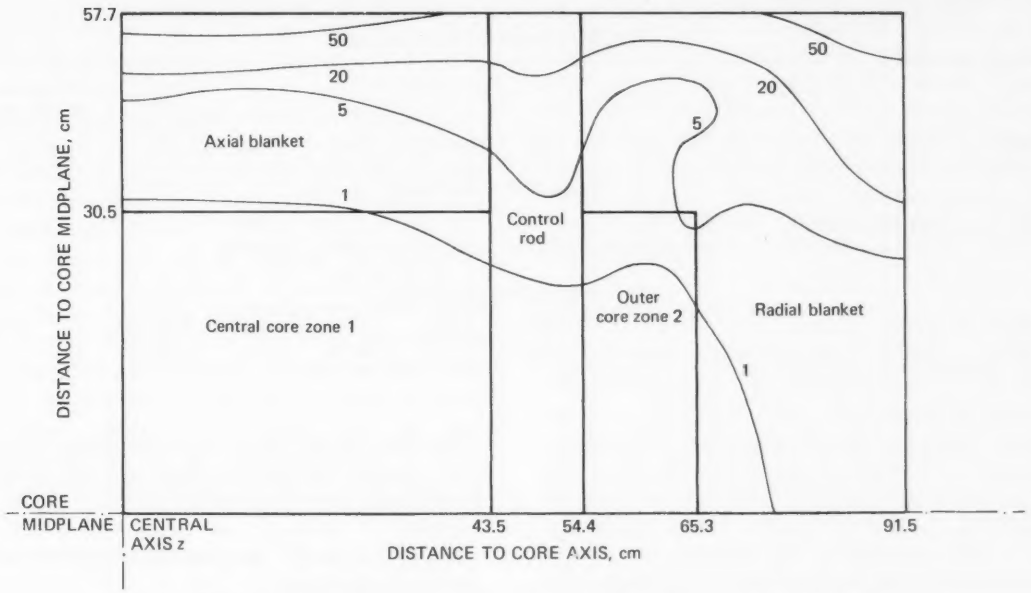

Fig. 9 Error (%) distribution for synthesized fission rate in SNEAK-2C. (Absorption rate in control rod.)

Table 7 Spatial Synthesis Calculation for a Two-Dimensional LMFBR Model at Middle of Cycle[26]

Calc.	k_{eff}	BR*	C1	C2	AB1	AB2	RB1	RB	$P_{max.}$ arbitrary units	$P_{max.}$ location, cm	
										r	z
			Regional Breeding Ratios								
DIF2D	1.003480	1.37081	0.50449	0.28833	0.24182	0.13552	0.11885	0.05181			
5 TF†	1.003058	1.37429	0.50592	0.28708	0.27193	0.13376	0.14979	0.05583			
3 TF	1.003015	1.38121	0.50634	0.28673	0.24187	0.13375	0.14980	0.06272			
1 TF	1.002440	1.39521	0.50886	0.28509	0.23832	0.13604	0.14903	0.07796			
			Regional Power Fractions								
DIF2D	1.003480	1.37081	0.5071	0.3816	0.0515	0.0235	0.0311	0.0052	0.75254	1.266	3.810
5 TF	1.003058	1.37429	0.5087	0.3798	0.0514	0.0233	0.0312	0.0055	0.75798	1.266	3.810
3 TF	1.003015	1.38121	0.5092	0.3793	0.0514	0.0234	0.0312	0.0055	0.76197	1.266	3.810
1 TF	1.002440	1.39521	0.5115	0.3773	0.0499	0.0249	0.0310	0.0054	0.76933	1.266	3.810

*BR = breeding ratio.
†TF = trial function.

performing such calculations for all regions in a planar slice through a reactor, a set of trial functions was constructed, each of which was analogous to a Green's function for the corresponding region. Trial functions 5 to 8 in Table 5 are examples. Such trial functions should be well-suited for describing changes taking place separately in the different regions. This means of choosing trial functions has worked well for coupled-core reactor models[31] but has been less successful for the analysis of more compact cores.[29]

Multichannel Blending Methods of Spatial Synthesis

Multichannel blending methods, as introduced by Wachspress and Becker[8] on a variational basis, have been extended to time-dependent problems by

Table 8 Spatial Synthesis Calculation for a Two-Dimensional LMFBR Model at Beginning of Cycle Using Middle-of-Cycle Trial Functions[26]

Calc.	k_{eff}	BR	C1	C2	AB1	AB2	RB1	RB2	$P_{max.}$ arbitrary units	$P_{max.}$ location, cm	
										r	z
			Regional Breeding Ratios								
DIF2D	1.042968	1.46050	0.46276	0.28740	0.27912	0.17329	0.17703	0.08090			
5 TF	1.040214	1.42670	0.47620	0.28065	0.28636	0.16808	0.14574	0.06966			
			Regional Power Fractions								
DIF2D	1.042968	1.46050	0.4858	0.4112	0.0398	0.0238	0.0324	0.0069	0.69292	1.266	3.810
5 TF	1.040214	1.42670	0.4998	0.4016	0.0407	0.0233	0.0286	0.0061	0.69032	1.266	3.810

Stacey[32] and rederived on a weighted-residual basis by Fuller et al.[33] This formalism allows the planar trial functions to be combined differently in different regions (channels) of the plane (or the use of different trial functions in different regions of the plane), which in essence allows the shape of the trial functions to be modified on a gross-region basis during the calculation. Such additional flexibility implies a greater accuracy and/or a greater range of applicable problems for a given set of planar solutions as trial functions, relative to the normal single-channel blending method, as has in fact been demonstrated by several tests.[32-36]

However, numerical difficulties have been encountered with the multichannel formalism which have hindered its implementation. The channel-to-channel coupling terms involve integrals over the mutual surface, and results have proved to be quite sensitive to numerical evaluation of these integrals. Moreover, the transport cross section is buried within these coupling terms following a series of matrix multiplications and inversions, making it burdensome to incorporate changes in the transport cross section (e.g., arising from density changes during a transient) into a calculation. Recent ideas on the use of overlapping polynomial domain functions to derive multichannel synthesis equations[37] eliminate these two difficulties, as well as provide a formalism that can be treated with existing single-channel codes with only minor modifications in the processing of the trial functions. The multichannel blending method should reemerge as the most promising of the spatial synthesis methods.

Synthesis of Reactivity Coefficients

Synthesis of reactivity coefficients can be performed as an adjunct calculation, once the synthesized flux and adjoint distributions are constructed, by performing the appropriate multidimensional perturbation integrals. Methods also have been developed for synthesizing three-dimensional reactivity coefficients directly[38,39] when it is not desirable or practical to construct explicitly the three-dimensional flux and adjoint distributions.

Anomalies

On occasion, anomalies have arisen in the application of spatial synthesis blending methods.[40,41] In addition, it has been possible to construct synthesis problems in which anomalous results were obtained for certain choices of cross sections and trial or weighting functions.[42-45] These situations occur because the synthesis approximation, in general, fails to preserve certain positivity properties associated with the direct finite-difference multigroup diffusion equations. Although that eigenvalue of the latter which is associated with the everywhere nonnegative (fundamental) eigensolution is always real and larger than the real part of any other eigenvalue, which ensures that iterative solution schemes that converge on the largest eigenvalue will converge to the fundamental eigensolution, this is not necessarily true of the synthesis approximation. Consequently it is possible for an iterative solution of the synthesis equations to converge to a solution that leads to a synthesized flux with negative components (harmonic) if the associated eigenvalue is larger than the eigenvalue corresponding to the fundamental eigensolution or not to converge at all if the eigenvalue with largest real part is complex.[41]

This situation represents a serious but not fatal flaw in synthesis approximations. The danger is not so much in the truly anomalous case, where a negative flux serves as a warning that something is amiss, which can be recognized and rectified by changing trial or

weighting functions. The real difficulty is that, in the vicinity of that combination of composition and trial/weighting functions which gives rise to an obvious anomaly, the synthesized result is quite sensitive to small changes in any of these quantities; inaccurate but not implausible results may be obtained. Practitioners have developed empirical tests to guard against this difficulty, but these are in the realm of black art and are rarely written down.

The situation is not so bleak as the preceding paragraph would indicate. Of the hundreds, perhaps thousands, of synthesis calculations that have been performed for realistic reactor models using reasonable trial and weighting functions, anomalies or associated difficulties have been found only a handful of times (the author knows of only three). Thus users and potential users of synthesis methods should be aware of but not distracted by the possibility of encountering such difficulties.

Polynomial Expansions in Space

Polynomial expansions in space were suggested[46-49] several years ago as a means for arriving at more accurate but more highly coupled coarse-mesh difference equations. Considering the polynomials, which were nonzero only over certain (generally overlapping) regions, as trial functions, the methods are very similar, if not entirely equivalent, to spatial synthesis methods.

A resurgence of interest has been kindled by the recent discovery (by reactor physicists/mathematicians) that the method has been highly developed by workers in structural mechanics, where it is known as the finite-element method.[50] The method is presently being investigated by several workers[51-57] for application to the neutron diffusion and transport equations.

In addition to yielding more accurate coarse-mesh equations than are obtained by the usual finite-difference approximation, which may or may not be a practical advantage for realistic reactor models in which description of the geometric detail requires a rather fine difference mesh, the finite-element method is convenient for the treatment of complex geometries. Elements (within which polynomial expansions are made) may be chosen in any shape or size (providing one is willing to work out the algebra) and may vary within a given model. Although this is also true, in principle, for the derivation of the ordinary finite-difference approximation, it has been exploited to a much greater extent in the finite-element approximation (e.g., Ohnishi's work[52,53]) and has come to be regarded as a unique characteristic of the latter.

Stacey[37] recently suggested a generalized nodal approximation in which spatial trial functions of the ordinary type are multiplied by polynomial domain functions, which may be considered as an extension of the finite-element method in which the polynomials are modulated by one or more spatial functions which account for details in the spatial distribution within an element. Henry[58] recently proposed the use of a single spatial trial function to modulate the polynomial within an element.

Coarse-Mesh Rebalancing

Coarse-mesh rebalancing as a means of accelerating the convergence of flux iteration procedures by using the most recent flux iterate as a single trial function, which could be used to collapse to a coarser spatial mesh, was introduced by Wachspress[59] within the context of variational synthesis. A theoretical foundation for the method was developed by Fröhlich[45,60] for the case of disjunctive, or nonoverlapping, coarse-mesh regions. He showed that the method retained the positivity properties of the fine mesh finite-difference equations for subdomain weighting and, under special circumstances, also for Galerkin weighting.

The method has been incorporated in many diffusion-theory and S_N codes. Gains in convergence attainable with coarse-mesh rebalancing in the GAMBLE-5 diffusion theory code are shown in Table 9, as reported by Fröhlich[61] for a typical high-temperature gas-cooled reactor (HTGR) application. Impressive improvements were also reported for TRIGA applications.

Nakamura[62-64] suggested the use of overlapping coarse mesh, obtained by superimposing overlapping domain functions on the most recent flux iterate, for rebalancing. Using "tent" domain functions, he demonstrated the superiority of the overlapping to the

Table 9 Efficiency of Variational Rebalancing for a Typical HTGR Two-Dimensional Diffusion Theory Problem[61]

Rebalancing	Iterations	Maximum relative flux change	k_{eff} error, %	Patch power error, %	Execution time, min (UNIVAC 1108)
No	70	0.01	0.02	84	6.0
No	140	0.003	0.0004	2.2	12.0
Yes	70	0.005	0.0004	2.0	8.2
Yes	140	0.0003	0.00001	0.06	14.7
No	300	0.00003	Reference case		26.6

disjunctive coarse-mesh rebalancing for a one-dimensional diffusion theory model,[62] as shown in Fig. 10. Here θ is the Chebyshev parameter, K is the number of coarse-mesh regions, and E_S is the error in the source. The rebalancing interrupted the normal Chebyshev accelerated iteration every n iterations. Nakamura[62] also considered a three-group two-dimensional diffusion theory model representative of a boiling-water reactor (BWR). He compared a coarse-mesh rebalanced (every five iterations) and a normal Chebyshev accelerated iteration and found the former to be much superior (see Fig. 11).

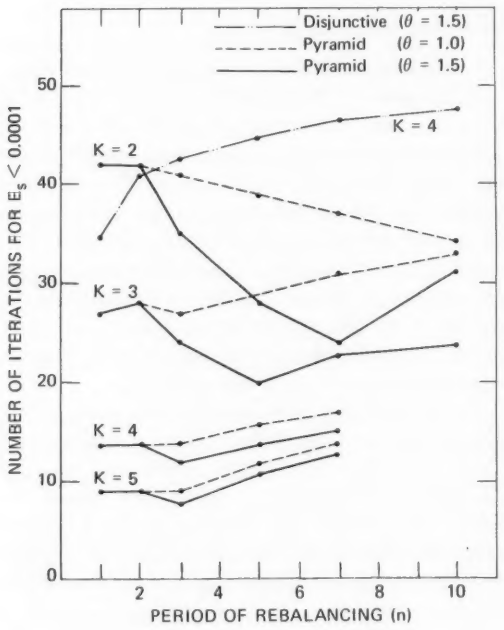

Fig. 10 Decay of error source for overlapping (pyramid) and disjunctive coarse-mesh rebalancing methods for a one-dimensional diffusion theory problem.[62]

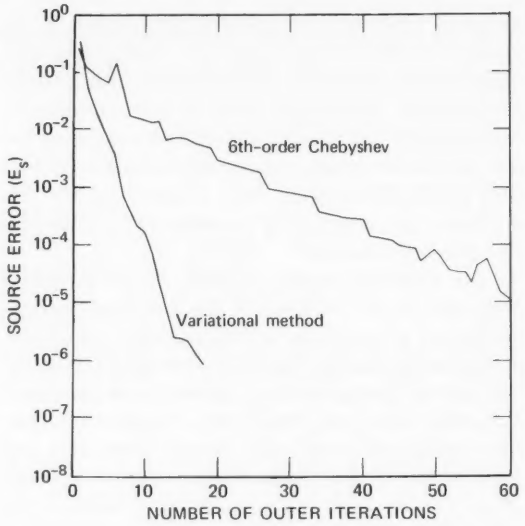

Fig. 11 Decay of source error for variational rebalanced and ordinary Chebyshev iteration procedures for a two-dimensional BWR diffusion theory calculation.[62]

Summary

Nonblending methods have been applied successfully to simple geometric configurations and, with iterative improvement of the trial functions, to relatively more complex geometries. However, for more realistic models, blending methods offer a distinct advantage and have been developed to a much greater extent. The single-channel synthesis method has been applied to quite complex geometrical models with rather impressive results, although the problem of obtaining trial functions for "driven" regions, such as blanket or reflectors, or for regions where the flux is highly nonseparable requires more work. Multichannel synthesis, which partially alleviates these difficulties, has encountered difficulties of a numerical type which, however, are eliminated by a new overlapping formulation. Thus it is expected that the development of an overlapping multichannel synthesis offers the potential for significant improvement in spatial synthesis blending methods.

The use of polynomial expansions in deriving coarse-mesh difference equations has been moderately successful in the past and currently is being investigated systematically. Coarse-mesh rebalancing, a special case of nonblending synthesis, has resulted in quite impressive gains when used to accelerate the iterative convergence of the finite-difference equations. Further development effort in both areas seems warranted on the basis of the results obtained to date.

SPECTRAL SYNTHESIS

Those methods in which precomputed spectral distribution functions (trial spectra) are blended together to obtain a (generally detailed) solution for the neutron-energy spectra are referred to as spectral

synthesis methods. The names energy-modal approximation, space–energy synthesis, and overlapping group have also been used to describe such methods. Calame and Federighi[4] were the first to develop and apply these methods. Subsequent authors have developed the theory,[65-68] and the methods have been successfully applied to cross-section interpolation and space- and time-dependent calculations in thermal and fast reactors.

Broad-Group Cross-Section Interpolation

Broad-group cross-section interpolation is a natural application of spectral synthesis methods, and it is not surprising that it was one of the first such applications. Differential nuclear data were averaged over two or more different flux spectra (corresponding to different compositions) to form two or more broad-group cross-section sets. When the averaging fluxes were considered as trial spectra, a spectral synthesis calculation yielded the appropriate combining coefficients for a given composition. These combining coefficients could then be used to interpolate directly among the cross-section sets.

Calame et al.[69] combined "hard" (high absorption) and "soft" (low absorption) thermal-neutron trial spectra calculated for media consisting of $1/v$ absorbers to calculate thermal-group diffusion theory parameters. They employed different trial spectra for each different moderator temperature considered. A comparison of interpolated (SPG) thermal-group cross sections with thermal-group cross sections averaged over a composition-dependent spectrum calculated for the thermal-energy region by the multigroup code SOFOCATE is given in Table 10 for a representative PWR composition. The interpolated cross sections are generally within 1% of the directly calculated values, yet the time required for synthesis solution and interpolation was approximately $\frac{1}{60}$ of that for the SOFOCATE calculation.

Ombrellaro et al.[70,71] considered the interpolation of fast-neutron broad-group cross sections. Using hard and soft trial spectra, Ombrellaro and Federighi[70]

Table 10 Comparison of Synthesized (SPG) and Directly Calculated (SOFOCATE) Thermal-Group Constants for a Representative PWR Composition[69]

Hydrogen N = 0.03136 Aluminum N = 0.002982
Oxygen N = 0.01568 ^{235}U N = 0.0001342
Zirconium N = 0.02067 ^{238}U N = 0.00000825

	68°F		300°F		500°F	
	SOFOCATE	SPG	SOFOCATE	SPG	SOFOCATE	SPG
Diffusion Theory Parameters						
Σ_a, cm^{-1}	0.07642	0.07551	0.06600	0.06519	0.05977	0.05903
$\nu\Sigma_f$, cm^{-1}	0.13640	0.13460	0.11750	0.11588	0.10620	0.10465
D, cm	0.34040	0.34330	0.36540	0.36720	0.38610	0.38690
Microscopic-Absorption Cross Section (σ_a)						
Unit $1/v$	0.7345	0.7258	0.6474	0.6397	0.5932	0.5863
Hydrogen	0.2438	0.2409	0.2149	0.2123	0.1969	0.1946
Oxygen	0.1469×10^{-3}	0.1451×10^{-3}	0.1295×10^{-3}	0.1279×10^{-3}	0.1186×10^{-3}	0.1172×10^{-3}
Zirconium	0.1322	0.1306	0.1165	0.1151	0.1068	0.1055
Carbon	0.2350×10^{-2}	0.2322×10^{-2}	0.2072×10^{-2}	0.2047×10^{-2}	0.1898×10^{-2}	0.1867×10^{-2}
Aluminum	0.1689	0.1669	0.1489	0.1471	0.1364	0.1348
^{235}U	0.4882×10^{3}	0.4824×10^{3}	0.4202×10^{3}	0.4150×10^{3}	0.3797×10^{3}	0.3750×10^{3}
^{238}U	0.2005×10^{1}	0.1981×10^{1}	0.1767×10^{1}	0.1746×10^{1}	0.1619×10^{1}	0.1600×10^{7}
^{135}Xe	0.2306×10^{7}	0.2227×10^{7}	0.2128×10^{7}	0.2071×10^{7}	0.1940×10^{7}	0.1895×10^{7}
^{232}U	0.4316×10^{3}	0.4271×10^{3}	0.3796×10^{3}	0.3763×10^{3}	0.3482×10^{3}	0.3456×10^{3}
Hydrogen transport	0.2938×10^{2}	0.2892×10^{2}	0.2590×10^{2}	0.2551×10^{2}	0.2370×10^{2}	0.2338×10^{2}
Microscopic Fission Production Cross Sections ($\nu\sigma_f$)						
^{235}U	0.1016×10^{4}	0.1003×10^{4}	0.8756×10^{3}	0.8635×10^{3}	0.7909×10^{3}	0.7798×10^{3}
^{233}U	0.1004×10^{4}	0.9927×10^{3}	0.8865×10^{3}	0.8763×10^{3}	0.8152×10^{3}	0.8055×10^{3}

interpolated fast broad-group cross sections (for representative PWR compositions) which compared favorably with broad-group cross sections obtained by averaging over a multigroup spectrum calculated for the composition of interest.

Ombrellaro and Snyder[71] applied spectral synthesis to interpolate one- and three-group constants for a range of LMFBR core mixtures. They calculated 50-group trial spectra for two extreme compositions (denoted by trial spectra 1 and 2 in Table 11), which were used to collapse to one- and three-group cross-section sets. Then a range of intermediate compositions, two of which are given in Table 11, was considered. Synthesis-extrapolated and directly calculated (i.e., collapsed over a 50-group spectrum calculated for that composition) group cross sections are compared in Table 12 for core 1. Similar results were obtained for core 2 and for cores in which the sodium was partially voided.

Table 11 Compositions for LMFBR Spectral Synthesis Calculations[71]

Isotope	Core 1	Core 2	Trial spectra 1	Trial spectra 2
^{16}O	0.012406	0.015531	0.009318	0.018640
^{56}Fe	0.008962	0.010685	0.007293	0.012684
^{238}U	0.004598	0.005905	0.003328	0.007214
^{239}Pu	0.000861	0.000976	0.000732	0.001085
^{52}Cr	0.002341	0.002791	0.001905	0.003313
^{59}Ni	0.000922	0.001099	0.000750	0.001305
^{241}Pu	0.000067	0.000068	0.000051	0.000076
^{240}Pu	0.000344	0.000390	0.000293	0.000434
^{23}Na	0.012107	0.009880	0.014312	0.007556
PFP1	0.000340	0.000426	0.000255	0.000511

These results indicate that the use of spectral synthesis to calculate composition-dependent combining coefficients for the interpolation among broad-group cross-section sets is an economic and relatively accurate means for obtaining composition-dependent broad-group cross sections. However, the ability of these methods to deal with the contribution of heavy-element resonance cross sections has not been adequately examined.

Calculation of Spatially Dependent Thermal-Neutron Spectra by Spectral Synthesis

Application of spectral synthesis to the calculation of spatially dependent thermal-neutron spectra was first carried out by Calame and Federighi.[4] They argued that the thermal-neutron spectrum in a two-region model consisted of two components: (1) neutrons which became thermal in region 1, with a thermal spectrum characteristic of that medium, and thereafter diffused throughout space while retaining that spectrum and (2) neutrons which became thermal in region 2 and thereafter diffused throughout space while retaining that characteristic spectrum. Thus they were led to blend infinite media spectra characteristic of the two regions, with the knowledge that one or the

Table 12 Comparison of Synthesized and Directly Calculated Few-Group Constants for a Typical LMFBR Composition[71]

Parameters	Exact values	Differences of synthesis values from exact values, %: One-group synthesis P_0	One-group synthesis P_1	Three-group synthesis P_0	Three-group synthesis P
		Groups 1–50			
D	0.20284 + 1	−0.05	0.003	0.02	0.21
$\nu\Sigma_f$	0.61550 − 2	−0.12	−0.04	−0.02	0.21
Σ_a	0.42335 − 2	−0.11	−0.11	−0.04	−0.12
Σ_t	0.56574 − 1	0.16	0.14	0.002	−0.025
$\langle\phi\rangle$	0.10764 + 3	0.12	0.04	0.02	−0.27
$\langle J\rangle$	0.10917 + 2	0.06	0.05	0.03	−0.08
$\langle\nu\Sigma_f\phi\rangle$	0.66254 + 0	−0.003	0.0	−0.008	−0.06
		Groups 1–18			
D	0.23432 + 1	0.003	0.04	−0.01	0.13
$\nu\Sigma_f$	0.65567 − 2	−0.04	0.03	−0.07	0.23
Σ_a	0.32667 − 2	−0.03	0.004	−0.043	0.10
Σ_t	0.53562 − 1	−0.01	−0.007	−0.02	0.01
$\langle\phi\rangle$	0.71918 + 2	−0.05	−0.01	0.08	0.05
$\langle J\rangle$	0.84263 + 1	−0.04	0.03	0.07	0.18
		Groups 19–30			
D	0.14266 + 1	0.009	0.01	0.003	0.022
$\nu\Sigma_f$	0.47841 − 2	−0.04	−0.04	−0.04	−0.05
Σ_a	0.51509 − 2	−0.07	−0.080	−0.06	−0.10
Σ_t	0.58163 − 1	0.02	0.014	0.03	0.001
$\langle\phi\rangle$	0.33108 + 2	0.51	0.20	−0.07	−0.83
$\langle J\rangle$	0.23616 + 1	0.52	0.21	−0.07	−0.80
		Groups 31–50			
D	0.98474 + 0	−1.2	−1.1	0.05	0.06
$\nu\Sigma_f$	0.12465 − 1	−0.76	−0.61	0.89	0.91
Σ_a	0.19206 − 1	−0.70	−0.56	0.77	0.79
Σ_t	0.11928 + 0	3.2	2.9	0.52	0.49
$\langle\phi\rangle$	0.26150 + 1	0.39	−0.42	−0.72	−1.8
$\langle J\rangle$	0.12876 + 0	−1.6	−1.5	−0.66	−1.7

other was appropriate far away from the interface between the two media and with the hope that a combination of the two infinite media spectra would be a good approximation in the vicinity of the interface. Calame and Federighi developed coupled equations for the spatially dependent combining coefficients and successfully applied the method to the analysis of experiments. The method subsequently has been incorporated into a number of codes and used extensively, yielding results comparable in accuracy to those obtained by a more expensive multigroup treatment of the thermal-energy spectrum in a spatially dependent calculation.

Extensions and refinements of this method, which is generally known as the two-overlapping-group method, have been suggested by several authors. Leslie[72] considered the terms that coupled the two equations for the combining coefficients as "removal" cross sections from one spectral distribution to another and established a physical basis for their definition and computation. Breen and Yasinsky[73] proposed a particular choice of weighting spectra which partially decoupled the two equations for the combining coefficients so that they could be solved with conventional two-group iteration schemes. Natelson[74] employed the method to develop a two-overlapping thermal-group approximation for the discrete-ordinates representation of the transport equation, used a technique similar to that of Breen and Yasinsky to simplify the equations, and obtained results that compared rather well with Monte Carlo calculations. Selengut[75] examined the choice of weighting spectra, which traditionally are chosen as E (the energy variable) and unity, and suggested that $\sqrt{E}$ was a better choice than E.

Fast Reactor Applications of Spectral Synthesis

Fast reactor applications of spectral synthesis were first investigated by Stacey[65] and by Storrer and Chaumont.[76] Stacey considered a two-region model (core and blanket) representing a fast reactor critical facility. As trial spectra he chose: (1) a zero leakage spectrum characteristic of the core medium and (2) the spectrum resulting from solving a source problem in an infinite medium of the blanket material, using as the source the ^{238}U fission spectrum characteristic of the core medium. He demonstrated that the first trial spectrum was appropriate at the center of the core, that the second trial spectrum was a good approximation deep in the blanket, and that a mixture of the two provided a reasonable approximation in the vicinity of the interface.

These early studies have been extended by several authors[77-84] in an attempt to establish the feasibility of spectral synthesis for fast reactor analysis, where the possibility of obtaining the necessary spectral detail by blending a few trial spectra promises significant economy relative to a direct calculation with the large number of groups which would be required for an equivalent multigroup spectral representation. Different choices of trial and weighting spectra have been compared, and the advantages of using different sets of trial or weighting spectra in different spatial regions has been examined. Neuhold and Ott[79] and Neuhold[80] introduced the idea of weighting with reaction rates, which they found to be generally superior to Galerkin weighting and comparable to adjoint weighting. Errors in the synthesis calculation of the absorption rate in a slab model of an LMFBR are shown in Fig. 12. Because

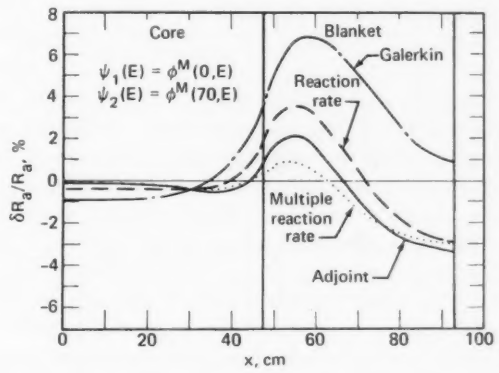

Fig. 12 Error in the synthesized absorption rate in a one-dimensional LMFBR model for different weighting functions.[80]

the purpose of this study was to assess different weighting spectra, the trial spectra were taken as the exact solutions at the center of the core and at the center of the blanket. The two weighting functions in the case designated "reaction rate" were the product of the core macroscopic fission cross section with the two trial spectra. For the case designated "multiple reaction rate," the two weighting functions used in the core were the products of the core macroscopic-absorption cross section with the two trial spectra, and the two weighting spectra used in the blanket were the products of the blanket macroscopic-absorption cross section with the two trial spectra. "Galerkin" refers to the use of the trial spectra also as weighting spectra, and "adjoint" refers to the use of the exact adjoint

spectra at the center of the core and at the center of the blanket as weighting spectra. Best results with reaction-rate weighting were obtained by using different reaction rates when calculating different integral quantities, which becomes impractical.

Several authors[79-83] have found that the use of different sets of trial and/or weighting spectra appropriate to the different regions of a reactor generally results in a better approximation than can be obtained by using the same number of trial spectra throughout the reactor. Neuhold and Ott[79] and Kiguchi et al.[81] found that, in regions where the spectrum was largely influenced by another region (e.g., a blanket), a spectrum calculated for the "driven" medium with a leakage source or a buckling representing the neighboring "driver" region was a better trial spectrum than an isolated fundamental-mode solution for the driven medium. Neuhold and Ott[79] demonstrated the importance of using an adequate fundamental-mode leakage representation for both core and blanket calculations.

Kiguchi et al.[81] found that the sodium-void worth in an LMFBR model was predicted more accurately by a spectral synthesis calculation than by a conventional few-group calculation requiring equivalent computing time. Stacey[84] concluded that the spectral synthesis method was superior to few-group methods (requiring equivalent computing time) for treating the reactivity worth of sodium voiding and the interacting Doppler worth during a transient in a space-independent LMFBR model. Both authors used trial spectra calculated for core regions with extremes in sodium concentration to synthesize the spectrum for intermediate sodium concentrations. Stacey[85] also demonstrated the ability of spectral synthesis to treat local sodium voiding in spatially dependent kinetics calculations.

Multidimensional Geometries in Spectral Synthesis Equations

Multidimensional geometries pose special problems for the solution of the spectral synthesis equations. Although the spectral synthesis and multigroup equations are formally identical, the coupling among equations is much greater for the former, with the result that the diffusion coefficient and removal matrices, which are diagonal for the multigroup equations, and the scattering matrix, which generally is lower triangular for the multigroup equations, are all full for the spectral synthesis equations. Thus the iterative solution techniques, which have been developed for the multigroup equations and which take advantage of the special nature of these equations, cannot be used directly for the solution of the spectral synthesis equations. This is particularly true for the inner iterations, which are used to invert matrices, and the acceleration of the outer iterations.

Although there are two possible means of resolving this difficulty, modification of the multigroup iteration schemes together with recasting of the spectral synthesis equations or the development of new iteration strategies especially for the spectral synthesis equations, only the former alternative has been explored. Robkin[86] and Lorenzini and Robinson[87] suggested a series of transformations which reduced the spectral synthesis equations to a form that can be solved by multigroup codes. Such transformations basically involved the diagonalization of the diffusion-coefficient matrix, followed by the addition to the fission source term of those parts of the scattering and removal matrix which do not conform to the multigroup structure. Lorenzini and Robinson[87] were able to solve two-dimensional LMFBR spectral synthesis problems with a standard multigroup code, although they generally found that more iterations were required than for multigroup problems with the same number of unknowns. Numerical instabilities associated with the complete coupling in the scattering matrix (they used a code that allowed upscattering and hence a full scattering matrix) were encountered, and modifications of the diagonal terms were introduced to suppress this difficulty. Although they compared spectral synthesis and few-group approximations, their results were inconclusive as to which was superior. They introduced the idea of using one-dimensional calculations to generate trial spectra appropriate to different regions in a two-dimensional model.

Greenspan[88] also applied spectral synthesis to two-dimensional LMFBR models, using a formulation similar to that of Lorenzini and Robinson to enable the equations to be solved with a standard multigroup code. His model consisted of two core regions, axial and radial blankets, and a radial reflector. Trial spectra (24 group) were: (1) a fundamental-mode solution for the dominant core material, (2) a source solution for the axial blanket material utilizing the leakage spectrum from the core trial spectrum as a source, and (3) a source solution for the reflector material utilizing the leakage spectrum from the blanket trial spectrum as the source. Greenspan employed subdomain (in energy) weighting whereby the 24 groups were distributed among three energy intervals and each weighting spectrum was unity within one energy interval and zero within the others. For comparison, he

performed several few-group calculations in which the few-group constants were collapsed over the spectrum of the dominant core region (i.e., the first trial spectrum). He found that the spectral synthesis calculations required on the order of 10% greater computing time than the few-group calculations with the same number of unknowns (i.e., in which the number of trial spectra and few groups were equal) but that considerably more few groups than trial spectra were required to obtain comparable accuracy, so that the spectral synthesis approximation was superior to the few-group approximation in this application. Computing time requirements and important reactor parameters are compared with the results of direct 24-group calculations in Tables 13 and 14.

Table 13 Comparison of k_{eff} and Computing Times for a Two-Dimensional LMFBR Problem[88]

	k_{eff}	Time, sec
Reference Case		
24 group	1.05883	414
3 TF synthesis	1.05911	109
3 group	1.07787	84
4 group	1.07064	102
8 group	1.06412	149
Sodium Voided in Dominant Core*		
24 group	1.05447	430
3 TF synthesis	1.04706	99
3 group	1.07446	88
4 group	1.06665	105

*Same trial functions and collapsing spectrum used as in the reference case.

Iterative Improvement of Trial Spectra

Iterative improvement of trial spectra has been investigated by several authors.[89-92] Two general methods have been considered; successive iteration between spectral and spatial synthesis[65,89,90] and the use of approximate solutions together with a single-group diffusion kernel to arrive at zero-dimensional equations from which an approximation to the spectrum at a point in a reactor can be obtained.[91,92]

Toivanen,[89] considering a small intermediate-spectrum reactor, found that asymptotic spectra representative of the different regions in the reactor were inadequate trial spectra. He found that iteration between spatial and spectral synthesis, as suggested by Stacey,[65] significantly improved the trial spectra and hence the accuracy of the calculation. A similar idea was pursued by Lancefield[90] in applying spectral synthesis to a fast reactor model. Lancefield also suggested the use of homogeneous functionals of the flux, such as reflector reaction rates, in deriving the synthesis equations so as to improve the accuracy of the flux solution in the reflector. This latter idea is similar to Neuhold's[80] use of multiple reaction-rate weighting.

Cockayne and Ott,[91] based on studies of a two-region (core-blanket) LMFBR model, concluded that the actual spectra occurring at selected points in a

Table 14 Power Fractions and Breeding Ratios for a Two-Dimensional LMFBR Problem[88]

	Core 1	Core 2	Axial blanket 1	Axial blanket 2	Radial blanket	Total
			Power Fraction			
24 group	0.6572	0.3233	0.0080	0.0032	0.0083	
3 TF synthesis	0.6609	0.3162	0.0105	0.0040	0.0084	
3 group	0.6458	0.3239	0.0130	0.0048	0.0125	
4 group	0.6513	0.3776	0.0089	0.0035	0.0087	
8 group	0.6541	0.3227	0.0096	0.0037	0.0099	
			Breeding Ratio			
24 group	0.5080	0.1496	0.2124	0.0691	0.1932	1.1323
3 TF synthesis	0.5096	0.1479	0.2178	0.0706	0.1908	1.1367
3 group	0.5032	0.1547	0.1877	0.0626	0.1805	0.0886
4 group	0.5048	0.1535	0.1930	0.0642	0.1828	1.0983
8 group	0.5077	0.1512	0.2035	0.0647	0.1891	0.1162

reactor made the best trial spectra. They examined several methods of approximating such spectra. The fundamental-mode spectrum of the core material was found to be a very good approximation to the actual spectrum over much of the core, but the fundamental-mode spectrum for the blanket material was found to be a very poor approximation to the actual spectrum in the blanket. The blanket spectrum, calculated using as a source the fundamental-mode core leakage spectrum, was found to be a good approximation to the actual spectrum over a portion of the blanket and resulted in a relatively accurate synthesis solution when used as a trial spectrum. These authors developed an approximate procedure for computing the spectrum at a point in a reactor model which consists of three steps: (1) calculation of an approximate flux from a two-spectra synthesis problem using two readily available spectra; (2) calculation of special "group constants" at the specific spatial location using as weight functions the approximate flux from step 1 and a single-group diffusion kernel; and (3) solution of the resulting zero-dimensional equation for the spectrum at the point, which is then used as a trial spectrum. Use of this procedure in one LMFBR problem significantly reduced the error in blanket absorption rates (from 1.27 to 0.6%) and fission rates (from 3.64 to 0.17%) relative to the results of step 1. This procedure may be limited, in practice, to one-dimensional problems because of complexities associated with the diffusion kernel in multidimensional geometries.

Summary

Spectral synthesis has been demonstrated to be an economical and accurate approximation to a detailed multigroup representation of the neutron spectrum for many applications and generally to be superior to the conventional few-group reduction of the multigroup representation. If detailed multigroup trial spectra are blended, the spectral synthesis method has the potential for representing the spectrum in great detail with a relatively simple calculational model. As was the case with spatial synthesis, the spectral synthesis approximation does not retain the positivity properties of the multigroup equations, and anomalous results can be obtained.

The use of spectral synthesis to interpolate among broad-group cross-section sets averaged over different fine-group spectra has been successfully demonstrated for the thermal- and fast-neutron energy regimes. However, treatment of the composition and temperature dependence of heavy-element (e.g., uranium) narrow-resonance cross sections should be developed and evaluated to a greater degree.

Spatially dependent spectral synthesis (overlapping thermal-group) methods have been successfully applied to the thermal-neutron regime for many years. Applications to the fast-neutron-energy regime and to fast reactors have been more recent. However, the adequacy and economy of spectral synthesis calculations for fast reactors seem to be relatively well established. The fact that the spectral synthesis equations (suitably modified) can be solved by standard multigroup codes enhances the attractiveness of the method. The calculation of trial spectra representative of "transition" regions near region interfaces substantially improves the accuracy in these transition regions. Two areas in which more work is needed are: (1) adaptation of standard multigroup iteration schemes and of the spectral synthesis equations to achieve an efficient means for solving the latter in multidimensional geometries and (2) development of economical means for computing trial spectra characteristic of "transition" regions and other regions where the asymptotic spectrum characteristic of the medium is a poor approximation to the actual spectrum.

TRANSPORT-THEORY APPLICATIONS OF SYNTHESIS METHODS

In the preceding sections the use of synthesis methods to solve the multigroup diffusion or P_1 equations has been emphasized. In this section, three types of applications of synthesis methods to neutron-transport theory are reviewed. The first such application is the derivation of approximations to the transport equation in which the continuous angular dependence is discretized. The second application is to the solution of these discretized equations, using methods similar to those which have been discussed in previous sections. Finally the application of spatial synthesis methods directly to the transport equation, preceding the discretization of the angular dependence, is discussed.

Discretization of Angular Dependence

Discretization of the angular dependence is the normal first step in seeking a solution to the neutron-transport equation. Expansion in spherical harmonics and direct discretization, leading to P_N and discrete-ordinates approximations, respectively, are traditional methods in reactor physics. Selengut[3] showed that, when the first two Legendre polynomials were con-

sidered as angular trial functions in a variational derivation, the resulting synthesis equations were the P_1 equations. This insight precipitated the development of a number of discrete approximations which were variants on the P_N or discrete-ordinates approximations.

Pomraning and Clark[93] derived an improved form of diffusion theory, which had an asymptotic transport-theory diffusion coefficient, by making a two-term expansion of the angular dependence of the neutron flux. Numerical comparisons based on a thermal-group cell problem indicated that his improved diffusion theory was comparable in accuracy to P_3 theory. Palveri-Fontana and Amster[94] also derived an alternate diffusion theory, featuring a different definition of the diffusion coefficient, based on a double P_0 expansion of the angular distribution and utilizing a discontinuous trial-function variational formulation.

Kaplan et al.[95] used circles and ellipses as angular trial functions to reduce the transport equation to an angular discrete approximation. They noted that discrete-ordinate approximations could be derived in this manner by choosing the angular trial functions as constant within each solid-angle element. Schreiner and Selengut[96] proposed a similar derivation of discrete-ordinate equations, using linear polynomials in the cosine of the angular variable within each solid-angle element.

Natelson[97] suggested a strategy for deriving a discrete approximation by using at each spatial point the angular distribution (in a high-order discrete-ordinate approximation) obtained from a reference calculation as an angular trial function. He also suggested some approximate strategies for obtaining the angular trial function when a high-order discrete-ordinate approximation was impractical. Using these angular trial functions (one at each spatial mesh point but different trial functions at different mesh points) obtained for a reference or "representative" problem, he derived diffusion-theory-type approximations that were then applied to similar problems. He obtained impressive results for this space-angle-synthesis (SAS) approximation for a variety of realistic problems. One such problem is depicted in Fig. 13, and the results obtained with SAS and P_1 diffusion theory are compared to a high-order discrete-ordinate (D_{16}) solution in Table 15.

Several authors[98-100] have examined the variational synthesis derivation of discrete-ordinate equations. Jauho and Kalli[98] proposed two methods for choosing the set of directions and weights to be used in

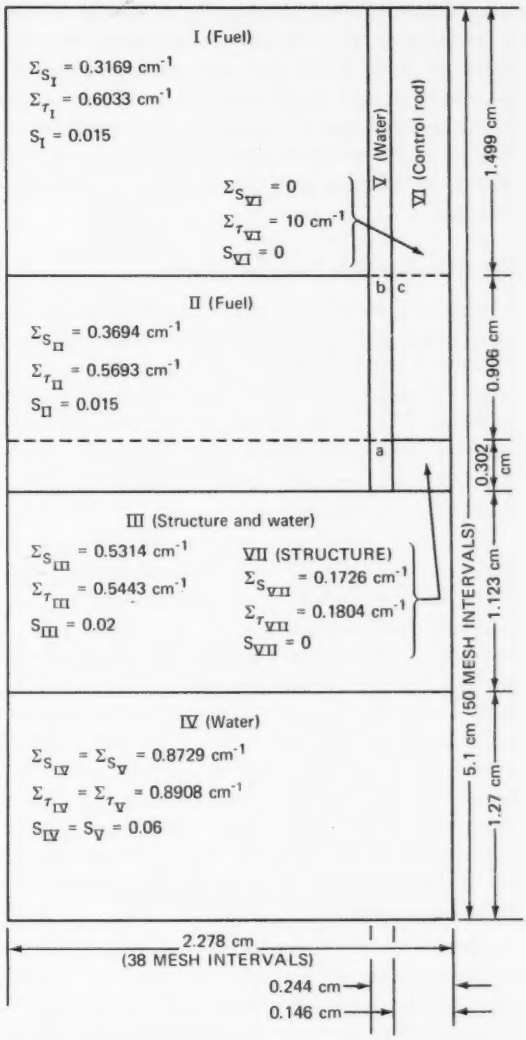

Fig. 13 Heterogeneous PWR cell model for space-angle-synthesis calculations.[97]

the standard S_N equations. Kaplan[99] used angular trial functions that were constant within each solid-angle element, but oriented the solid-angle elements differently at adjacent spatial mesh points, in seeking discrete-ordinate equations that would be free of the troublesome "ray" effect.

Natelson[100] found that a variational derivation of the standard discrete-ordinate approximation in two dimensions also yielded a relation between the weights and the directions but that use of this relation did not produce results significantly different from those of

the standard discrete-ordinate scheme. He also derived a modified discrete-ordinate approximation that consisted of pairs of coupled diffusion-type equations, with each increase in the order of the approximation adding another pair of equations. The potential advantage of the modified approximation is its inherent ability to mitigate ray effects, thus to serve as a standard.

Spatial Synthesis in Transport Theory

Spatial synthesis in transport theory has developed along two lines. One procedure involves the blending of discretized transport-theory solutions of lower dimensional (in space) problems to obtain higher dimensional solutions.[101-103] A second procedure consists in reducing the spatial dimensionality by blending spatial trial functions, then carrying out the angular discretization on the spatially reduced equations.[104-106]

The first procedure is typified by the work of Natelson and Gelbard,[102] who blended two-dimensional discrete-ordinate solutions with combining coefficients which depended on the third spatial variable but not on the angular variable. The equations that resulted for the combining coefficients were of the same form as in the case of diffusion theory synthesis, which facilitated implementation of the method in an existing diffusion-theory spatial synthesis code. This method has the potential for synthesizing angular distributions in the plane of the trial-function calculation but has no provision for treating angular effects not in that plane (i.e., it can handle azimuthal but not polar angular effects).

Cobb's[106] work represents the most extensive development of the second procedure. He blended one-dimensional spatial shapes, with combining coefficients which depended on the other spatial variable and the angular variable, to reduce a two-dimensional transport equation (one group) to a coupled set of one-dimensional transport equations. A discrete-ordinate approximation was then made for the latter. He used the multichannel synthesis approximation to allow different combining coefficients to be used in different spatial regions. A comparison with a direct S_4 two-dimensional calculation is given in Table 16 for a small 10-cm square fuel assembly with a 4-cm-square absorber in one corner. The two trial functions were one-dimensional S_4 calculations along traverses that did and did not pass through the absorber. These results indicate that this type of synthesis approximation can yield rather accurate results, even for this highly nonseparable problem, together with a considerable savings in computing time relative to the direct solution.

Lancefield's[90] work with spectral synthesis also utilized the second procedure. He used trial spectra to discretize the energy representation of the transport equation and then used a discrete-ordinates approximation to solve the resulting equations.

Summary

The use of variational synthesis methods to discretize the angular dependence of the neutron-transport equation not only provides a consistent means of deriving the standard (e.g., S_N, P_N) approximations but also provides a systematic procedure for deriving alternate approximations. Exploitation of this technique has been limited, but the results have been promising, suggesting that further effort in this area is warranted.

Standard spatial synthesis methods, involving the blending of two-dimensional transport solutions with angle-independent combining coefficients, are inherently incapable of treating angular effects not in the plane of the two-dimensional solutions. An extension of these methods to use angle-dependent combining coefficients would seem to be worthwhile.

A second type of spatial synthesis, in which a spatial expansion is used to reduce the dimensionality of the problem prior to the discretization of the angular dependence, also has been employed with encouraging results. Further investigation is required to determine if this type of spatial synthesis has any advantage or disadvantage with respect to the standard type.

VARIATIONAL PRINCIPLES

Significant advances in flux synthesis methods have proceeded, almost without exception, from advances in the underlying variational theory. Although the entire theory of flux synthesis methods can be constructed with the method of weighted residuals, and all the advances can be derived therefrom without recourse to variational methods, the fact remains that variational theory has played a central role in the development of flux synthesis methods. Thus this section is devoted to a review of those developments in variational theory which are relevant to flux synthesis methods. Construction of variational principles, extension of variational principles to admit a wider class of trial functions, and the transformations that relate different variational principles will be discussed.

Table 15 Space-Angle-Synthesis Calculations for PWR Cell Model[97]

	Total absorptions in region									
	I	II	III	IV	V	VI	VII	a	b	c
Representative Problem										
$D_{1\phi}$ (standard result)	0.8989×10^{-1}	0.9642×10^{-1}	0.1234×10^{-1}	0.2784×10^{-1}	0.5015×10^{-3}	0.9605×10^{-1}	0.8415×10^{-4}	0.1339×10^{-3}	0.1877×10^{-3}	0.5367×10^{-1}
% error in SAS	−0.78%	−0.41%	−0.6%	−0.47%	−0.8%	1.3%	−1.66%	−2.17%	0.45%	1.68%
% error in P_1 approx.	−8.12%	−9.3%	−10.5%	−15.6%	−8.9%	22.4%	−12.9%	−16.9%	0.5%	27.7%
Test Problem I (Beginning-of-Life Configuration) $S_I = S_{II}$ Becomes 0.022383, S_{III} Becomes 0.027014, and $S_{1V} = S_V$ Becomes 0.051743										
$D_{1\phi}$ result	0.1045	0.1048	0.1273×10^{-1}	0.2708×10^{-1}	0.5427×10^{-1}	0.1060	0.8804×10^{-4}	0.1404×10^{-3}	0.2010×10^{-3}	0.5762×10^{-1}
% error in SAS	−1.05%	−0.29%	−0.26%	1.15%	0.46%	1.05%	0.56%	−1.43%	1.4%	1.75%
% error in P_1 approx.	−7.76%	−9.7%	−15.7%	−14.8%	−8%	23.2%	−13.05%	−17.1%	1.05%	28%
Test Problem II (End-of-Life Configuration) Sources Are as in Test Problem I, $\Sigma_{\tau I}$ Becomes 0.48 in.$^{-1}$, and $\Sigma_{\tau II}$ Becomes 0.427 in.$^{-1}$; Σ_{S_I} and $\Sigma_{S_{II}}$ Are Unchanged										
$D_{1\phi}$ result	0.9965×10^{-1}	0.4429×10^{-1}	0.1551×10^{-1}	0.3119×10^{-1}	0.8066×10^{-3}	0.1642	0.1128×10^{-3}	0.1829×10^{-3}	0.2942×10^{-3}	0.8360×10^{-1}
% error in SAS	2.2%	−2.6%	2.1%	3.4%	2.5%	1%	2.2%	0.16%	2.2%	0.88%
% error in P_1 approx.	−12.6%	−18%	−20.6%	−18.2%	−10%	18.3%	−18.2%	−22.8%	−3.7%	20.2%

Table 16 Comparison of Two-Dimensional Transport Results with Spatial Transport Synthesis[106]

Assembly region	DOT S_4 results	% deviations from DOT results: S_4 synthesis (N channels) $N=1$	$N=2$	$N=3$	$N=4$	Diffusion theory
Total assembly						
Absorption rate	0.37060	+0.111	−0.067	+0.040	+0.002	−4.55
Leakage rate	0.62940	−0.065	+0.039	+0.041	−0.001	+2.68
Fission source	1.0	0.0	0.0	0.0	0.0	0.0
Eigenvalue (k_{eff})	1.10699	−0.404	−0.019	+0.017	−0.004	−12.85
Fuel region						
Absorption rate	0.31449	−0.456	−0.017	+0.022	−0.008	−10.2
Leakage rate	0.67207	+0.135	+0.010	−0.003	−0.002	+3.94
Fission source	0.98656	−0.054	+0.001	+0.005	−0.004	−0.556
Absorber region						
Absorption rate	0.05612	+3.28	−0.364	−0.602	+0.040	+26.9
Leakage rate	−0.04265	−3.15	+0.370	+0.598	−0.043	−22.6
Fission source	0.01347	+3.70	−0.345	−0.62	+0.047	+40.5
Computing time, sec	18.03	2.70	5.94	9.33	12.84	3.84

Construction of Variational Principles for Neutron Transport and Diffusion Theory

Construction of variational principles for neutron transport and diffusion theory has been, one suspects, largely a matter of inspiration. However, some effort has been devoted to the development of procedures for systematically deriving variational principles.

Pomraning[107-110] and Lewins[111,112] have suggested a method to derive variational principles for the estimation of some integral parameter. They adjoined the neutron transport/diffusion equations to the functional which defined a parameter of physical interest by means of Lagrange multipliers, in the way that constraints are treated in the formulation of a problem in the classical calculus of variations. It turned out that the Lagrange multipliers must satisfy the adjoint equations in order for the resulting functional to be a variational principle.

Becker[113] and Mikhlin[114] suggested "least-squares" variational principles formed by "squaring" the neutron transport/diffusion equations and integrating over the independent variables. Such principles, which have the advantage of not requiring the use of an adjoint but the disadvantage of higher order differential operators in the final synthesis equations, have been little used.

Selengut[115] and Pomraning[108] developed variational principles by considering a functional Taylor's series expansion of the functional which defined the integral parameter of interest. Termination of the series with the quadratic term, plus the requirement of accuracy to second order in the trial function, led to the appropriate variational principle.

Pomraning[108] related this latter derivation to perturbation theory and indicated that retention of higher order terms in the series led to higher order variational principles (i.e., principles for which errors in the trial function led to nth order ($n > 2$) errors in the value of the functional) of the type proposed by Kostin and Brooks.[116] Devooght[117] also derived higher order variational principles. These higher order principles do not seem to have been employed yet in the derivation of flux synthesis approximations.

Extended Variational Principles in Flux Synthesis Methods

Extended variational principles have played a major role in the development of more powerful and more flexible flux synthesis methods. A variational principle for the neutron transport/diffusion problem must not only have the appropriate balance equations as Euler equations but must also embody the associated boundary, initial, and continuity conditions, either directly or indirectly through restrictions on the admissible class of trial functions. Significant advances have been made in embodying these associated "side" conditions directly in the variational principle, thus increasing the class of admissible trial functions and thereby the flexibility and power of the flux synthesis method.

Several authors[6,118-127] have considered the problem of embodying external surface boundary conditions directly in the variational principle, thus enabling the derivation of a synthesis approximation in which the trial functions were not constrained to satisfy the external boundary conditions. Such variational principles were also employed in the derivation of appropriate external boundary conditions for the P_N equations.

Lewins[128] and Becker[129] noted that the variational principle of Kaplan et al.[12] rigorously admitted only flux trial solutions satisfying a known final condition and introduced an initial value term to replace this physically unrealistic condition by initial value conditions on the trial solutions. Pomraning[130] and Yasinsky[18] suggested initial and final value terms, which embodied flux initial conditions and adjoint final conditions directly in the principle, and temporal continuity terms, which embodied flux and adjoint temporal continuity directly in the principle. The former enabled physically realistic initial and final conditions to be derived for the flux and adjoint, respectively, combining coefficients in a synthesis approximation, and the latter enabled different sets of trial functions to be blended within different time intervals.

Wachspress and Becker[8] incorporated flux and current spatial continuity conditions directly into a variational principle, thereby enabling the use of trial solutions that need not satisfy the physical conditions of flux and current continuity. Multichannel blending synthesis[8] and discontinuous synthesis[9] were direct results of this added flexibility. Initially it was held necessary to work with a variational principle for the P_1 equations in order to embody spatial continuity conditions. However, Pomraning[130] and Buslik[131] introduced appropriate variational principles for the neutron diffusion equation, and Lambropoulos and Luco[132] subsequently provided mathematical arguments as to the validity of such principles. Goldstein and Lancefield[133] have suggested a potentially useful theory in which the locations of the spatial interfaces are determined variationally.

Transformations and Complementary Variational Principles in Transport Theory

Neutron-transport theory can be characterized by many different equations that are related to each other by various transformations. To each characterization corresponds a different variational principle. It was recently shown that many of these variational principles are related among themselves by transformations of two special types, canonical and involutory. Moreover, it has been demonstrated that the pair of extremum (minimum and maximum) variational principles that are related through an involutory transformation are complementary, i.e., the functions that minimize one maximize the other.

Kaplan[134] drew an analogy between reactor physics and classical mechanics to demonstrate that the diffusion-theory variational principles of Selengut[3] and Kaplan[5] were related to the P_1 theory variational principle of Wachspress and Becker[8] in the same manner that Hamilton's principle is related to the canonical integral. Kaplan and Davis[135] demonstrated the relation among four variational principles for the neutron-transport problem. Beginning with a generalized form of one of Vladimirov's principles,[136] which has the even-parity second-order form of the transport equation as its Euler equation, they applied a canonical transformation to obtain essentially Davis' principle[123] F_a, but in a form that did not contain adjoint functions. Then they applied an involutory transformation that resulted in a principle related to Pomraning and Clark's principle[6] $F[\phi^-]$, but with surface terms, which has the odd-parity second-order form of the transport equation as an Euler equation. Applying a canonical transformation to this involutory principle produced essentially Davis' principle[123] F_b, which, with F_a, has the transport equation in coupled first-order form as Euler equations. Adding a variable surface term to Vladimirov's principle resulted in a family of principles, each of which has canonical and involutory forms. One of the canonical forms turned out to be essentially Selengut's principle.[118]

Kaplan[137] extended the theory for canonical and involutory transformations to variational problems with higher derivatives. Pomraning[138] further extended the theory to allow an arbitrary number of linear operators, including derivatives of all order, in the variational problem.

Kaplan and Davis[135] pointed out that the generalized form of Vladimirov's principle and the principle obtained after a canonical and an involutory transformation are complementary (for monoenergetic transport theory) in the sense that the minimum value of the former equals the maximum value of the latter. Their suggestion that this fact might lead to a means for obtaining error bounds or figures of merit for approximate solutions was investigated by Yasinsky and Kaplan.[139] These latter authors applied the idea to obtain a figure of merit for synthesis approximations in neutron-diffusion theory with some success but concluded that the computational effort involved rendered the procedure unfeasible for large multidimensional problems.

Pomraning[138,140] used involutary transformations to construct complementary variational principles for self-adjoint neutron-transport and diffusion problems. He invoked these complementary principles to compute bounds for several quantities of interest in neutron-transport and reactor theory.

Davis[141] formulated complementary variational principles for the monoenergetic one-dimensional neutron-transport equation. He utilized these complementary principles to show that even-order P_N approximations converge monotonically from below, and odd-order P_N approximations converge monotonically from above, as the order N increases.

The work on transformations of variational principles serves mainly to unify the basic theory. However, the bounding property of complementary variational principles could have practical application to self-adjoint, or extremum, problems. Complementary principles could be employed to define upper and lower bounds on integral properties or to obtain figures of merit for approximate (e.g., synthesis) solutions.

SUMMARY

Flux synthesis methods provide a powerful means for constructing neutron-flux distributions in a degree of detail which is impractical, if not impossible, by direct solution methods. It is paradoxical that the essential feature of flux synthesis methods, the combination of detailed lower dimensional solutions to obtain a detailed higher dimensional solution, is simultaneously their principal advantage and disadvantage. For it can be said fairly of synthesis methods that their strongest point is that one can incorporate physical insight to reduce an otherwise intractable problem to manageable proportions, and, conversely, their weakest point is that one must. This, obviously, strikes different people in different ways.

The power and economy of flux synthesis methods have been amply demonstrated by numerous applica-

tions to realistic reactor models. These applications have also illustrated the need to exercise some ingenuity in the selection of trial functions, if accurate solutions are required for complex models in which the flux is highly nonseparable, and the need to be wary of the possibility of anomalous solutions. In the hands of an experienced user, flux synthesis methods constitute one of the most powerful tools available for the analysis of realistic reactor models.

ACKNOWLEDGMENT

This work was performed under the auspices of the U. S. Atomic Energy Commission.

REFERENCES

1. J. E. Meyer, Synthesis of Three-Dimensional Power Shapes, in *Proceedings of the Second United Nations International Conference on the Peaceful Uses of Atomic Energy, 1958,* Vol. 11, p. 519, United Nations, New York, 1958.
2. E. L. Wachspress, R. D. Burgess, and S. Baron, Multichannel Flux Synthesis, *Nucl. Sci. Eng.*, **12:** 381 (1962).
3. D. S. Selengut, Variational Analysis of a Multidimensional System, USAEC Report HW-59126, p. 89, Hanford Laboratory, 1959.
4. G. P. Calame and F. D. Federighi, A Variational Procedure for Determining Spatially Dependent Thermal Spectra, *Nucl. Sci. Eng.*, **10:** 190 (1961).
5. S. Kaplan, Some New Methods of Flux Synthesis, *Nucl. Sci. Eng.*, **13:** 22 (1962).
6. G. C. Pomraning and M. C. Clark, Jr., The Variational Method Applied to the Monoenergetic Boltzmann Equation, Parts I and II, *Nucl. Sci. Eng.*, **16:** 147, 155 (1963).
7. D. S. Selengut, Knolls Atomic Power Laboratory, personal communication, 1964.
8. E. L. Wachspress and M. Becker, Variational Synthesis with Discontinuous Trial Functions, in Proceedings of Conference on Application of Computational Methods to Reactor Problems, USAEC Report ANL-7050, p. 191, Argonne National Laboratory, 1965; also, Variational Multichannel Synthesis with Discontinuous Trial Functions, USAEC Report KAPL-3095, Knolls Atomic Power Laboratory, 1965.
9. J. B. Yasinsky and S. Kaplan, Synthesis of Three-Dimensional Flux Shapes Using Discontinuous Sets of Trial Functions, *Nucl. Sci. Eng.*, **28:** 426 (1967).
10. A. Travelli and F. Helm, Calculation of the Sodium Void Effect by Flux Synthesis, *Trans. Amer. Nucl. Soc.*, **10:** 275 (1967).
11. B. L. Hutchins, M. D. Kelly, and G. L. Gyorey, Multigroup Two-Dimensional Synthesis Calculations for Fast Power Reactors, *Trans. Amer. Nucl. Soc.*, **10:** 526 (1967).
12. S. Kaplan, O. J. Marlowe, and J. Bewick, Application of Synthesis Techniques to Problems Involving Time Dependence, *Nucl. Sci. Eng.*, **18:** 163 (1964).
13. J. B. Yasinsky, Combined Space–Time Synthesis with Axially Discontinuous Trial Functions, USAEC Report WAPD-TM-736, Bettis Atomic Power Laboratory, 1967.
14. E. L. Wachspress, On the Use of Different Radial Trial Functions in Different Axial Zones of a Neutron Flux Synthesis Computation, *Nucl. Sci. Eng.*, **34:** 342 (1968).
15. V. Luco and G. K. Leaf, Variational Flux Synthesis with Discontinuous Trial Functions, in Reactor Physics Division Annual Report, July 1, 1967, to June 30, 1968, USAEC Report ANL-7410, p. 400, Argonne National Laboratory, 1969.
16. W. L. Woodruff, Some Improvements in Variational Flux Synthesis Methods, USAEC Report ANL-7696, Argonne National Laboratory, 1970.
17. W. B. Terney, Interface Conditions for Discontinuous Flux Synthesis Methods, *Nucl. Sci. Eng.*, **41:** 303 (1970).
18. J. B. Yasinsky, The Solution of the Space–Time Neutron Group Diffusion Equations by a Time-Discontinuous Synthesis Method, *Nucl. Sci. Eng.*, **29:** 381 (1967).
19. M. Becker, Asymmetric Discontinuities in Synthesis Techniques for Initial Value Problems, *Nucl. Sci. Eng.*, **34:** 343 (1968).
20. J. B. Yasinsky and A. F. Henry, Some Numerical Experiments Concerning Space–Time Reactor Kinetics Behavior, *Nucl. Sci. Eng.*, **22:** 171 (1965).
21. R. A. Rydin, Time Synthesis—A Study of Synthesis Modes and Weighting Functions, *Trans. Amer. Nucl. Soc.*, **10:** 559 (1967).
22. C. H. Adams, R. A. Rydin, and W. M. Stacey, Jr., A Numerical Study of Single-Channel Flux Synthesis, *Trans. Amer. Nucl. Soc.*, **11:** 169 (1968).
23. J. B. Yasinsky, Numerical Studies of Combined Space–Time Synthesis, *Nucl. Sci. Eng.*, **34:** 158 (1968).
24. H. Larsen, Experience with Flux Synthesis for Burnup Calculations on Light Water Reactors, in *Proceedings of IAEA Seminar on Numerical Reactor Calculations, Vienna, 1972,* Paper IAEA/SM-154/24, to be published.
25. S. Pilate et al., A Three-Dimensional Synthesis Method Tested and Applied in Fast Breeders, German Report KFK-1345, Kernforschungszentrum Karlsruhe, 1971; also, G. Buckel et al., Three-Dimensional Space Synthesis in Hexagonal Geometry, in *Proceedings of IAEA Seminar on Numerical Reactor Calculations, Vienna, 1972,* Paper IAEA/SM-154/43, to be published.
26. V. Luco, Single-Channel Continuous-Trial-Function Calculations in a Fast Reactor Configuration, in Applied Physics Division Annual Report, July 1, 1970, to June 30, 1971, USAEC Report ANL-7910, Argonne National Laboratory, to be published.
27. V. Luco, Synthesis Calculations in a Highly Nonseparable Fast Reactor Cell, in Applied Physics Division Annual Report, July 1, 1970, to June 30, 1971, USAEC Report ANL-7910, Argonne National Laboratory, to be published.
28. D. E. Doughterty and C. N. Shen, The Space–Time Neutron Kinetics Equations Obtained by the Semidirect Variational Method, *Nucl. Sci. Eng.*, **13:** 141 (1962).

29. R. J. Hooper and M. Becker, Flux Synthesis Using Modified Green's Function Modes, *Trans. Amer. Nucl. Soc.*, **9**: 471 (1966).
30. K. Kobayashi, Flux Synthesis Using Green's Function in Two-Dimensional Group Diffusion Equations, *Nucl. Sci. Eng.*, **31**: 91 (1968).
31. J. B. Yasinsky, On the Application of Time-Synthesis Techniques to Coupled Core Reactors, *Nucl. Sci. Eng.*, **32**: 425 (1968).
32. W. M. Stacey, Jr., A Variational Multichannel Space–Time Synthesis Method for Nonseparable Reactor Transients, *Nucl. Sci. Eng.*, **34**: 45 (1968).
33. E. L. Fuller, D. A. Meneley, and D. L. Hetrick, Weighted Residual Methods in Space-Dependent Reactor Dynamics, *Nucl. Sci. Eng.*, **40**: 206 (1970).
34. E. L. Wachspress, Numerical Studies of Multichannel Variational Synthesis, *Nucl. Sci. Eng.*, **26**: 373 (1966).
35. E. L. Wachspress, Some Mathematical Properties of the Multichannel Variational Synthesis Equations and 2D Synthesis Numerical Studies, USAEC Report KAPL-M-6588, Knolls Atomic Power Laboratory, 1966.
36. P. C. Rohr and M. Becker, Modal Analysis of Power Tilting, *Trans. Amer. Nucl. Soc.*, **11**: 169 (1968).
37. W. M. Stacey, Jr., Variational Flux Synthesis Methods for Multigroup Neutron Diffusion Theory, *Nucl. Sci. Eng.*, **47**: 4, 449 (1972); also, Variational Flux Synthesis Approximations, in *Proceedings of IAEA Seminar on Numerical Reactor Calculations, Vienna, 1972*, Paper IAEA/SM-154/47, to be published.
38. S. Kaplan, O. J. Marlowe, and W. R. Caldwell, Equations and Programs for Solutions of the Neutron Group Diffusion Equations by Synthesis Approximations, USAEC Report WAPD-TM-377, Bettis Atomic Power Laboratory, 1963.
39. J. L. Bear, F. D. Judge, and E. R. Venerus, The Application of Synthesis Techniques to the Calculation of Three-Dimensional Reactivity–Coefficient Distributions, *Nucl. Sci. Eng.*, **31**: 349 (1968).
40. J. B. Yasinsky and S. Kaplan, Anomalies Arising from the Use of Adjoint Weighting in a Collapsed Group–Space Synthesis Model, *Nucl. Sci. Eng.*, **31**: 354 (1968).
41. C. H. Adams and W. M. Stacey, Jr., An Anomaly Arising in the Collapsed-Group Flux Synthesis Approximation, *Nucl. Sci. Eng.*, **36**: 444 (1969).
42. R. Froehlich, Anomalies in Variational Flux Synthesis Methods, *Trans. Amer. Nucl. Soc.*, **12**: 150 (1969).
43. V. Luco and W. L. Woodruff, Another Anomaly in Variational Flux Synthesis, *Trans. Amer. Nucl. Soc.*, **13**: 739 (1970).
44. V. Luco, On the Eigenvalues of the Flux Synthesis Equations, *Trans. Amer. Nucl. Soc.*, **14**: 203 (1971).
45. R. Fröhlich, Flux Synthesis Methods Versus Finite Difference Approximation Methods for the Efficient Determination of Neutron Flux Distributions in Fast and Thermal Reactors, in *Proceedings of IAEA Seminar on Numerical Reactor Calculations, Vienna, 1972*, Paper IAEA/SM-154/14, to be published.
46. J. W. Riese, A Variational Technique for Space–Time Neutron Diffusion, *Trans. Amer. Nucl. Soc.*, **7**: 22 (1964); also, USAEC Report WANL-TNR-133, Westinghouse Astronuclear Laboratory, 1963.
47. G. C. Pomraning, Approach to Space-Energy Problems, *Nukleonik*, **7**: 192 (1965).
48. G. C. Pomraning, A Numerical Study of the Method of Weighted Residuals, *Nucl. Sci. Eng.*, **24**: 291 (1966).
49. K. F. Hansen, S. R. Johnson, and R. E. Storat, A Numerical Method for the Three-Dimensional Multigroup Equations, *Trans. Amer. Nucl. Soc.*, **10**: 174 (1967).
50. W. H. Guilinger, The Finite Element Method, *Trans. Amer. Nucl. Soc.*, **14**: 199 (1971).
51. H. G. Kaper, G. K. Leaf, and A. J. Lindeman, Application of Finite-Element Techniques for the Numerical Solution of the Neutron Transport and Diffusion Equations, Proceedings of Second Conference on Transport Theory, USAEC Report CONF-710107, p. 258, 1971. Also, Applications of Finite-Element Methods in Reactor Mathematics. Numerical Solution of the Neutron Diffusion Equation, USAEC Report ANL-7925, Argonne National Laboratory, 1972.
52. T. Ohnishi, Application of the Finite-Element Solution Technique to Neutron Diffusion and Transport Equations, Proceedings of Conference on New Developments in Reactor Mathematics and Applications, USAEC Report CONF-710302, Vol. II, p. 723, 1971.
53. T. Ohnishi, Finite-Element Solution Technique for Neutron Transport Equations, in *Proceedings of IAEA Seminar on Numerical Reactor Calculations, Vienna, 1972*, Paper IAEA/SM-154/57, to be published.
54. C. M. Kang and K. F. Hansen, Finite Element Methods for the Neutron Diffusion Equations, *Trans. Amer. Nucl. Soc.*, **14**: 199 (1971).
55. L. A. Semenza, E. E. Lewis, and E. C. Rossow, The Application of the Finite-Element Method to the Multigroup Neutron Diffusion Equation, *Nucl. Sci. Eng.*, **47**: 302 (1972).
56. W. F. Miller et al., Transport Solutions Using Finite Elements in Space-Angle Phase Space, *Trans. Amer. Nucl. Soc.*, **14**: 651 (1971).
57. S. Nakamura and T. Ohnishi, The Iterative Solutions for the Finite Element Method, in *Proceedings of IAEA Seminar on Numerical Reactor Calculations, Vienna, 1972*, Paper IAEA/SM-154/57, to be published.
58. A. F. Henry, Refinements in Accuracy of Coarse Mesh Finite-Difference Solution of the Group Diffusion Equations, in *Proceedings of IAEA Seminar on Numerical Reactor Calculations, Vienna, 1972*, Paper IAEA/SM-154/21, to be published.
59. E. L. Wachspress, *Iterative Solution of Elliptic Systems*, Prentice-Hall, Inc., Englewood Cliffs, N. J., 1966, pp. 270–287.
60. R. Fröhlich, A Theoretical Foundation for Coarse Mesh Variational Techniques, in Proceedings of International Conference on Research Reactor Utilization and Reactor Computation, Mexico, Report CNM-R-2, Vol. 1, p. 219 (CONF-670501), 1967.
61. R. Fröhlich, Computer Independence of Large Reactor Physics Codes with Reference to Well Balanced Computer Configurations, in Proceedings of Conference on Effective Use of Computers in the Nuclear Industry, USAEC Report CONF-690401, p. 451, 1969.

62. S. Nakamura, A Variational Rebalancing Method for Linear Iterative Convergence Schemes of Neutron Diffusion and Transport Equation, *Nucl. Sci. Eng.*, **39**: 278 (1970).

63. S. Nakamura, Coarse Mesh Acceleration of Iterative Solution of Neutron Diffusion Equation, *Nucl. Sci. Eng.*, **43**: 116 (1971).

64. S. Nakamura, New Formulation and Coarse Mesh Acceleration for Two-Dimensional DS_N and P_N Methods, in *Proceedings of IAEA Seminar on Numerical Reactor Calculations, Vienna, 1972*, Paper IAEA/SM-154/54, to be published.

65. W. M. Stacey, Jr., *Modal Approximations: Theory and an Application to Reactor Physics*, The MIT Press, Cambridge, Mass., 1967; also, Fast Reactor Calculation Models, *Nucl. Sci. Eng.*, **28**: 443 (1967).

66. A. F. Henry, Few-Group Approximations Based on a Variational Principle, *Nucl. Sci. Eng.*, **27**: 493 (1967).

67. M. Becker, Overlapping Group Methods with Discontinuous Trial Functions, *Nucl. Sci. Eng.*, **34**: 339 (1968).

68. W. M. Stacey, Jr., General Multigroup and Spectral Synthesis Equations, *Nucl. Sci. Eng.*, **40**: 73 (1970).

69. G. P. Calame, F. D. Federighi, and P. A. Ombrellaro, A Two Mode Variational Procedure for Calculating Thermal Diffusion Theory Parameters, *Nucl. Sci. Eng.*, **10**: 31 (1961).

70. P. A. Ombrellaro and F. D. Federighi, A Variational Procedure for Calculating Fast Group Constants, *Nucl. Sci. Eng.*, **16**: 343 (1963).

71. P. A. Ombrellaro and M. A. Snider, Synthesis of Fast Reactor Energy Spectra, *Nucl. Sci. Eng.*, **46**: 150 (1971).

72. D. C. Leslie, The Calculation of Removal Cross Sections Between Overlapping Thermal Groups, *J. Nucl. Energy, Parts A and B*, **16**: 303 (1962).

73. R. J. Breen and J. B. Yasinsky, An Approximate Solution of the Two-Overlapping Thermal-Group Diffusion Equations, *Nucl. Sci. Eng.*, **22**: 392 (1965).

74. M. Natelson, A Two-Overlapping-Group Transport Approximation for Thermal-Neutron Problems, *Trans. Amer. Nucl. Soc.*, **13**: 189 (1970).

75. D. S. Selengut, Adjoint Spectra for Calculating Thermal Group Constants, *Nucl. Sci. Eng.*, **44**: 447 (1971).

76. F. Storrer and J. M. Chaumont, The Application of Space-Energy Synthesis to the Interpretation of Fast Multizone Critical Experiments, in Proceedings of International Conference on Fast Critical Experiments and Analysis, USAEC Report ANL-7320, p. 439, Argonne National Laboratory, 1967.

77. T. E. Murley and J. W. Williamson, Techniques for Fast Reactor Calculations, *Trans. Amer. Nucl. Soc.*, **11**: 174 (1968).

78. E. V. Vaughan, P. F. Rose, and D. F. Hausknecht, Spectrum Synthesis in Fast Reactor Analysis, USAEC Report AI-AEC-12820, Atomics International, 1969.

79. R. J. Neuhold and K. Ott, Improvements in Fast Reactor Space-Energy Synthesis, *Nucl. Sci. Eng.*, **39**: 14 (1970).

80. R. J. Neuhold, Multiple Weighting Functions in Fast-Reactor Space-Energy Synthesis, *Nucl. Sci. Eng.*, **43**: 74 (1971).

81. T. Kiguchi, S. An, and A. Oyama, Energy Modal Synthesis Method in Fast Reactor Analysis, *Nucl. Sci. Eng.*, **43**: 328 (1971).

82. P. A. Ombrellaro, Synthesis of Fast Reactor Space-Energy Spectra, *Nucl. Sci. Eng.*, **44**: 204 (1971).

83. W. O. Olson and A. H. Robinson, Space-Energy Flux Synthesis with Spatially Discontinuous Trial Functions, *Trans. Amer. Nucl. Soc.*, **14**: 204 (1971).

84. W. M. Stacey, Jr., Spectral Synthesis Applied to Fast-Reactor Dynamics, *Nucl. Sci. Eng.*, **41**: 249 (1970); also, Spectral Synthesis Methods in Fast-Reactor Dynamics, in *Dynamics of Nuclear Systems*, David L. Hetrick (Ed.), The University of Arizona Press, 1972, pp. 453–466.

85. W. M. Stacey, Jr., Application of the Spectral Synthesis Method to the Analysis of Spatially-Dependent Fast-Reactor Transients, *Nucl. Sci. Eng.*, **45**: 221 (1971).

86. M. A. Robkin, The Application of a Standard Diffusion Theory Code to the Overlapping Group Method, General Electric Report MAR-4096, General Electric, 1967.

87. P. G. Lorenzini and A. H. Robinson, Solutions of the Diffusion Equation by the Spectral-Synthesis Method, *Nucl. Sci. Eng.*, **44**: 27 (1971).

88. H. Greenspan, Evaluation of Spectral Flux Synthesis for LMFBR Applications, *Trans. Amer. Nucl. Soc.*, **15**: 300 (1972); also, *Nucl. Sci. Eng.*, submitted for publication.

89. T. Toivanen, On the Variational and Bubnov–Galerkin Synthesis of the Epithermal Spatially Dependent Neutron Energy Spectra, *J. Nucl. Energy, Parts A and B*, **22**: 283 (1968).

90. M. J. Lancefield, Space-Energy Flux Synthesis in Neutron Transport, *Nucl. Sci. Eng.*, **37**: 423 (1969).

91. J. E. Cockayne and K. O. Ott, Successive Space-Energy Synthesis for Neutron Fluxes in Fast Reactors, *Nucl. Sci. Eng.*, **43**: 159 (1971).

92. R. P. Savio et al., Applications of Iterative and Successive Space-Energy Synthesis to Fast-Reactor Problems, *Trans. Amer. Nucl. Soc.*, **14**: 638 (1971).

93. G. C. Pomraning and M. Clark, Jr., A New Asymptotic Diffusion Theory, *Nucl. Sci. Eng.*, **17**: 227 (1963).

94. S. L. Paveri-Fontana and H. Amster, An Altered Diffusion Theory Based on the Double P–O Approximation for All Geometries, *Nucl. Sci. Eng.*, **44**: 44 (1971).

95. S. Kaplan, J. A. Davis, and M. Natelson, Angle-Space Synthesis—An Approach to Transport Approximations, *Nucl. Sci. Eng.*, **28**: 364 (1967).

96. S. Schreiner and D. S. Selengut, Variational Development of S_N Theory, in Proceedings of International Conference on Research Reactor Utilization and Reactor Computation, Mexico, Report CNM-R-2, Vol. 1, p. 238 (CONF-670501), 1967.

97. M. Natelson, A Strategy for the Application of Space-Angle Synthesis to Practical Problems in Neutron Transport, *Nucl. Sci. Eng.*, **31**: 325 (1968).

98. P. Jauho and H. Kalli, A Variational Approach to the Selection of the Direction Sets in the Discrete S_n Approximation to Neutron Transport Theory, *Nucl. Sci. Eng.*, **33**: 251 (1968).

99. S. Kaplan, A New Derivation of Discrete Ordinate Approximations, *Nucl. Sci. Eng.*, **34**: 76 (1968).

100. M. Natelson, Variational Derivation of Discrete Ordinate-Like Approximations, *Nucl. Sci. Eng.*, **43**: 131 (1971).

101. B. D. O'Reilly, A Variational Synthesis Method for Calculating Structure Shielding Data, USAEC Report AI-68-51, Atomics International, 1968.
102. M. Natelson and E. M. Gelbard, Synthesis of Three-Dimensional Problems Using Transport Trial Functions, *Trans. Amer. Nucl. Soc.*, **12**: 728 (1969). Also, M. Natelson, Synthesis of Three-Dimensional Transport Problems Using Two-Dimensional Trial Functions, *Nucl. Sci. Eng.*, **48**: 16 (1972).
103. R. E. Alcouffe, A Study of Two-Dimensional S_N Transport Synthesis Via Angle-Collapse, *Trans. Amer. Nucl. Soc.*, **14**: 217 (1971).
104. G. C. Pomraning and M. Clark, Jr., Spatial Expansion of the Transport Equation, *J. Nucl. Energy, Parts A and B*, **18**: 191 (1964).
105. H. S. Zwibel and B. Bowes, Space-Angle Synthesis, *Nucl. Sci. Eng.*, **36**: 435 (1969).
106. W. R. Cobb, Multichannel Spatial Transport Synthesis, *Trans. Amer. Nucl. Soc.*, **14**: 216 (1971).
107. G. C. Pomraning, A Variational Principle for Linear Systems, *J. Soc. Ind. Appl. Math.*, **13**: 511 (1965).
108. G. C. Pomraning, A Variational Principle for Eigenvalue Equations, *J. Math. Phys.*, **8**: 149 (1967).
109. G. C. Pomraning, A Derivation of Variational Principles for Inhomogeneous Equations, *Nucl. Sci. Eng.*, **29**: 220 (1967).
110. G. C. Pomraning, Generalized Variational Principles for Reactor Analysis, in Proceedings of International Conference on Research Reactor Utilization and Reactor Computation, Mexico, Report CNM-R-2, Vol. 1, p. 250 (CONF-670501,), 1967.
111. J. Lewins, *Importance: The Adjoint Function*, Pergamon Press, Ltd., London, 1965.
112. J. Lewins, Time-Dependent Variational Theory, *Nucl. Sci. Eng.*, **31**: 160 (1968).
113. M. Becker, *The Principles and Applications of Variational Methods*, The MIT Press, Cambridge, Mass., 1964.
114. S. G. Mikhlin, *Variational Methods in Mathematical Physics*, The Macmillan Company, New York, 1964.
115. D. S. Selengut, On the Derivation of a Variational Principle for Linear Systems, *Nucl. Sci. Eng.*, **17**: 310 (1963).
116. M. D. Kostin and H. Brooks, Generalization of the Variational Method of Kahan, Rideau, and Roussopoulos and Its Application to Neutron Transport Theory, *J. Math. Phys.*, **5**: 1691 (1965).
117. J. Devooght, Higher Order Variational Principles and Iterative Process, *Nucl. Sci. Eng.*, **41**: 399 (1970).
118. D. S. Selengut, Transport Corrections to Diffusion Theory, *Trans. Amer. Nucl. Soc.*, **5**: 40 (1962).
119. G. C. Pomraning, An Improved Free-Surface Boundary Condition for the P-3 Approximation, *Nucl. Sci. Eng.*, **18**: 528 (1964).
120. G. C. Pomraning, The Treatment of Boundary Terms in a Variational Principle Characterizing Transport Theory, *Nucl. Sci. Eng.*, **22**: 259 (1965); also, Variational Boundary Conditions for the Spherical Harmonics Approximation to the Neutron Transport Equation, *Ann. Phys.*, **27**: 193 (1964).
121. F. D. Federighi, Vacuum Boundary Conditions for the Spherical Harmonics Method, *Nukleonik*, **6**: 277 (1964).
122. H. J. Amster, A More Straightforward Use of Variational Principles with Boundary Conditions, *Nucl. Sci. Eng.*, **22**:254 (1965).
123. J. A. Davis, Variational Vacuum Boundary Conditions for a P_N Approximation, *Nucl. Sci. Eng.*, **25**: 189 (1966).
124. T. Toivanen, A Self-Adjoint Variational Principle for Deriving Vacuum and Interface Boundary Conditions in the Spherical Harmonics Method, *Nucl. Sci. Eng.*, **25**: 275 (1966).
125. J. R. Mika, On the Variational Method to the Monoenergetic Boltzmann Equation, *Nucl. Sci. Eng.*, **19**: 377 (1964).
126. W. H. Kohler, Variational Method for Prompt Neutron Kinetics, *Nukleonik*, **8**: 203 (1966).
127. W. M. Stacey, Jr., Variational Functionals for Space–Time Neutronics, *Nucl. Sci. Eng.*, **30**: 448 (1967).
128. J. Lewins, Time-Dependent Variational Principles for Nonconservative Systems, *Nucl. Sci. Eng.*, **20**: 517 (1964).
129. M. Becker, On the Inclusion of Boundary Terms in Time-Dependent Synthesis Techniques, *Nucl. Sci. Eng.*, **22**: 385 (1965).
130. G. C. Pomraning, A Variational Description of Dissipative Processes, *J. Nucl. Energy, Parts A and B*, **20**: 617 (1966).
131. A. J. Buslik, A Variational Principle for the Neutron Diffusion Equation Using Discontinuous Trial Functions, USAEC Report WAPD-TM-610, Bettis Atomic Power Laboratory, 1966; also, *Trans. Amer. Nucl. Soc.*, **9**: 199 (1966).
132. P. Lambropoulos and V. Luco, Functionals for Discontinuous Trial Function Flux Synthesis, *J. Nucl. Energy, Parts A and B*, **24**: 551 (1970); also, USAEC Report ANL-7627, Argonne National Laboratory, 1969.
133. R. Goldstein and M. Lancefield, Variational Functionals with Trial Functions Having Arbitrary Points of Discontinuity, *Trans. Amer. Nucl. Soc.*, **12**: 723 (1969).
134. S. Kaplan, An Analogy Between the Variational Principles of Reactor Theory and Those of Classical Mechanics, *Nucl. Sci. Eng.*, **23**: 234 (1965).
135. S. Kaplan and J. A. Davis, Canonical and Involutory Transformations of the Variational Problems of Transport Theory, *Nucl. Sci. Eng.*, **28**: 166 (1967).
136. V. S. Vladimirov, Mathematical Problems in the One-Velocity Theory of Particle Transport, Atomic Energy of Canada Limited, 1963, translated from *Trans. V. A. Steklov Math. Inst.*, **61**: (1961).
137. S. Kaplan, Canonical and Involutory Transformations of Variational Problems Involving Higher Derivatives, *J. Math. Anal. Appl.*, **22**: 45 (1968).
138. G. C. Pomraning, Reciprocal and Canonical Forms of Variational Problems Involving Linear Operators, *J. Math. Phys.*, **47**: 155 (1968).
139. J. B. Yasinsky and S. Kaplan, On the Use of Dual Variational Principles for the Estimation of Error in Approximate Solutions of Diffusion Problems, *Nucl. Sci. Eng.*, **31**: 80 (1968).
140. G. C. Pomraning, Complementary Variational Principles and Their Application to Neutron Transport Problems, *J. Math. Phys.*, **8**: 2096 (1967).
141. J. A. Davis, Transport Error Bounds Via P_N Approximations, *Nucl. Sci. Eng.*, **31**: 127 (1968).

General References

W. M. Stacey, Jr., Variational Flux Synthesis Approximations, in *Proceedings of IAEA Seminar on Numerical Reactor Calculations, Vienna, 1972,* Paper IAEA/SM-154/47.

E. L. Wachspress, Variational Methods and Neutron Flux Synthesis, in Proceedings of Conference on Effective Use of Computers in Nuclear Industry, USAEC Report CONF-690401, p. 271, 1969.

S. Kaplan, Synthesis Methods in Reactor Analysis, in *Advances in Nuclear Science and Technology,* Vol. 3, Academic Press Inc., New York, 1966.

M. L. Steele, Variational Techniques as a Method for Multidimensional Reactor Calculations, *Reactor Technol.*, 13(1): 73 (Winter 1969–1970).

S. Kaplan, Variational Methods in Nuclear Engineering, in *Advances in Nuclear Science and Technology,* Vol. 5, Academic Press Inc., New York, 1969.

Selected Recent or Recently Released Publications*

Unless otherwise stated, the publications listed here are available from the National Technical Information Service (NTIS), U.S. Department of Commerce, Springfield, Va. 22151.

SIMULATING STRONG MOTION EARTHQUAKE EFFECTS ON NUCLEAR POWER PLANTS

Authors: J. Chrostowski, C. M. Duke, Mary C. Hart, G. Howard, P. Ibanez, R. DiJulio, Y. Kharraz, R. B. Matthiesen, C. B. Smith, University of California, Nuclear Energy Laboratory, Los Angeles, Calif.

Abstract: Tests using high explosives to simulate the ground motion produced by earthquakes are described. The tests were conducted at the Experimental Gas-Cooled Reactor (EGCR) facility at Oak Ridge National Laboratory. The objectives of the tests were to determine the feasibility of dynamic-response measurements using blast-induced vibrations and to determine the nonlinear response of structures due to high force levels typical of moderate- to strong-motion earthquakes. The test results are described and compared to results obtained by using structural vibrators. (HDR)

Available as UCLA-ENG-7119. Date of report, February 1972.

HIGH-TEMPERATURE STRUCTURAL DESIGN METHODS FOR LMFBR COMPONENTS. Quarterly Progress Report for Period Ending March 31, 1972.

Authors: W. L. Greenstreet, J. M. Corum, and C. E. Pugh, Oak Ridge National Laboratory, Oak Ridge, Tenn.

Abstract: The ORNL program to develop high-temperature structural design methods for LMFBR vessels, components, and core structures is described. Effects of temperature on the tensile properties of 304 stainless steel are measured. 46 references. (auth)

Available as ORNL-TM-3845. Date of report, June 1972.

*Compiled by the Reactor Technology Section of the AEC Technical Information Center, Oak Ridge, Tenn. 37830.

FFTF DESIGN FLEXIBILITY FOR HYPOTHETICAL ACCIDENT MITIGATION

Author: R. E. Peterson, Hanford Engineering Development Laboratory, Richland, Wash.

Abstract: The capability of the Fast Flux Test Facility (FFTF) containment to withstand consequences associated with a hypothetical core-disruptive accident (HCDA) is investigated over a wide range of energy release. Responses of the primary-coolant-system boundary, the reactor cavity, and the containment building to a theoretically available work energy of 150 MW-sec are evaluated. The sensitivity of the design to work energy was also assessed by extending the calculations to 350 MW-sec. The design is evaluated for higher energy releases up to 1000 MW-sec. In these evaluations the responses of the following design features were analytically obtained: reactor-vessel head, reactor-cavity pressures with and without vapor-bubble collapse, piping interferences, plugs in the reactor-vessel head, head-compartment-pressure sensitivity to postulated sodium release, reactor and guard vessel, and reactor support system. (auth)

Available as HEDL-71-125(Rev. 1). Date of report, Oct. 25, 1971.

DESIGN AND SITING CRITERIA FOR ONCE-THROUGH COOLING SYSTEMS BASED ON A FIRST-ORDER THERMAL PLUME MODEL

Authors: D. W. Pritchard and H. H. Carter, Johns Hopkins University, Baltimore, Md.

Abstract: The processes that control the distribution of excess temperature in the heated plume resulting from the discharge of a heated effluent into a natural water body are discussed, and the relative importance of each process for various plant design and environmental conditions is assessed. The distributions of excess temperature and the time–temperature history of exposure of organisms entrained into the thermal plume resulting from the discharge of condenser cooling water from a 1000-MW(e) nuclear power plant are given for several alternate sets of design criteria for the discharge structure. It is shown that, in order to minimize adverse effects on natural water bodies used to supply condenser cooling-water flow for once-through cooling systems, the power plant should be located on a waterway having large

dilution capacity, and the discharge structure should be designed to promote rapid dilution of the heated effluent by the cooler receiving waters. Intake structures should be designed to provide for low intake velocities and to provide an effective means of diverting fish and other aquatic organisms away from the intake. Time of travel of the condenser cooling-water flow from the condensers to the point of discharge should be kept small in order to minimize the time of exposure of entrained organisms to the maximum temperature rise. 16 references. (auth)

Available as COO-3062-3. Date of report, April 1972.

COMPARISON OF THERMAL–HYDRAULIC RESPONSE OF LOFT AND A LARGE PRESSURIZED-WATER REACTOR TO LOCA CONDITIONS

Authors: G. K. Cederberg, H. D. Curet, P. R. Davis, J. Dugone, R. F. Jiminez, R. C. Schmitt, R. W. Shumway, and R. P. Wadkins, Aerojet Nuclear Company, Idaho Falls, Idaho.

Abstract: An analytical study was performed to determine how closely the thermal–hydraulic response of the Loss-of-Fluid Test (LOFT) pressurized-water reactor [55 MW(t)] with a 5.5-ft-long core compares with that of a large four-loop pressurized-water reactor [3000 MW(t)] with a 12-ft-long core under loss-of-coolant accident conditions. The analysis employed the thermal–hydraulic computer codes RELAP3 and THETA1-B to determine the hydraulic response of the primary systems during blowdown and the thermal responses of the cores during blowdown. An additional analysis was performed to assess the core thermal response during ECC reflooding. On the basis of the results of the analyses, the conclusion was reached that a 5.5-ft core operating in the LOFT system can produce thermal–hydraulic behavior representative of that calculated to occur in a large four-loop PWR with a 12-ft core during a double-ended inlet pipe break. The inlet pipe break analyzed is generally considered to result in the highest core temperatures for large PWRs. (auth)

Available as ANCR-1053. Date of report, April 1972.

INDEXED BIBLIOGRAPHY OF THERMAL EFFECTS LITERATURE—2

Authors: J. G. Morgan and C. C. Coutant, Oak Ridge National Laboratory, Oak Ridge, Tenn.

Abstract: The second volume in the series of indexed bibliographies of thermal-effects literature published by the Nuclear Safety Information Center is presented. It contains new material that has appeared in the literature during 1970 and 1971. The sources for this bibliography include technical journals, government-sponsored reports, technical reports from universities, and conferences dealing with thermal discharges. (auth)

Available as ORNL-NSIC-97. Date of report, May 1972.

RADIATION-INDUCED VOIDS IN METALS

AEC Symposium Series

An international symposium sponsored by
U. S. Atomic Energy Commission and
State University of New York at Albany

Held at State University of New York at Albany
June 9–11, 1971

EDITORS
James W. Corbett and **Louis C. Ianniello**

884 pages, 6 by 9, paperback
Library of Congress Catalog Number: 72-600048

This book summarizes the remarkable progress achieved in just a few years on the important problem of voids and swelling in metals subjected to high-temperature irradiation. This swelling implies an additional cost of several billions of dollars in the cost of fast breeder reactors planned for the United States alone by the year 2000. The book contains the 40 papers, discussions of the papers, a list of participants, and name and subject indexes.

Published as No. 26 in the AEC Symposium Series, this book is available as CONF-710601 for $9.00 from

National Technical Information Service
U. S. Department of Commerce
Springfield, Virginia 22151

Recent USAEC publication of special interest

Sodium Technology 1962–1971 (TID-3334 Part II)

8½ X 11, paperback, 1052 pages, $6.00

Prepared by the USAEC Technical Information Center for the Division of Reactor Development and Technology.

This bibliography covers the literature cited in *Nuclear Science Abstracts* for 1962 (Vol. 16) through Mar. 31, 1972 (Issue 6, Vol. 26). The search was limited to metallic sodium and NaK technology, and the main emphasis of the literature covered is on sodium as applied to reactor-coolant technology.

A subject index is provided, and all literature cited is publicly available. Part I of this two-part bibliography (TID-3334 Part I) is in preparation. It will cover the literature cited in *NSA* from 1948 (Vol. 1) through 1961 (Vol. 15).

Available from
National Technical Information Service
U. S. Department of Commerce
Springfield, Virginia 22151

AEC SYMPOSIUM SERIES

Available from the National Technical Information Service, U. S. Department of Commerce, Springfield, Virginia 22151

1 Progress in Medical Radioisotope Scanning
(TID-7673), Oak Ridge Institute of Nuclear Studies 1963, $6.00

2 Reactor Kinetics and Control
(TID-7662), The University of Arizona, 1964, $6.00

3 Dynamic Clinical Studies with Radioisotopes
(TID-7678), Oak Ridge Institute of Nuclear Studies, 1964, $6.00

4 Noise Analysis in Nuclear Systems
(TID-7679), University of Florida, 1964, $6.00

5 Radioactive Fallout from Nuclear Weapons Tests
(CONF-765), U. S. Atomic Energy Commission, 1965, $6.00

6 Radioactive Pharmaceuticals
(CONF-651111), Oak Ridge Institute of Nuclear Studies, 1966, $6.00

7 Neutron Dynamics and Control
(CONF-650413), The University of Arizona, 1966, $6.00

8 Luminescence Dosimetry
(CONF-650637), Stanford University, 1967, $6.00

9 Neutron Noise, Waves, and Pulse Propagation
(CONF-660206), University of Florida, 1967, $6.00

10 Use of Computers in Analysis of Experimental Data and the Control of Nuclear Facilities
(CONF-660527), Argonne National Laboratory, 1967, $6.00

11 Compartments, Pools, and Spaces in Medical Physiology
(CONF-661010), Oak Ridge Associated Universities, 1967, $6.00

12 Thorium Fuel Cycle
(CONF-660524), Oak Ridge National Laboratory, 1968, $6.00

13 Radioisotopes in Medicine: In Vitro Studies
(CONF-671111), Oak Ridge Associated Universities, 1968, $6.00

14 Abundant Nuclear Energy
(CONF-680810), Oak Ridge Associated Universities, 1969, $6.00

15 Fast Burst Reactors
(CONF-690102), The University of New Mexico, 1969, $6.00

16 Biological Implications of the Nuclear Age
(CONF-690303), Lawrence Radiation Laboratory, 1969, $6.00

17 Radiation Biology of the Fetal and Juvenile Mammal
(CONF-690501), Pacific Northwest Laboratory, 1969, $6.00

18 Inhalation Carcinogenesis
(CONF-691001), Oak Ridge National Laboratory, 1970, $6.00

19 Myeloproliferative Disorders of Animals and Man
(CONF-680529), Pacific Northwest Laboratory, 1970, $9.00

20 Medical Radionuclides: Radiation Dose and Effects
(CONF-691212), Oak Ridge Associated Universities, 1970, $6.00

21 Morphology of Experimental Respiratory Carcinogenesis
(CONF-700501), Oak Ridge National Laboratory, 1970, $6.00

22 Precipitation Scavenging (1970)
(CONF-700601), Pacific Northwest Laboratory, 1970, $6.00

23 Neutron Standards and Flux Normalization
(CONF-701002), Argonne National Laboratory, 1971, $6.00

24 Survival of Food Crops and Livestock in the Event of Nuclear War
(CONF-700909), Brookhaven National Laboratory, 1971, $9.00

25 Biomedical Implications of Radiostrontium Exposure
(CONF-710201), 1972, $6.00

26 Radiation-Induced Voids in Metals
(CONF-710601), 1972, $9.00

NUCLEAR SCIENCE ABSTRACTS

The U. S. Atomic Energy Commission publishes *Nuclear Science Abstracts (NSA)*, a semimonthly journal containing abstracts of the literature of nuclear science and engineering.

NSA covers (1) research reports of the U. S. Atomic Energy Commission and its contractors; (2) research reports of government agencies, universities, and industrial research organizations on a worldwide basis; and (3) translations, patents, books, and articles appearing in technical and scientific journals.

Complete indexes covering subject, author, source, and report number are included in each issue. These indexes are cumulated and sold separately.

Availability

SALE *NSA* is available on subscription from the Superintendent of Documents, U. S. Government Printing Office, Washington, D. C. 20402, at $42.00 per year for the semimonthly abstract issues and $34.50 per year for the cumulated-index issues. Subscriptions are postpaid within the United States, Canada, Mexico, and all Central and South American countries, except Argentina, Brazil, Guyana, French Guiana, Surinam, and British Honduras. Subscribers in these Central and South American countries, and in all other countries throughout the world, should remit $52.50 per year for subscriptions to semimonthly abstract issues and $43.00 per year for the cumulated-index issues. The single-copy price for the abstract issues is $1.75 postpaid, with this exception: Add one-fourth of $1.75 for mailing to the countries to which the $52.50 subscription rate applies.

EXCHANGE *NSA* is also available on an exchange basis to universities, research institutions, industrial firms, and publishers of scientific information. Inquiries should be directed to the USAEC Technical Information Center, P. O. Box 62, Oak Ridge, Tennessee 37830.